LOCAL DRUG DELIVERY TARGETING MAST CELLS TO IMPROVE THE FUNCTIONAL LIFETIME OF CONTINUOUS GLUCOSE SENSORS

by

Mahender nath Avula

A dissertation submitted to the faculty of
The University of Utah
in partial fulfillment of the requirements for the degree of

Doctor of Philosophy

Department of Bioengineering

The University of Utah

December 2013

The University of Utah Graduate School

STATEMENT OF DISSERTATION APPROVAL

The dissertation of **Mahender nath Avula**

has been approved by the following supervisory committee members:

Florian Solzbacher	, Chair	**10/17/2013** Date Approved
David W. Grainger	, Member	**10/21/2013** Date Approved
Lawrence D. McGill	, Member	**10/29/2013** Date Approved
Robert W. Hitchcock	, Member	**10/29/2013** Date Approved
Jules J. Magda	, Member	**10/24/2013** Date Approved

and by **Patrick A. Tresco**, Chair/Dean of

the Department/College/School of **Bioengineering**

and by David B. Kieda, Dean of The Graduate School.

ABSTRACT

Diabetes mellitus affects 5% of the world's population and requires constant monitoring to avoid fatality. Tight control of blood glucose levels has shown to reduce the long-term effects of diabetes. Finger-stick blood glucose measurements are the gold standard for glucose monitoring that are painful and only provide intermittent glucose values. Continuous glucose monitoring (CGM) is an improvement in this technology but is severely limited in its performance abilities beyond the currently approved implantation time lasting up to a week. CGM is still performed as an adjunct to finger-stick measurements since they are unreliable even during the approved usage durations. Implantation of a biomaterial induces a wound (catheter, hernia meshes, etc.) or disturbance in local tissue (contact lens, etc.). Wound healing response in the host mediates the formation of scar tissue and healing of the injury site. Host foreign body response (FBR) deviates from its healing response in the presence of a foreign body i.e, an implant, and tries to isolate it from the host via fibrous encapsulation. FBR is considered as one of the primary reasons for CGM sensor failure. FBR encapsulates the sensor implant, creating a barrier between the sensing electrode and essential analytes (glucose, oxygen, etc.) required for measuring glucose levels. This phenomenon results in painful and expensive CGM sensor replacements.

Work described in this dissertation focuses on improving the clinical performance of CGM sensors by extending their functional lifetimes. Combination device strategies involving the use of a drug (dexamethasone, etc.), or a biologic (VEGF, siRNA, etc.), or a combination of these have been studied to reduce implant-associated FBR. In this

dissertation, we targeted mast cells that are believed to orchestrate the FBR by secreting several key granules containing inflammatory cytokines, vasodilators, chemokines, etc. that result in an increased influx of inflammatory cells to the wound site. A novel tyrosine kinase inhibitor- masitinib was used to target the c-KIT receptor on the cell surface of mast cells. Stem cell factor and its ligand c-KIT are considered critical for mast cell survival, proliferation, and degranulation and the hypothesis driving this research is that *targeting mast cell degranulation via the c-KIT pathway results in a reduced foreign body response.*

To test our hypothesis, we developed a local drug delivery formulation comprised of PLGA microsphere drug carriers embedded in a PEG matrix around implants. The effect of the drug was initially evaluated in wild-type (mast cell competent) and sash (mast cell-deficient) mice for up to 28 days. The results from these studies confirmed previous claims that mast cells play an important role in mediating FBR-associated fibrosis around implanted biomaterials and that the use of a mast cell stabilizing tyrosine kinase inhibitor reduced fibrous capsule thickness around implants in wild-type mice but had no effect in sash mice. The drug-releasing coating was then tested in CGM sensors in a wild-type murine percutaneous model for 21 days. Results from the CGM study indicate that drug-releasing coated sensors exhibit relatively stable response compared to control implants, suggesting that reduced fibrosis resulting from stabilizing mast cells results in improving CGM performance. The translation of these results to human subjects would enable better control of diabetes and provide the ability to better diagnose long-term effects of diabetes through long-term continuous glucose monitoring.

TABLE OF CONTENTS

ACKNOWLEDGEMENTS

Pursuing this very ambitious project given my background and limited experience with medical devices would not have been possible without the constant support, technical advice, and motivation of many people. I am incredibly grateful to my family for supporting me through this endeavor. I would like to firstly thank my advisors, Dr. Florian Solzbacher and Dr. David Grainger, for encouraging me and mentoring me on this project. I would like to also thank my committee members, Dr. McGill, Dr. Hitchcock, and Dr. Magda, who mentored and advised me on the technical aspects of the project. I would like to thank all my colleagues from the Solzbacher lab and the Grainger group, especially Dr. Archana Rao, whose constant guidance and motivation enabled me to complete this Ph.D. work in such a short duration. My sincere gratitude to Dr. Ben Feldman and Brian Cho at Abbott Diabetes Care for supplying CGM sensors and for technical advice. Finally, I would like to thank the University of Utah Research foundation for supporting this work through various grants.

PREFACE

Host reaction to an implanted foreign body remains one of the foremost challenges hindering the extension of *in vivo* operational lifetimes of continuous glucose monitoring (CGM) sensors. This research focuses on locally controlling early-stage mast cell reactions inducing the host reaction around the implanted CGM sensor. Many previous elaborate and sophisticated methods to address the foreign body response (FBR) issue have exploited drugs, designs, and materials, but they have not addressed the biological source of the problem. **The central theme of our proposal is the local delivery of the tyrosine kinase inhibitor (TKI), masitinib, to inhibit mast cell c-KIT and FCεRI receptors, thereby stabilizing these potent inflammatory mediators around the implant.** This will serve to reduce the intensity of the acute inflammatory reaction, attenuating cytokine releases that attract fibroblasts to sites to prompt production of a fibrous capsule. Drug-loaded degradable polymer microspheres in temporary polymer carrier coatings on the CGM implant surface constitute the local controlled release matrix. The coating-modified CGM devices have been exploited both as an analytical tool to gauge the intensity of the FBR by measuring the change in CGM output signals *in situ* and also to report glucose changes over time as required.

Innovation resides in the use of locally delivered TKI, specifically masitinib, to control the tissue site reactivity. This drug class has not been used in this sensor application before, either to control mast cell (MC) behavior, or in combination device formulations in the context of the FBR or any implant application. Our focus on MC-centered control points in inflammation and the FBR is not novel, but the focus on

control of MC behavior locally around implants, and CGMs, is innovative. Exploiting the W-sash MC-deficient mouse compared to wild-type implant models under local drug control exploits this previous MC-FBR connection in an innovative mechanistic way toward elucidating their involvement in the FBR. Lastly, the focus on a clinically important but modest, incremental improvement for CGM performance *in vivo* (i.e., increasing sensor performance from 5-7 days to 14-21 days) is a much more realistic goal that should provide profound clinical impact if achieved, compared to 4 decades of unrealized claims to extend implant life indefinitely.

In this dissertation, Chapter 2 is a review of combination medical devices: approved clinical implants with functions that are modified by the addition of add-on drug loads. This chapter (accepted book chapter published as Avula M, Grainger DW. Addressing medical device challenges with drug/device combination. In: Siegel R, Lyu SP, editors. Drug-Device Combinations for Chronic Diseases. New York: Jon Wiley & Sons; 2013.) serves to introduce the reader to the concept of combination medical devices and the aspects of their design and pharmacology in modern clinical use. It gives a comprehensive review of FDA-approved combination devices focusing on the different host responses (inflammatory response, thrombosis, coagulation, and infection mitigation) to implantable medical devices and the drug-device combination strategies employed to overcome the host response. Drug-eluting stents, antimicrobial catheters, vascular grafts with antithrombotic coatings, and orthopedic drug-eluting implants are mainly discussed with the various pharmaceutical drugs and formulation strategies involved. This chapter further leads us to possible future strategies that are in development to provide a more personalized strategy for the next generation of combination devices.

Chapter 3 is a reprint of a published full manuscript in the leading journal, Biomaterials (M. Avula, A. Rao, L.D. McGill, D.W. Grainger, F. Solzbacher, “Modulation

of the foreign body response to implanted sensor models through device-based delivery of the tyrosine kinase inhibitor, masitinib," Biomaterials, published, 2013) and describes release of a tyrosine kinase inhibitor – masitinib – from the sensor implant to target tissue resident mast cells as key mediators of the FBR. Model implants are coated with a composite polymer hydrophilic matrix that rapidly dissolves upon tissue implantation to deposit slower-degrading polymer microparticles containing masitinib. Matrix dissolution limits coating interference with sensor function while establishing a local controlled-release delivery depot formulation to alter implant tissue pharmacology and addressing the FBR. Drug efficacy was evaluated in a murine subcutaneous pocket implant model. Drug release extends to more than 30 days *in vitro*. The resulting FBR *in vivo*, evaluated by implant capsule thickness and inflammatory cell densities at 14, 21, and 28 days, displays statistically significant reduction in capsule thickness around masitinib-releasing implant sites compared to control implant sites.

Chapter 4 (Avula M, Rao AN, McGill LD, Grainger DW, Solzbacher F. Foreign Body Response to Implanted Biomaterials in a Mast Cell-deficient $Kit^{w\text{-}Sh}$ Murine Model. Acta Biomater 2013; Submitted) is a reprint of a full manuscript submitted to *Acta Biomaterialia* and describes the modulation of foreign body response in the absence of mast cells in a mast cell-deficient sash mouse model. Mast cells are recognized for their functional role in wound healing, allergic, and inflammatory responses, host responses that are frequently detrimental to implanted biomaterials if extended beyond acute reactivity. These tissue reactions are especially impacting to the performance of sensing implants such as continuous glucose monitoring (CGM) devices. That effective blockade of mast cell activity around implants could alter the host foreign body response (FBR) and enhance the *in vivo* lifetime of these implantable devices motivated this study. Stem cell factor (SCF) and its ligand c-KIT receptor are critically important for mast cell survival, differentiation, and degranulation. Therefore, a mast cell-deficient sash mouse

model was used to assess mast cell relationships to CGM implants. Additionally, local delivery of a tyrosine kinase inhibitor (TKI) that inhibits c-KIT activity was also used to evaluate the role of mast cells in modulating the FBR. Model sensor implants comprising polyester fibers coated with a rapidly dissolving polymer coating containing drug-releasing degradable microspheres were implanted subcutaneously in sash mice for various time points, and the FBR was evaluated for chronic inflammation and fibrous capsule formation around the implants. No significant differences were observed in the foreign body capsule formation between control and drug-releasing implant groups in mast cell-deficient mice. However, fibrous encapsulation was significantly greater around the drug-releasing implants in sash mice compared to drug-releasing implants in wild-type (e.g., mast cell competent) mice. These results provide insights into the role of mast cells in the FBR, suggesting that mast cell deficiency provides alternative pathways for host inflammatory responses to implanted biomaterials.

Chapter 5 (Local release of masitinib affects implantable continuous glucose sensor performance) describes the use of mast cell-targeting tyrosine kinase inhibitor, masitinib, released from polymer microspheres delivered from the surfaces of commercial CGM needle-type implanted sensors. Targeting the mast cell c-Kit receptor and inihibting mast cell activation and degranulation, the local masitinib delivery around the CGM sought to reduce fibrosis around the sensor and extend its functional lifetime in subcutaneous sites. Drug-releasing and control CGM implants were tested in murine percutaneous implant studies for 21 days continuously. Drug-releasing implants showed reduced fibrosis around implant sites and relatively stable sensor responses over the period of the study compared to blank microsphere controls.

Chapter 6 produces some analysis of current deficiencies in the approach based on the results reported and describes follow-on experiments that would be prudent to pursue in this strategy with potentially fruitful new results.

CHAPTER 1

BACKGROUND AND INTRODUCTION

Implantable medical devices (IMDs) undergo a spontaneous host-mediated foreign body response (FBR) upon implantation as a result of local tissue disturbance or wound creation. FBR is the aberrant wound healing mechanism seeking ultimately to eliminate foreign objects from host tissue sites to restore normal wound repair and tissue remodeling. The FBR is mediated by complex spatial and temporal cellular and protein components recruited to the wound site as a part of initially normal inflammatory processes in acute wounding. However, the FBR results from abnormal chronic inflammatory processes at the wound site resulting from implant placement. Initial biochemical and physical cellular events seeking to degrade, engulf, and eliminate the foreign body become frustrated if sustained beyond the acute temporal window. This inability to physically expel the foreign body from the tissue site leads eventually in chronic phases to fibrous encapsulation of the foreign object. In the case of sensor IMDs such as the clinically important continuous glucose monitoring (CGM) sensors, FBR results in unreliable tissue glucose measurements, requiring frequent CGM replacements. This frequent tissue replacement makes CGMs expensive, inconvenient, and uncomfortable to the user. Since CGM sensors have shown significant reduction in glucose excursions in chronic diabetic patients, efforts to extend their performance and reliability in tissue sites are warranted. These can be approached through device engineering, redesign, signal processing, and local pharmacologic strategies that modify the reactivity of the local tissue site.

1.1 Diabetes and Glucose Monitoring Significance

Nearly 350 million people (5% of world population) suffer from diabetes worldwide [1], including the 25.8 million Americans (8.3% of the population) who require regular glucose monitoring. Treatment has direct and indirect costs of about $218 billion annually (2007) [2]. The rate of diabetes incidence in adults aged 18 or above in the United states has increased from 4.5% in 1990 to 8.2% in 2010 [3]. Tight regulation of blood glucose has been convincingly shown to reduce diabetes morbidity and mortality [4], leading to a standard of care that demands intensive glucose monitoring. This has traditionally used painful, invasive, and costly percutaneous sampling (i.e., finger sticks) through skin to extract blood that is measured on a hand-held calibrated monitor. Estimates are that 1.4 million diabetics (1.1 million Type 1 and nearly 0.3 million Type 2) in the US use insulin and measure blood glucose levels at least twice daily [5]. Innovations that improve the ease, convenience, access, compliance, and routine of glucose monitoring are needed. Patient avoidance of “finger sticks” is regularly attributed to diabetic noncompliance with glucose monitoring, and costly morbidities and mortalities associated with poor glucose control [6].

A miniature implantable electrical transducer to monitor glucose continuously and remotely was first developed by Updike and Hicks [6] in 1967. Many of their concepts were based on glucose oxidase electrode designs described by Clark in 1956 [7-9]. In the early 1970s, several groups reported progress with glucose electrodes, including Soeldner et al., [10], Bessman et al., [11, 12] Gough and Andrade [13], and Williams et al., [14]. The mid-1970s saw the emergence of continuous glucose monitoring (CGM) via extrapolation of blood through a double-lumen catheter, used for the development of glucose sensor-controlled insulin infusion systems by Albisser, Leibel, et al. [15, 16] and by Clemens, Pfeiffer, et al. [17, 18]. Less exotic, more routine continuous glucose monitoring systems were produced in the 1990s, with the first reports on CGM by

subcutaneous microdialysis implants in 1992 [19, 20]. Subcutaneous implanted needle-type CGM glucose sensing systems were available in 1999 [21-24].

1.2 Continuous Glucose Monitors (CGMs)

Currently, four subcutaneous CGM systems are approved and marketed with "real-time" glucose reporting every 1–5 minutes, and with alarm functions for hypo- and hyperglycemia [25, 26]. Three are needle-type subcutaneous designs: the Freestyle Navigator (Abbott Diabetes Care, Alameda, CA), the Guardian Real-Time (Medtronic MiniMed, Northridge, CA), [27-29] and the Dexcom SEVEN (Dexcom, San Diego, CA). The fourth (GlucoDay, Menarini Diagnostics) is a microdialysis-type sensor. All measure glucose in situ amperometrically via the classic Clark glucose-oxidase reaction shown below [4-6].

$$Glucose + GO_X\text{-}FAD^+ \longrightarrow Glucolactone + GO_X\text{-}FADH_2$$
$$GO_X\text{-}FADH_2 + O_2 \longrightarrow GO_X\text{-}FAD^+ + H_2O_2$$
$$H_2O_2 \longrightarrow 2H^+ + O_2 + 2e^-$$

GO_X - Glucose oxidase
FAD - Flavin adenine dinucleotide (redox cofactor of GO_X)

CGMs are now used internationally by thousands of diabetic patients for daily glucose monitoring, particularly for asymptomatic hypoglycemia or rapidly fluctuating blood sugars (so-called "brittle" patients). Given this explosion in CGM use, the current performance issues dogging CGMs are notable:

- Up to 21% CGM inaccuracy when compared with actual plasma glucose values, (expressed as mean absolute difference, i.e., [CGM glucose − plasma glucose]/plasma glucose) [30, 31]. Assay inaccuracy is even more profound in the hypoglycemic range or during rapid fluctuations in plasma glucose [32]. Lag times between physiologic glucose and instrumental delay inherent to current real-time CGMs contribute to CGM inaccuracy [33].

- Costs of CGM devices are a major downside. CGM monitoring costs about $4,930–7,120 per person-year compared with $550–2,740 for traditional self-monitoring using finger sticks [5]. CGMs have been FDA-approved only for short-term, transient implant use, often using traditional finger sticks as a required “back-up” control [34]. Part of current CGM cost issue is the FDA mandate for CGM removal and replacement every 3-7 days [34, 35].
- All four FDA-approved sensors exhibit instability over the approved implantation and sensing period (3-7 days), and their calibration is thought to be good for only 12 hours [25]. Also, many of the electrochemical sensors exhibit a “run-in period” in which the sensitivity drops by 10-30% immediately after implantation [25, 36, 37], followed by a period of stability that lasts 1 to 7 days before removal and costly replacement.

1.3 CGM Performance Issues and Current Combination Device Strategies

Clinical realization of improved implantable glucose sensors with extended lifetimes *in vivo* (>1 week) remains elusive primarily due to the host’s acute and chronic foreign body response (FBR) to the implanted sensor [38, 39]. CGM sensor biofouling, including protein adsorption on or infiltrated into the implanted sensors, as well as inflammatory wound-site reactions that limit analyte diffusion into the CGM contribute to the observed decrease in sensitivity upon acute implantation [37, 39, 40]. In addition to ubiquitous sensor fouling, the host inflammatory response to the implanted foreign body produces a sustained cascade of cellular reactions that alter the local environment around the implant, modify local metabolism and homeostasis, and trigger a departure from normal wound healing. Leukocyte and mast cell invasion proceeds to fibroblast recruitment and proliferation. Release of inflammatory cytokines like IL-4 and IL-13

accelerate the recruitment of inflammatory and immune cells to the site of implant [41]. This further results in an intense expression of collagens around the implant within days of implantation. This excess connective tissue is rapidly remodeled into a dense fibrous capsule (fibrosis) that “walls off” the implant, separating the sensor from its physiological surroundings after 7-10 days of subcutaneous implantation. This foreign body capsule is the hallmark of the FBR, and a primary barrier to sustained CGM function. Despite intensive research over two decades, CGM glucose sensing performance under sustained chronic implantation (>14 days) remains a major challenge.

As a result of sustained, persistent host tissue assault, continuous glucose monitoring exhibits substantial clinical performance issues, limiting patient utility and FDA approvals for long-term implant use. The host foreign body response (FBR) to implanted devices is often the limiting issue to implant longevity and performance [41]. Nonetheless, as a real-time *in vivo* data-reporting implant, the CGM provides a unique reporting tool in research to monitor and report real-time *in vivo* responses to both the implant’s acute phase host reaction as well as chronic host-implant integration reactions. That is, the implanted CGM provides both a relevant clinical metric, i.e., glucose determinations, and also an analytical metric, i.e., sensor signal fluctuations and attenuation corresponding to acute host inflammatory and more chronic foreign body response. This provides unique implant site information on the host response to the device and local physiology. Such an approach has been exploited by Reichert [37] and Klueh [42, 43] in producing new information on host tissue responses to CGMs in order to supply new rational design criteria for CGM improvements.

The focus on reducing sensor surface fouling *in vivo* has predominantly been accomplished by applying specific coatings to sensor surfaces to inhibit protein adhesion. Hydrogels, polymers, flow-based systems, surfactants, naturally derived materials, and others have been used with only limited effectiveness *in vivo* [39,

44]. Modifying the CGM into a combination device that releases drug locally from the implant seeks to overcome these limitations [45-48]. Surface coatings containing nitric oxide [49-51], dexamethasone [45, 52, 53], and vascular endothelial growth factor (VEGF) [54, 55] attempt to limit biofouling while exploiting a local pharmacological strategy for modulating the intensity of the acute phase inflammatory reaction. Each locally released drug has formulation, loading and stability issues, different potencies, and different targets: dexamethasone seeks to inhibit fibroblast production of collagen around the sensor, while VEGF prompts local angiogenesis to make the FBR fibrotic capsule around the sensor effectively permeable, sufficiently perfused for glucose transport. Significantly, these drug-release approaches have addressed cell targets and behaviors well downstream, and temporally and spatially distinct from the early acute-phase FBR mast cell and leukocyte initiators around the implant.

1.4 Role of Mast Cells in the Foreign Body Reaction to CGMs

Mast cells (MC) play an important critical role in mediating acute phases of the tissue inflammatory response following sensor implantation: they are located perivascularly throughout all tissues and are mobilized during any inflammatory response [56]. MC degranulation of histamine and other pro-inflammatory mediators including heparin, cytokines (TNF-alpha), chemokines, and many proteases together with fibrinogen adsorption are recognized as powerful inducers of acute inflammatory responses to implanted biomaterials [57, 58]. MC-released cytokines and chemotaxis along with histamine and serotonin result in vasodilation and increased recruitment of phagocytes to the implant site. Their connection with the foreign body reaction is recognized [47, 48, 59]. **Figure 1.1** illustrates mast cell degranulation in the presence of an allergen or foreign antigen.

Specific to CGMs, Klueh et al. [42] have recently compared *in vivo* CGM sensor implant performance in both wild-type and MC-deficient mice. Significantly, they confirmed based on CGM signal-to-noise ratio (S/N) and analyte response time as a function of implant time that MCs play a major role in the host FBR around CGMs. Importantly, this was linked to subsequent fibrous capsule formation around the CGM that impedes sensor function [42].

The operative mechanism behind apparent MC regulation of the host FBR has been elusive. One new clue is that stem cell factor (SCF), the ligand of the MC-specific c-KIT tyrosine kinase receptor, is an important growth factor for MC survival, proliferation, differentiation, and degranulation processes [60]. The link between the MC-specific SCF/MC c-KIT pathway and the intensity of acute phase of the inflammatory response is critical in MC function and degranulation reactions [60]. *Central to the research in this dissertation, recent work shows that masitinib, a newly screened tyrosine kinase inhibitor (TKI), is effective in inhibiting the SCF receptor c-KIT on mast cells and is a potent inducer controlling MC reactivity [61, 62] by binding competitively to the ATP binding c-KIT receptor, and blocks its critical tyrosine kinase signaling activity*. ***Importantly, this drug action stabilizes mast cells from degranulating or activating***.

A recent study [61] concludes that masitinib is a potent TKI that stabilizes mast cell reactivity both *in vitro* and *in vivo* when compared to imatinib mesylate - another widely used TKI to inhibit c-KIT [63]. As an indicator of common TKI bioactivity pathways, masitinib mesylate has already been shown to reduce production of extracellular matrix and prevent the development of experimental nonimplant fibrosis [64]. Nonetheless, masitinib is selective in inhibiting recombinant human c-KIT receptor (IC_{50} 200 ± 40nM), and platelet-derived growth factor receptor (PDGFR) while weakly inhibiting other type III tyrosine kinase receptors, including fibroblast growth factor

receptor 3 (FGFR3) and FCεRI receptor. Imatinib inhibits a broader range of receptors [61]. These receptors when bound to ligands like IgE, SCF, C3a, PAMPs etc., result in mast cell activity and degranulation [65], leading to increased inflammatory cell activity. Masitinib is currently in clinical trials as an oral therapeutic for Alzheimer's disease [66], pancreatic cancer [67], canine mastocytosis [62], gastro-intestinal stromal tumors [68], and rheumatoid arthritis [69].

Masitinib has been found to be effective against mast cell activity and has been found to have very less toxicity in mouse models [61] as it has high specificity for its target receptor, c-Kit. The structure of masitinib is shown in **Figure 1.2**.

Our hypothesis is that stabilizing and avoiding degranulation of mast cells around the site of implantation could delay the cascade of events in the foreign body response to the host, thereby increasing the useful lifetime of the implants. To validate our hypothesis technically, a glucose sensor capable of continuous glucose monitoring (CGM) is coated with a composite polymer matrix comprising soluble PEG loaded with degradable PLGA/PLA microporous microspheres containing masitinib. This strategy produces a combination device for subcutaneous use, seeking to alter the local wound bed pharmacology by local drug release over extended time periods. The strategy intends to reduce mast cell reactivity, degranulation, and inflammatory responses leading to the FBR. Both model sensor implants (model polymer fibers of the same dimensions as the CGM implant) and functional human CGM devices are coated with this matrix and implanted in a murine subcutaneous implant model and the effect of masitinib and mast cell stabilization on FBR and the resulting CGM response are evaluated.

Model sensor implants were tested in C57BL/6 mice and their mast cell-deficient mutant knockout strain (B6.Cg-*KitW-sh*/HNihrJaeBsmGlliJ). These models were used

before to compare the effects of mast cells on CGM sensor and hence were chosen for this study [42].

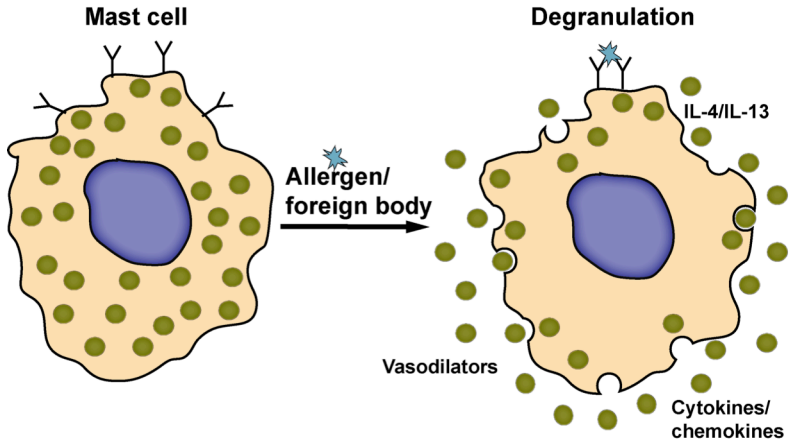

Figure 1.1: Mast cell degranulation in the presence of a foreign object or allergen

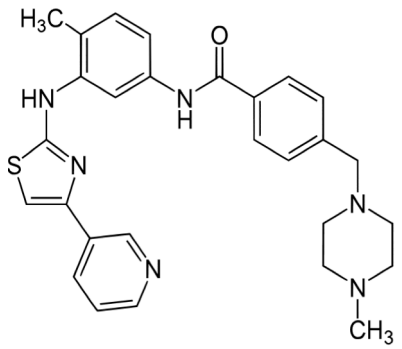

Figure 1.2: Structure of masitinib (AB1010)

1.5 References

[1] Danaei G, Finucane MM, Lu Y, Singh GM, Cowan MJ, Paciorek CJ, et al. National, regional, and global trends in fasting plasma glucose and diabetes prevalence since 1980: systematic analysis of health examination surveys and epidemiological studies with 370 country-years and 2.7 million participants. The Lancet. 2011;378:31-40.

[2] Centers for Disease Control and Prevention. National diabetes fact sheet: national estimates and general information on diabetes and prediabetes in the United States. In: Services DoHaH, editor. Atlanta, GA: U.S.: Centers for Disease Control and Prevention; 2011.

[3] CDC. Increasing Prevalence of Diagnosed Diabetes — United States and Puerto Rico, 1995–2010. Morb Mortal Wkly Rep: CDC; 2012.

[4] Coster S, Gulliford MC, Seed PT, Powrie JK, Swaminathan R. Monitoring blood glucose control in diabetes mellitus: a systematic review. Health Technol Assess. 2000;4:i-iv, 1-93.

[5] Pham M. Medtronic diabetes: sizing the market for realtime, continuous blood glucose monitors from MDT, DXCM, and ABT. HSBC Global Research; 2006.

[6] Updike SJ, Hicks GP. The enzyme electrode. Nature. 1967;214:986-8.

[7] Clark Jr. LC. Monitor and Control of Blood and Tissue Oxygen Tensions. ASAIO J. 1956;2:41-8.

[8] Clark Jr. LC. Membrane Polarographic Electrode System and Method With Electrochemical Compensation. United States: Leland Jr., Clark C.; 1970.

[9] Clark Jr. LC. How the first enzyme electrode was invented. Biosens Bioelectron. 1993;8.

[10] Chang KW, Aisenberg S, Soeldher JS, Hiebert JM. Validation and Bioengineering Aspects of An Implantable Glucose Sensor. ASAIO J. 1973;19:352-60.

[11] Bessman SP, Schultz RD. Progress toward a glucose sensor for the artificial pancreas. Adv Exp Med Biol. 1974;50:189-96.

[12] Layne EC, Schultz RD, Thomas LJ, Slama G, Sayler DF, Bessman SP. Continuous extracorporeal monitoring of animal blood using the glucose electrode. Diabetes. 1976;25:81-9.

[13] Gough DA, Andrade JD. Enzyme Electrodes. Science. 1973;180:380-4.

[14] Williams DL, Doig AR, Korosi A. Electrochemical-enzymatic analysis of blood glucose and lactate. Anal Chem. 1970;42:118-21.

[15] Albisser AM, Leibel BS, Ewart TG, Davidovac Z, Botz CK, Zingg W. An artificial endocrine pancreas. Diabetes. 1974;23:389-96.

[16] Albisser AM, Leibel BS, Ewart TG, Davidovac Z, Botz CK, Zingg W, et al. Clinical control of diabetes by the artificial pancreas. Diabetes. 1974;23:397-404.

[17] Pfeiffer EF, Thum C, Clemens AH. The artificial beta cell--a continuous control of blood sugar by external regulation of insulin infusion (glucose controlled insulin infusion system). Horm Metab Res. 1974;6:339-42.

[18] Fogt EJ, Dodd LM, Jenning EM, Clemens AH. Development and evaluation of a glucose analyzer for a glucose controlled insulin infusion system ((Biostator). Clin Chem. 1978;24:1366-72.

[19] Bolinder J, Ungerstedt U, Arner P. Microdialysis measurement of the absolute glucose concentration in subcutaneous adipose tissue allowing glucose monitoring in diabetic patients. Diabetologia. 1992;35:1177-80.

[20] Bolinder J, Ungerstedt U, Arner P. Long-term continuous glucose monitoring with microdialysis in ambulatory insulin-dependent diabetic patients. Lancet. 1993;342:1080-5.

[21] Bode BW, Gross TM, Thornton KR, Mastrototaro JJ. Continuous glucose monitoring used to adjust diabetes therapy improves glycosylated hemoglobin: a pilot study. Diabetes Res Clin Pract. 1999;46:183-90.

[22] Chase HP, Kim LM, Owen SL, MacKenzie TA, Klingensmith GJ, Murtfeldt R, et al. Continuous subcutaneous glucose monitoring in children with type 1 diabetes. Pediatrics. 2001;107:222-6.

[23] Ludvigsson J, Hanas R. Continuous subcutaneous glucose monitoring improved metabolic control in pediatric patients with type 1 diabetes: a controlled crossover study. Pediatrics. 2003;111:933-8.

[24] Tanenberg R, Bode B, Lane W, Levetan C, Mestman J, Harmel AP, et al. Use of the Continuous Glucose Monitoring System to guide therapy in patients with insulin-treated diabetes: a randomized controlled trial. Mayo Clinic proceedings Mayo Clinic. 2004;79:1521-6.

[25] Wilson GSZ, Y. Introduction to the Glucose Sensing Problem. In Vivo Glucose Sensing. Hoboken, NJ: John Wiley; 2010.

[26] Liao KC, Hogen-Esch T, Richmond FJ, Marcu L, Clifton W, Loeb GE. Percutaneous fiber-optic sensor for chronic glucose monitoring in vivo. Biosens Bioelectron. 2008;23:1458-65.

[27] Jungheim K, Wientjes K, Heinemann L, Lodwig V, Koschinsky T, Schoonen A. Subcutaneous continuous glucose monitoring. Diabetes Care. 2001;24:1696.

[28] Koschwanez H, Reichert W. In vitro, in vivo and post explantation testing of glucose-detecting biosensors: Current methods and recommendations. Biomaterials. 2007;28:3687-703.

[29] Wilson G, Hu Y. Enzyme-based biosensors for in vivo measurements. Chem Rev. 2000;100:2693-704.

[30] Hirsch IB. Realistic Expectations and Practical Use of Continuous Glucose Monitoring for the Endocrinologist. J Clin Endocrinol Metab. 2009;94:2232-8.

[31] Kovatchev B, Anderson S, Heinemann L, Clarke W. Comparison of the numerical and clinical accuracy of four continuous glucose monitors. Diabetes Care. 2008;31:1160-4.

[32] Wentholt IM, Hoekstra JB, Devries JH. Continuous glucose monitors: the long-awaited watch dogs? Diabetes Technol Ther. 2007;9:399-409.

[33] Wentholt IM, Hart AA, Hoekstra JB, Devries JH. Relationship between interstitial and blood glucose in type 1 diabetes patients: delay and the push-pull phenomenon revisited. Diabetes Technol Ther. 2007;9:169-75.

[34] Burge MR, Mitchell S, Sawyer A, Schade DS. Continuous glucose monitoring: the future of diabetes management. Diabetes Spectrum. 2008;21:112.

[35] Kondepati VR, Heise HM. Recent progress in analytical instrumentation for glycemic control in diabetic and critically ill patients. Anal Bioanal Chem. 2007;388:545-63.

[36] Gifford R, Kehoe J, Barnes S, Kornilayev B, Alterman M, Wilson G. Protein interactions with subcutaneously implanted biosensors. Biomaterials. 2006;27:2587-98.

[37] Wisniewski N, Moussy F, Reichert W. Characterization of implantable biosensor membrane biofouling. Fresenius' J Anal Chem. 2000;366:611-21.

[38] Frost MC, Meyerhoff ME. Implantable chemical sensors for real-time clinical monitoring: progress and challenges. Curr Opin Chem Biol. 2002;6:633-41.

[39] Wilson GS, Gifford R. Biosensors for real-time in vivo measurements. Biosens Bioelectron. 2005;20:2388-403.

[40] Gerritsen M, Jansen JA, Lutterman JA. Performance of subcutaneously implanted glucose sensors for continuous monitoring. Neth J Med. 1999;54:167-79.

[41] Anderson JM, Rodriguez A, Chang DT. Foreign body reaction to biomaterials. Semin Immunol. 2008;20:86-100.

[42] Klueh U, Kaur M, Qiao Y, Kreutzer DL. Critical role of tissue mast cells in controlling long-term glucose sensor function in vivo. Biomaterials. 2010;31:4540-51.

[43] Klueh U, Dorsky DI, Kreutzer DL. Enhancement of implantable glucose sensor function in vivo using gene transfer-induced neovascularization. Biomaterials. 2005;26:1155-63.

[44] Wisniewski N, Reichert M. Methods for reducing biosensor membrane biofouling. Colloids Surf B Biointerfaces. 2000;18:197-219.

[45] Hickey T, Kreutzer D, Burgess D, Moussy F. Dexamethasone/PLGA microspheres for continuous delivery of an anti-inflammatory drug for implantable medical devices. Biomaterials. 2002;23:1649-56.

[46] Hickey T, Kreutzer D, Burgess D, Moussy F. In vivo evaluation of a dexamethasone/PLGA microsphere system designed to suppress the inflammatory tissue response to implantable medical devices. J Biomed Mater Res. 2002;61:180-7.

[47] Ward WK, Wood MD, Casey HM, Quinn MJ, Federiuk IF. The effect of local subcutaneous delivery of vascular endothelial growth factor on the function of a chronically implanted amperometric glucose sensor. Diabetes Technol Ther. 2004;6:137-45.

[48] Ward WK, Troupe JE. Assessment of chronically implanted subcutaneous glucose sensors in dogs: The effect of surrounding fluid masses. ASAIO J. 1999;45:555-61.

[49] Nichols SP, Le NN, Klitzman B, Schoenfisch MH. Increased In Vivo Glucose Recovery via Nitric Oxide Release. Anal Chem. 2011;83:1180-4.

[50] Nablo BJ, Prichard HL, Butler RD, Klitzman B, Schoenfisch MH. Inhibition of implant-associated infections via nitric oxide release. Biomaterials. 2005;26:6984-90.

[51] Hetrick EM, Prichard HL, Klitzman B, Schoenfisch MH. Reduced foreign body response at nitric oxide-releasing subcutaneous implants. Biomaterials. 2007;28:4571-80.

[52] Bhardwaj U, Sura R, Papadimitrakopoulos F, Burgess DJ. Controlling acute inflammation with fast releasing dexamethasone-PLGA microsphere/pva hydrogel composites for implantable devices. J Diabetes Sci Technol. 2007;1:8-17.

[53] Ju YM, Yu B, West L, Moussy Y, Moussy F. A dexamethasone-loaded PLGA microspheres/collagen scaffold composite for implantable glucose sensors. J Biomed Mater Res A. 2010;93:200-10.

[54] Golub JS, Kim Y-t, Duvall CL, Bellamkonda RV, Gupta D, Lin AS, et al. Sustained VEGF delivery via PLGA nanoparticles promotes vascular growth. Am J Physiol Heart Circ Physiol. 2010;298:H1959-H65.

[55] Sung J, Barone PW, Kong H, Strano MS. Sequential delivery of dexamethasone and VEGF to control local tissue response for carbon nanotube fluorescence based micro-capillary implantable sensors. Biomaterials. 2009;30:622-31.

[56] Krishnaswamy G, Ajitawi O, Chi DS. The human mast cell: an overview. Methods in molecular biology (Clifton, NJ). 2006;315:13-34.

[57] Zdolsek J, Eaton J, Tang L. Histamine release and fibrinogen adsorption mediate acute inflammatory responses to biomaterial implants in humans. J Transl Med. 2007;5:31.

[58] Tang L, Jennings TA, Eaton JW. Mast cells mediate acute inflammatory responses to implanted biomaterials. Proc Natl Acad Sci U S A. 1998;95:8841-6.

[59] Thevenot PT, Baker DW, Weng H, Sun M-W, Tang L. The pivotal role of fibrocytes and mast cells in mediating fibrotic reactions to biomaterials. Biomaterials. 2011;32:8394-403.

[60] Reber L, Da Silva CA, Frossard N. Stem cell factor and its receptor c-Kit as targets for inflammatory diseases. Eur J Pharmacol. 2006;533:327-40.

[61] Dubreuil P, Letard S, Ciufolini M, Gros L, Humbert M, Casteran N, et al. Masitinib (AB1010), a potent and selective tyrosine kinase inhibitor targeting KIT. PLoS ONE. 2009;4:e7258.

[62] Paul C, Sans B, Suarez F, Casassus P, Barete S, Lanternier F, et al. Masitinib for the treatment of systemic and cutaneous mastocytosis with handicap: a phase 2a study. Am J Hematol. 2010;85:921-5.

[63] Savage DG, Antman KH. Imatinib Mesylate — A New Oral Targeted Therapy. N Engl J Med. 2002;346:683-93.

[64] Distler JH, Jungel A, Huber LC, Schulze-Horsel U, Zwerina J, Gay RE, et al. Imatinib mesylate reduces production of extracellular matrix and prevents development of experimental dermal fibrosis. Arthritis Rheum. 2007;56:311-22.

[65] Gilfillan AM, Tkaczyk C. Integrated signalling pathways for mast-cell activation. Nat Rev Immunol. 2006;6:218-30.

[66] Piette F, Belmin J, Vincent H, Schmidt N, Pariel S, Verny M, et al. Masitinib as an adjunct therapy for mild-to-moderate Alzheimer's disease: a randomised, placebo-controlled phase 2 trial. Alzheimers Res Ther. 2011;3:16.

[67] Mitry E, Hammel P, Deplanque G, Mornex F, Levy P, Seitz JF, et al. Safety and activity of masitinib in combination with gemcitabine in patients with advanced pancreatic cancer. Cancer Chemother Pharmacol. 2010;66:395-403.

[68] Le Cesne A, Blay JY, Bui BN, Bouche O, Adenis A, Domont J, et al. Phase II study of oral masitinib mesilate in imatinib-naive patients with locally advanced or metastatic gastro-intestinal stromal tumour (GIST). Eur J Cancer. 2010;46:1344-51.

[69] Tebib J, Mariette X, Bourgeois P, Flipo RM, Gaudin P, Le Loet X, et al. Masitinib in the treatment of active rheumatoid arthritis: results of a multicentre, open-label, dose-ranging, phase 2a study. Arthritis Res Ther. 2009;11:R95.

CHAPTER 2

ADDRESSING MEDICAL DEVICE CHALLENGES WITH DRUG/DEVICE COMBINATIONS

Mahender N. Avula[1] and David W. Grainger[1,2*]

[1]Department of Bioengineering, University of Utah, Salt Lake City, UT 84112 USA

[2]Department of Pharmaceutics and Pharmaceutical Chemistry, University of Utah, Salt Lake City, UT 84112-5820 USA

**to whom correspondence should be addressed:* David W. Grainger, david.grainger@utah.edu

Keywords: medical device, drug delivery, blood coagulation, foreign body response, infection, fibrosis, implant complications, local therapy

Reprinted with permission from: Drug-Device Combinations for Chronic Diseases. New York: Jon Wiley & Sons; 2013.

2.1 Introduction

Implanted medical devices (IMDs) comprising synthetic biomaterials have seen exponential growth in their applications and clinical use over the past five decades [1]. The scope and fields of use for IMDs have increased multiple-fold with the advent of new technologies, innovation and improved understanding of human physiology and its underlying problems. Increasing rates of medical device adoption can be attributed to various factors, including aging median populations worldwide,[2] innovations in design and function that increase performance and reliability, rising standards of living among patients in developing nations and noted improvements in patient quality of life offered by the devices. New IMDs continue to offer improved treatment alternatives for cardiovascular, orthopedic, oncologic, and many other diseases [3]. Given these factors, the global medical device market is expected to continue growing, reaching approximately US $302 billion in 2017 with an annual growth rate of ~6% over the next six years (2011-2017) [4]. Tens of millions of people in the United States alone have some kind of IMD in their body. Despite enhanced safety and efficacy, new device design strategies are required to understand and address complex human factors affecting device performance *in vivo*. Innovations in design, biomaterials, surface modifications and biocompatible coatings, and device-based on-board drug delivery mechanisms are among strategies employed to improve clinical IMD performance.

Drug-device combination medical products are innovative biomedical implants with enhancements to device function provided by the on-board formulation and local pharmacology of selected drugs at the implant site [5]. Combination devices couple a drug loading and releasing mechanism onto an approved prosthetic implant. Together, these seek to provide several improvements to the *in vivo* performance and lifetime of implantable medical devices in various classes and capacities, including cardiovascular, ophthalmic, orthopedic, diabetes and cancer applications. Drug-device combination

products represent relatively new device class among implantable medical devices, one that is drawing increasing attention from both the pharmaceutical and device manufacturing industries as well as clinicians to address several long-standing problems associated with IMDs. In 2003, the Food and Drug Administration (FDA) approved a coronary drug-eluting stent (Cordis CYPHER™, Johnson and Johnson, USA) opening the market to similar officially designated "drug-device combination products" in the United States [6]. Several notable medical devices with locally delivered drugs had earlier precedent, namely steroid-releasing pacemaker leads, hormone-releasing intrauterine devices, antibiotic-impregnated catheters, aerosolized drug inhalers, drug-infused condoms, and several other precedents. Additionally, several combination products also existed earlier in Europe than elsewhere, e.g., antibiotic-releasing bone cements, drug-eluting stents, heparin-coated catheters, and others (approved with the CE mark). FDA's Office of Combination Products (OCP) was established in 2002 to provide a pathway for assigning principal FDA oversite and review policies for drug/biologic/device combinations that could otherwise be confused or compromised by traditional FDA review file assignments [7]. The objective was to provide a streamlined and consistent process for assigning these new products to FDA Centers based on claimed primary modes of action (i.e., device or drug). The OCP defines a "combination device" under 21 CFR 3.2(e) as "*A product comprised of two or more regulated components, i.e., drug/device, biologic/device, drug/biologic, or drug/device/biologic, that are physically, chemically, or otherwise combined or mixed and produced as a single entity; or two or more separate products packaged together in a single package or as a unit and comprised of drug and device products, device and biological products, or biological and drug products*". Table 2.1 summarizes this classification system. Most combination devices add a drug bioactivity adjunct to an already-approved implanted device to counteract challenges faced by the device in the context of the local host tissue

environment. This can include inflammation, fibrosis, coagulation, and infection, improving performance in several conditions. One prominent example is the use of the drug-eluting stent, where local release of micrograms of drug to the vascular bed has reduced the need for surgical intervention by 40-70% over bare metal stents [8-10]. However, combination products are often optimized into an integrated system from separate drug and device products: they were never designed de novo to complement each other in structure and function, i.e., controlled drug delivery often is an add-on feature to an existing FDA-approved medical device design that is sub-optimally adapted to the structural, mechanical or electronic function of the device [6]. New strategies and new technologies that combine drugs, devices and biologics de novo as coordinated, unified new designs are expected to provide a new generation of combination products, more intelligently incorporating and merging new technologies, changes and refinements of both existing drug delivery mechanisms and medical device functions, shifts from traditional devices and drugs, while remaining compliant with regulations [6].

Diverse classes of drugs are used in combination devices to enhance medical device and implant performance. Anti-inflammatory, antifibrotic, antiproliferative, antithrombotic and antibiotic drugs are primary classes of pharmaceutical agents often combined with a controlled delivery mechanism suited to the application. Site-specific and implant-specific drug interventions before, during and after medical device implantation can be used to alleviate several adverse host responses, providing a local therapeutic strategy when device design or systemic drug delivery alone are insufficient. For example, anticoagulants are applied to cardiovascular and intravascular implants to reduce device-based thrombosis, while antifibrotic, anti-inflammatory and antiproliferative drugs are used for soft tissue implants and endovascular stents susceptible to fibrous tissue in-growth and smooth muscle proliferation. Antibiotics are

released from orthopedic implants, shunts and percutaneous and urinary catheters that exhibit high infection incidence.

Conventional therapeutics are administered in different ways, including nasal, oral, parenteral (intravascular, intramuscular, subcutaneous and intra-peritoneal), topical, transdermal and other administrative routes [11]. While systemic administration has its merits, local drug administration can in some cases provide comparable results with significantly lower doses of drugs while limiting the drug efficacy and toxicity to the tissue surrounding the implant site. Drugs are combined with delivery technologies to control rates and local dosing of therapeutics to tissue beds surrounding implanted devices. Typically, drugs are released systematically from the device surface using impregnated resins, or rate-controlling polymer films. Occasionally, drugs are eluted from the bulk device as in the case of antibiotic-loaded bone cement. Local drug release limits drug dosing to low quantities, reduces systemic toxicity, increases durations of release and limits the area of release to the tissue bed surrounding the implant [6]. Local drug release mechanisms offer several advantages over conventional systemic drug administration. An ideal drug delivery system with a combination device should provide continuous and effective drug doses to the site of implantation while also offering possibilities to continue drug release for prolonged periods [12]. Rates and durations of drug delivery depend on several factors such as the implant size, local tissue physiology and morbidity, drug pharmacology and potency in therapy, duration and location of drug release, its kinetics, drug and local clearance and toxicity.

Due to the widespread development and use of combination products, a comprehensive understanding of drug delivery mechanisms and device functional improvements in the drug's presence is necessary to improve their efficacy and scope of medical applications. Mechanisms involved in drug delivery should be exploited to better match release to the local needs of each specific combination product. The major

challenges faced by IMDs in clinical applications are shown in Figure 2.1: 1) nonspecific host response/foreign body reaction; 2) device thrombosis, and 3) biomaterial-associated infections. These all share some interrelated failure mechanisms that may amplify tissue-site adverse reactions and host responses. For example, the link between thrombosis and infection is increasingly identified to be synergistic, as is the relationship between the host foreign body response and implant-centered infection. These increasingly complex host response relationships can be difficult to solve using a single device design, or biomaterials-based approach alone. Use of local pharmaceutics with the device provides options to exploit device strengths and also drug targeting against multiple challenges in the implant site. The remainder of this chapter serves to describe combination device approaches in the context of the current medical device and implant challenges in host tissue sites.

2.2 The Host Foreign Body Reaction

The host's acute and chronic foreign body response (FBR) remains an unsolved challenge for many IMDs. As the implantation of almost every medical device creates a wound (e.g., knee arthroplasty, pacemaker), or local disturbance of a tissue bed (e.g., contact lens), a normal host tissue wounding response is spontaneously initiated. This reaction is primarily an abnormal tissue healing response that alters normal wound site healing in the presence of a foreign body (IMD), yielding a chronic unresolved tissue response, often resulting in excessive fibrosis. Extending the functional clinical lifetime of IMDs while reducing their adverse events *in vivo* remains an important goal. Nonetheless, despite many device improvements and design changes, this goal remains elusive. For example the host's acute and chronic FBR are well-known to limit the lifetime of implanted sensors (i.e., glucose real-time monitoring devices) [13-15]. Lack of tissue mechanisms preclude rational implant improvements and other more direct

therapeutic approaches. IMDs spontaneously adsorb a diverse array of plasma proteins within the first few seconds of implantation [16]. Neither the types and amounts nor orientations of these proteins on the implant can be controlled *in vivo*, but despite many assertions otherwise, this might not have much significance to the final tissue reaction. Surface properties of the implanted biomaterial certainly govern aspects of protein adsorption, but exactly how this then modulates the host reaction to the implant is less certain. Many biomaterials of distinctly different bulk chemical and surface composition result in very similar endpoints *in vivo* in soft tissue, encased by fibrous overgrowth and an avascular capsule. The IMD as a foreign body destabilizes homeostasis and hemostasis in host tissue and results in a modified "healing response" that adversely affects both the implant's performance and host tissue surrounding it.

The FBR is a consequence of aborted wound healing and the complex interplay between the complement and coagulation cascades with the host immune system. The complement system comprises cascades of blood and cell surface proteins triggered by pathogens and other "foreign" substances, including implanted biomaterials [17]. Blood's potent intrinsic and extrinsic protease cascades are triggered by procoagulant stimulus [18]. In both systems, procoagulant and complement proteins are zymogen proteases activated by the foreign body interacting with the precursor zymogens through proteolytic cleavage [19], and each acting to amplify host cell-signaling and cell-recruiting capacity. FBR results from continuous host exposure to combinations of specific (activating) and nonspecific (activating) proteins on the foreign body and their protease activation. Subsequent chemotaxis and reactions from host immune and inflammatory cells lead to unresolved chronic healing responses, sustained inflammation, recruitment of fibroblasts and fibrotic encapsulation, and foreign body giant cell presence as a terminal response to the implanted device. In this dynamic wound site response, normal wound site acute cell infiltrates comprising neutrophils and other leukocytes, and later monocyte and

macrophage invasion, stimulate release of inflammatory cytokines like IL-6, TNF-alpha, IL-4 and IL-13 (i.e., from mast cells) to accelerate recruitment of inflammatory and immune cells to the site of implant [15]. In normal wounds these abate, but a foreign body provides continuous inflammatory stimulus for sustained, abnormal cell signaling. Fibroblasts then arrive at the implant site and mediate the formation of an avascular fibrous tissue via exuberant collagen production around the implant that can act as a physical barrier blocking access to essential components of the tissue surrounding the implants, an area of local hypoxia and poor perfusion to create an infection niche, and also a physical impediment of prosthetic motion if required (i.e., joint arthroplasty) or adjacent tissue-on-tissue motion (e.g., surgical adhesions) that are highly painful. Chronically, the excess connective tissue remodels into a dense fibrous capsule (fibrosis) that "walls off" the implant, separating the IMD from its physiological surroundings. This foreign body capsule is the hallmark of the FBR, and adversely affects the general performance of IMDs, limiting their reliability and long-term success. Reactions of both the host on the implant and the implant on the host/blood/tissue need to be understood to enhance IMD performance. Figure 2.2 illustrates the sequence of host-materials events following the implantation of a biomaterial/ medical device into host tissue.

While some implants remain unaffected functionally by the FBR, certain types of IMDs are highly compromised. In particular, sensor implants like continuous glucose monitoring (CGM) sensors [20-22], pacemaker electrical leads [23], and neural deep brain stimulation arrays [24] undergo fibrosis that hinders function. The avascular fibrous tissue surrounding the implant impedes the implant's electrical [25] and chemical contact with the surrounding tissue while also depriving it of essential analytes [26-28] and nutrients, rendering implants less efficient. Pacemaker leads underwent early drug modification, with steroid reservoirs and elution from their porous electrode tips enhancing their

impedance and conductance properties with tissue and their functioning lifetime, enhancing battery life and reducing fibrous tissue encapsulation [29,30]. Many CGM sensors are placed subcutaneously where normal sensor fouling, including protein adsorption on or infiltrated into the implanted sensors, as well as inflammatory wound-site cellular reactions eventually limit analyte diffusion (mostly glucose and oxygen) into the sensing element, and contribute to the observed continual decreased analyte sensitivity with prolonged implantation [14,21,31]. In addition to ubiquitous sensor fouling and encapsulation, the host's acute inflammatory response to the implanted foreign body produces an immediate, sustained cascade of local tissue cellular reactions that alter the local environment around the implant, substantially modifying local metabolism and homeostasis. This triggers a departure from normal tissue analyte levels and causes the sensors to produce highly altered analyte levels from acute inflammation -- an acute reporting phenomenon called "break-in" [32].

As the host foreign body response in soft and hard tissue sites typically produces device-based challenges associated with excess or unresolved inflammation, fibrosis, and infection, combination device strategies seeking to address this issue have used drugs with known pharmacological actions against these specific problems.

2.2.1 Anti-inflammatory drug candidates to inhibit the foreign body response

Anti-inflammatory steroidal drugs (e.g., dexamethasone) are clinically familiar and used to reduce inflammation and the host FBR in tissues surrounding implant sites [33,34]. Dexamethasone, a glucocorticoid agonist, crosses cell membranes and binds to glucocorticoid receptors controlling different inflammatory pathways with high affinity by inhibiting leukocyte infiltration at sites of inflammation, suppressing humoral immune responses, and reducing edema and scar tissue. Molecular basis for dexamethasone's

anti-inflammatory actions are thought to involve the inhibition of cyclo-oxygenase enzyme [35] that regulates arachidonic acid metabolism responsible for production of inflammatory prostaglandins.

Local controlled-release systems containing the steroid, dexamethasone, have been used in intraocular application post-surgery in cataract treatments [36-40]. Local dexamethasone release [41] has also been used to reduce neointimal formation in the arterial wall after balloon angioplasty [42,43], and to prevent restenosis in intravascular drug-eluting stents [44]. Dexamethasone has also been used for improve the performance of pacemaker leads [45]. Dexamethasone release from PLGA microspheres coated onto a cotton suture implant has shown to decrease the acute inflammatory reaction around the implanted suture material [46]. Dexamethasone has been used in combination with angiogenesis factors like vascular endothelial growth factor (VEGF) to promote new blood vessel growth while reducing inflammation in the tissue surrounding a hydrogel (PVA) scaffold implant [47]. Sequential or simultaneous release of dexamethasone and VEGF has been shown to improve the performance of implanted biosensors [47-51].

2.2.2 Antiproliferative drug candidates to inhibit the foreign body response

Sirolimus, also called rapamycin, is a potent immune-suppressive drug used in combination with medical devices. As a potent inhibitor of cytokine and growth factor-mediated cell proliferation. sirolimus acts by inhibiting activation of the intracellular protein enzyme, mTOR (mammalian target of rapamycin) [52], a downstream mediator of the PI3K/Akt phosphorylation signaling pathway regulating several key cell functions. Receptor-based inhibition of mTOR results in the blockage of cell-cycle proliferation in the late G1 to S phase, causing antiproliferative and antihyperplastic actions [53,54]. Over 70 related “limus” derivatives are known drug candidates. Everolimus, temsirolimus,

deforolimus, tacrolimus, and ABT-578 are also used as potent antiproliferative drugs. Paclitaxel is another commonly used antiproliferative drug used with medical devices such as drug-eluting stents. Paclitaxel inhibits cell proliferation, cell motility, shape and transport between organelles [55]. Both rapamycin and paclitaxel have substantial clinical records as approved therapeutics for a number of indications independent of devices.

2.3 Device-based Thrombosis

Under normal, steady-state circulation conditions (hemostasis), blood continuously contacts host endothelium with an intrinsic, active anticoagulant and antithrombotic system. Injury to blood vessels exposes subendothelial components, releases pro-coagulant stimulants and disrupts hemostasis. Natural host response to this disruption involves blood platelet adhesion, activation, and aggregation in combination with activation of intrinsic, extrinsic coagulation cascades terminating in the formation of a crosslinked fibrin clot. These natural coagulation cascades are depicted in Figure 2.2. The combination of platelet and procoagulant cascade activation rapidly produces a thrombus/clot that stabilizes the injury and prevents further blood loss. Thrombus formation plays an important role in the maintenance of hemostasis. Thrombin-mediated fibrin polymer traps and stabilizes clusters of activated platelets to yield a stable thrombus critical for survival and also contributing powerfully to local wound healing.

Endothelial cells (ECs) lining the walls of the endothelium continuously synthesize and regulate several key molecules necessary for the maintenance of host hemostasis and the intrinsic blood compatibility of vasculature. The EC surface is a dense, brush-like layer of hydrated proteoglycans, called the glycocalyx. Glycocalyx glycoproteins enzyme-grafted with glycosaminoglycans (GAG) side chains [56] including heparan, dextran and chondroitin sulfate proteoglycans, and hyaluronic acid, are

negatively charged and highly hydrated, acting as a barrier and a lubricant between the ECs and blood components [57]. ECs also actively produce and release nitric oxide and prostacyclin (PGI_2) that actively prevent platelet adhesion and activation [58,59]. Heparan sulfate proteoglycan synthesized by the ECs inhibits platelet adhesion and activation [60] while also functioning as a catalytic cofactor for binding antithrombin-III and thrombin together to facilitate thrombin inhibition and anticoagulation [61,62]. ECs also produce tissue-type plasminogen activator (t-PA) and urokinase that act to initiate fibrin degradation and aid in clot dissolution [63,64]. This t-PA activity is tightly regulated by the EC-produced plasminogen activator inhibitor type-I [65-67].

Cardiovascular medical devices are placed into contact with patient's blood for varying periods of time, ranging from minutes (e.g., vascular access devices) to many hours (blood pumps, dialysis filters, central lines), to years (e.g., stents, heart valves, vascular grafts, pacemaker leads). The blood-contacting surfaces on these devices are critical to their performance, seeking to minimize activation of both platelets and the coagulation cascades. However, no materials chemistry or coatings used on these devices have proven clinically reliable in limiting risks of device-based thrombosis to date. Some blood-contacting biomaterials are grafted with heparin-like coatings, or polymers mimicking the EC glycocalyx[68]. Figure 2.3 shows one example of this device-based surface modification approach using heparin. Other approaches are designed to release anticoagulant and antiplatelet drugs for short durations[69]. No materials yet provide all the passive, active and functional aspects of ECs in maintaining hemostasis, and therefore all induce thrombosis in contact with blood to varying degrees. Device-induced thrombosis is a major cause of failure in blood-contacting biomaterials, mainly cardiovascular implants – that constitute a major class of chronic disease-related IMDs. Implantation of a medical device lacking the properties of a healthy endothelium constitutes the introduction of a foreign object into circulation. Blood-material interactions

after implantation spontaneously and immediately trigger a series of complex reactions involving protein and platelet absorption on the biomaterial surface, formation of clots and emboli, and activation of the host's immune system.

2.3.1 Platelet activation in device-based thrombosis

Platelets are anuclear cytoplasmic fragments present in blood essential for rapid, reliable blood clotting and wound healing [70]. Platelets play an essential role in controlling blood loss and maintain hemostasis. One common platelet mode of action is the formation of a stable platelet plug when the blood vessel wall is damaged and the endothelial cell layer is disrupted, exposing the underlying basement membrane and extracellular matrix. With every surgical device implantation, blood vessels in the tissue surrounding an implant are injured, exposing collagen IV in the subendothelial layers to blood which results in the activation of circulating platelets. Additionally, platelets also get activated when they undergo shear stress caused by flow disturbances common to implanted devices. Platelet activation is followed by platelet degranulation, then aggregation and adhesion to each other and to the implanted material. Degranulation serves to release a broad array of potent platelet-derived biochemicals that potentiate local thrombosis by accelerating both local coagulation cascade reactions and platelet activation by release of highly procoagulant stimulants, enzyme substrates and co-factors. The aggregated platelets are stabilized into a thrombus/clot by the newly formed fibrin polymer. Circulating platelets get activated under three major circumstances: a) by contacting the basal lamina of the endothelial vessel wall, b) by contact with a biomaterial surface, and c) due to flow disturbances caused in the presence of a biomaterial. Platelet adhesion, activation and aggregation is combined with simultaneous thrombin-mediated fibrin polymerization that together result in thrombus formation.

2.3.2 Extrinsic and intrinsic coagulation cascades

A biomaterial surface exposed to blood is coated with thousands of plasma proteins within seconds [71]. This adsorption activates some plasma proteins by inducing conformational changes or cleaving small fragments that trigger coagulation and inflammatory responses to the implanted device [72-74]. The coagulation cascade comprises two main branches: the intrinsic pathway (activated by contact with a biomaterial surface) and the extrinsic pathway (induced by EC injury). Both pathways converge at the proteolytic formation of thrombin from its prothrombin zymogen, the penultimate cascade step to converting soluble plasma and platelet-derived fibrinogen to fibrin polymer. Fibrin polymer is a major protein component of the natural clot. Activation of intrinsic and extrinsic proteolytic reactions following blood contact with biomaterials actively and consistently produces thrombin-mediated fibrin clots unless pharmacological treatments attenuate these natural responses, typically by inhibiting key enzymes. The series of coagulant events triggered by the activation of intrinsic or extrinsic pathways following the implantation of a medical device into blood are shown in Figure 2.3. Adherent platelets – both on the biomaterial as well as trapped by the clot – activate to release numerous potent thrombotic promoters and catalysts by degranulation. They also recruit more circulating platelets to the device surface. Subsequent device-based thrombosis and thromboemboli formation produce many clinical complications, causing failure in small-diameter grafts, stents, valves, pumps, catheters and other cardiovascular implants. Furthermore, causal links between device thrombosis and device-centered infection are increasing.

2.3.3 Biomaterials-associated infection

All implantable devices – from short-term devices like contact lens, glucose sensors, urinary catheters, endotracheal tubes, to long-term surgically implanted devices

like pacemakers, cardiac valves, endothelial grafts, orthopedic implants, suffer commonly from varying risks of biomaterials-associated infections (BAIs), or implant-associated infections [41]. BAIs remain a major cause of IMD failure despite years of device innovation, improved quality of care and surgical techniques [75]. In the United States, approximately 2 million nosocomial infections costing $11 billion occur annually [76]. A majority of nosocomial infections (60-70%) are biomaterial-associated infections caused from the increasing use of urinary and, venous catheters, orthopedic implants, shunts and other implants, [77] and involving significant mortality and economic costs. Infection mitigation is a common problem with IMDs and a primary focus of surgical antibiotic prophylaxis in device placement. BAIs most often result from bacterial contamination of implants intra-operatively during the implantation procedure. They are able to colonize implants using the implant-adherent protein layer and thrombus, proliferating at rates that outpace host wound healing. Bacterial adhesion leading to the formation of mature biofilms on the surface of a biomaterial is shown in Figure 2.4. Bacteria and other pathogens have multiple sources during surgery: no surgical suites, surgical personnel or patients are sterile, Pathogen seeding of implants and surgical sites is likely, yet only small fractions of implants actually colonize and lead to clinically symptomatic infections as BAIs. Nonetheless, BAIs can result in difficult-to-treat systemic infections with costly adverse complications and mortality. BAIs are most prevalent in orthopedic [78,79], dental [80], cardiovascular [81-83], neural and ophthalmological implants [84,85] and involve a broad spectrum of pathogens, many in polymicrobial implant infections. Rates of infection at the site of implantation post-surgery increase with the severity of the vascular and tissue injury [86]. Upon detection, BAIs often fail systemic administration of antibiotics. Therefore, common treatment most often involves immediate implant removal followed by long-term parenteral administration of antibiotics and then replacement with a second new implant. This often comes with associated

morbidity and high treatment costs. Little change in BAI incidence has resulted from changes in surgical practice, device design, or antibiotic usage, prompting re-examination of the entire medical device infection scenario [87]. Since systemic antibiotic therapies have failed to bring down implant infection rates, local release antiseptics and antibiotics has been sought in combination device form.

2.4 Combination Medical Devices

2.4.1 Drug-eluting stents

Coronary stent restenosis has been a major challenge since the introduction of percutaneous coronary intervention for coronary artery disease [88]. Use of rigid but flexible endovascular scaffolds such as stents prevents the recoil and collapse of the vessel while also mitigating the vessel restenosis experienced after balloon angioplasty [89,90]. Although development and use of stents in percutaneous coronary interventions (PCI) has demonstrated improvements over balloon angioplasty, vessel restenosis or in-stent restenosis after bare metal stent deployment also poses challenges to successful PCIs, resulting in past patient re-interventions in up to 50% in several patient classes depending on stent placement and patient pathophysiology [91,92]. Systemic administration of drugs to reduce in-stent restenosis is ineffective [93-95] mainly due to poor drug bioavailability, toxicity and insufficient drug dosing to the implant site. Popularity of drug-eluting stent (DES) is due to proven success in mitigating the effects of tissue hyperplasia-caused vessel occlusion [9,96,97]. DES use has reduced the occurrence of repeated PCIs and surgical revascularization procedures to treat restenosis by 40% to 70% [8-10]. Emerging classes of DES coated with bioactive agents (DNA, proteins and viral vectors) and biopharmaceuticals provide improved safety and efficacy in certain cases but also pose challenges during their fabrication and require specific formulations and delivery mechanisms for reliability and efficacy [98].

In coronary applications, DES devices are typically localized expandable, slotted metal tubes (~4mm long) coated with a polymer carrying a small dose (micrograms) of pharmacological agent. DES are collapsed around a deployment catheter and installed at a coronary lesion vessel by catheter-initiated intraluminal expansion. This provides structural support to the vessel while releasing drug locally to the vessel wall at the stent implant site [99]. The DES provides the advantage of effective localized drug delivery and therapeutic efficacy at the lesion site while avoiding excessive dose exposures through systemic delivery [100,101]. Other advantages include directional delivery of drug to the vessel wall tissue and only small fractions entering the blood stream. Additional new stent designs can build drug depots in spatially designated locations on-stent [102], with versatility to carry multiple drugs, releasing with different release kinetics, and also two distinct therapeutic functions – antithrombosis on the blood side and antiproliferatives on the tissue side [103].

Sirolimus-eluting stents originally were the pioneer DES, showing noticeable improvements over early bare metal stent designs in PCI procedures, reducing cell proliferation, migration and restenosis from the vessel bed at the stenting site. The sirolimus-eluting stent (Cordis CYPHER™) was the first DES to receive clinical approval [104,105] in Europe, and the first "official" combination device approved by the FDA in 2003. Sirolimus is now the most extensively studied drug to reduce in-stent neo-intimal hyperplasia following coronary stent deployment [106]. Sirolimus-eluting and paclitaxel-eluting stents (TAXUS®**,** Boston Scientific, USA) are the two commercially available, first-generation DES. These are coated with a very thin (~μm) nondegradable polymer layer (e.g., polyisobutylene or polymethacrylate copolymers) containing very little drug within the coated polymer (~μg/mm length of stent), released with an early significant burst (up to 50%) within the first 24-36 hours postimplantation followed by slower release lasting more than 6 weeks in some cases [6].

After initial enthusiasm with the first-generation DES, controversial debate has ensued over long-term DES safety, with a shift in clinical focus to increased risks of late stent thrombosis [107,108]. Although both CYPHER and TAXUS effectively achieved primary goals of reducing cellular restenosis across almost all lesion and patient subsets over bare metal stents, their safety has been limited by sub-optimal polymer biocompatibility, delayed stent endothelialization leading to late stent thrombosis, and local drug toxicity [109-113]. The permanent presence of the noneroding polymer covering the stent struts and wires has been correlated with tissue inflammatory response and local toxicity in preclinical studies [114,115]. Stent thrombosis risk gained primary focus after the dominant restenosis issue had been resolved using drug-eluting stents: DES are comparable to bare metal stents in occurrence of stent-associated thrombosis [116]. This has prompted new technologies and designs to overcome the thrombosis problem using new stent designs, stents with multiple drug reservoirs containing both antithrombotics and anti-proliferatives, absorbable or biodegradable polymers, nonpolymer drug-loaded surfaces and changes in the types and doses of currently used antiproliferative drugs placed on-stent.

Recent clinical introduction of the biodegradable polymer-coated DES [117] seeks to overcome stent thrombosis attributed to the permanent polymer layer on first generation DES. Biodegradable stent coatings have been designed to release loaded drug for an intended amount of time before completely degrading. Clinically familiar poly(L-lactic acid) (PLA), poly(lactic-co-glycolic acid) (PLGA) and poly(D,L-lactide) (PDLLA) remain popular choices for biodegradable polymer DES coatings. BioMatrix (Biosensors Inc, USA) is a stainless steel stent containing Biolimus A9 (a derivative of sirolimus) as drug on the abluminal surface facing the vessel wall targeting the mTOR protein, loaded in a PLA coating. The drug is released to the vessel wall over 2 to 4 weeks and the PLA coating is gradually absorbed between 6 and 9 months. Several

other novel DES with biodegradable coatings are in development. Cardiomind (Cardiomind Inc., USA), ELIXIR-DES (Elixir Medical Corporation, USA), JACTAX (Boston Scientific Corporation, USA) and NEVO (Cordis, USA) are example stents in development and clinical trials with degradable coatings used to deliver anti-proliferative drugs to mitigate neointimal tissue hyperplasia in PCI procedures.

As the model and precedent combination product approved by the FDA, DES are an excellent example of combining a drug with a device to target and address a specific problem unsolved by either component alone or used together but separately. Despite improvements in early prototypes and first-generation stents using new designs, materials, drugs, drug loading methods, drug release kinetics, release duration and improved understanding of local pharmacology and complications arising several months to years after DES placement, new technology should better address newer DES problems associated with late stent thrombosis, endothelialization and local drug toxicity. Additionally, expansion of DES use to other challenging luminal lesions, both in vasculature, gut/digestive, and reproductive tissues will require further innovation of drugs on devices.

2.4.2 Antimicrobial central venous catheters

Central venous catheters are a critical component for fluid delivery and retrieval, parenteral drug and nutritional fluid administration in a variety of clinical settings for critically ill patients. In the United States, physicians insert more than 5 million central venous catheters every year [118]. The two major complications associated with catheters are bacteremia (infection) and thrombosis [119]. Catheters coated with both antimicrobial and antithrombotic agents have been developed and commercialized. Antimicrobial-coated catheter use and efficacy have been studied for more than a decade [120].

Infections associated with catheters are classified as catheter-related blood-

stream infections (CRBSI). CRBSI can occur in 3-10% of all patients using central venous catheters [121], affecting over 300,000 patients in the United States annually [122] and causing more than 25,000 patient deaths [123,124]. Systemic administration of antibiotics to treat CRBSI either prophylactically or therapeutically is not a clinically preferred nor reliably efficacious route. Local administration of antimicrobial agents from properly designed combination devices seeks to provide small efficacious doses of therapeutics released into local tissue sites without requiring high systemic drug dosing.

Techniques developed to reduce CRBSI incidence include modified catheter designs, use of antimicrobial impregnated catheters, use of cuffed tunneled catheters, local topical treatments, and use of antimicrobial lock solutions [125]. Coating or impregnating the surface of central venous catheters with antimicrobial agents helped to markedly reduce the risk of CRBSI, and their use has now become the standard of care [126,127]. Antimicrobial-coated catheters employ different methods to immobilize the antimicrobial agents onto catheter surfaces – both luminal and external. One method is to simply add the antimicrobial agent to the precursor polymer granules used to fabricate the catheter, similar to adding other constituents like pigmentation or stabilization compounds prior to injection molding [128]. Another procedure involves electrostatically coating catheter surfaces layer-by-layer with antimicrobial agents and a binding material with opposite electrostatic charge. Hydrophobic alkylated regions of cationic surfactants like tridodecylmethylammonium chloride (TDMAC) have been adsorbed on catheter surfaces, presenting a cationic surface to anionic drug molecules binding to the surfactant-coated surface [129,130]. Recently, a zwitterionic polymer brush grafted layer has shown preclinical efficacy as an antimicrobial coating [131,132]. Addition of active drug release capability to this layer would provide enhanced bioactivity.

These strategies facilitate incorporation of different antimicrobials onto catheter surfaces to reduce CRBSI. Multiple antimicrobial agents are preferred (typically

combinations of an antiseptic and antibiotic agent) to reduce the development of antimicrobial resistance to any single agent [133]. According to Centers for Disease Control and Prevention (CDC) guidelines, catheters containing combinations of minocycline/rifampin (MR) antibiotics, and combinations of chlorhexidine/silver sulfadiazine (CS) antiseptics are the two most effective antimicrobial catheters to treat CRBSI [126,127]. Catheters coated with both antibiotics and antiseptics are FDA and CE approved and commercialized (e.g., CS: ARROWgard®, Arrow international, USA; MR: Cook Specturm® series catheters, Cook Critical Care, USA). Both ARROWgard® and Spectrum® series catheters have antimicrobial agents impregnated on internal and external surfaces using TDMAC adlayers [134]. Both MR and CS have shown broad-spectrum antimicrobial activity to both Gram negative and Gram positive organisms and fungi. Several randomized trials [135,136] conducted with MR and CS showed superior performance from MR-impregnated catheters versus CS-impregnated catheters in preventing CRBSI specially in patients needing catheter-based access for more than 7 days up to 50 days *in situ* [137]. Catheters impregnated with MR have been shown to exhibit higher anti-adherence activity and prolonged antimicrobial durability compared to catheters with CS against vancomycin-resistant Staphylococcus aureus and multidrug-resistant (MDR) Gram negative organisms other than Pseudomonas [138]. Although MR shows high antimicrobial activity against staphylococci and most of the Gram negative bacilli [138], they are less effective against Pseudomonas aeruginosa (contributing 3 to 5% of CRBSI) and Candida species (contributing about 12% of CRBSI) [138]. *In vitro* studies using catheters coated with a combination of MR and CS have shown to be effective against vancomycin-resistant Staphylococcus aureus, Gram negative bacilli, Pseudomonas aeruginosa and Candida species [139].

Silver nanoparticle-impregnated catheters (SNP: Medex Logicath AgTive®, Smith Medical International Ltd, UK) are CE-approved and commercially available in Europe.

Catheters coated with silver-based zeolite (SZ) on blood-contacting surfaces (e.g., Lifecath PICC Expert with AgION™ from Vygon international in Europe) use controlled release of silver nanoparticles from the coating to provide antimicrobial properties to the catheter. In a recent study [140] conducted over 14 months involving 246 central venous catheter insertions (122 silver zeolite-impregnated and 124 nonimpregnated catheters), the AgION™ catheters showed reduced CRBSI compared to uncoated catheters. In silver nanoparticle-impregnated catheters, a recent study has shown that platelets colliding with silver nanoparticles exposed on the coating surface accelerate the process of catheter-related thrombosis while simultaneously exhibiting strong antimicrobial properties [141].

Catheters with antithrombotic coatings are used to reduce the incidence of coagulation. The Carmeda® BioActive Surface (CBAS) on Spire Biomedical® catheter products (Spire Biomedical, Inc., Bedford, MA) and the Trillium® Biosurface developed by BioInteractions Ltd. (UK) are two commercially available antithrombotic-coated catheters. Both catheters use heparin-bonded polymer surfaces as an anticoagulant interface. Heparin is a polysaccharide with anticoagulant properties and has been used as an antithrombotic agent for clinical applications [142]. The CBAS treatment consists of heparin molecules covalently bonded to the catheter surface, exposing active heparin sequences to bind ATIII and thrombin from the bloodstream while shedding other protein components. Schematic representation of thrombin inhibition on a bioactive heparin-coated surface to limit device-based thrombosis is presented in Figure 2.5. The Trillium® Biosurface treatment combines a hydrophilic polyethylene oxide layer with negatively charged sulfate polymers to retain hydration at the catheter surface and reduce blood adsorption. In addition, it has heparin covalently bonded to the polyethylene oxide layer for anticoagulation [143]. Although catheters coated with active antithrombotic layers are clinically used, the effects of these coatings on catheter complications are yet to be

evaluated in the hemodialysis population where these complications also exist. Importantly, many such technologies have not been shown to produce significant cost-benefit using placebo-controlled blinded prospective studies.

Catheter lock solution (CLS) is another strategy used to reduce CRBSI incidence from central venous catheters. A biocompatible solution containing a combination of antimicrobial and anticoagulant agents constitutes the CLS. The CLS is injected into the lumen of the catheter after a hemodialysis session and retained there to reduce incidence of thrombus and associated biofilm formation. Catheter thrombosis can be limited using heparin solutions or treated by infusing a thrombolytic agent such as urokinase or tissue plasminogen activator [tPA] into the lumen of the catheter [144,145]. In a recent study, athrombogenic Camouflage™-coated (artificial glycocalyx) catheters have exhibited reduced need for urokinase injections for successful catheter tap and blood drawing over uncoated catheters in cancer patients with long-term catheters [68].

2.4.3 Antimicrobial urinary catheters

Urinary catheters allow passage of urine for treatment for patients with urinary retention, general surgery recovery, bladder obstruction, paralysis or loss of sensation in the perineal area [6]. Urinary catheters are generally used to manage urinary incontinence in elderly patients or in patients with long-term spinal cord injuries. More than 30 million urinary catheters are employed in patients annually [146]. Unfortunately, catheter-associated urinary tract infections (CUTI) remain the most common nosocomial infection [147]. Catheter surfaces in contact with the urethral epithelia facilitate bacterial contamination, adhesion, retention, and biofilm formation on both the abluminal and luminal surfaces eventually leading to infection of the urethra, then the bladder, and ascending into the ureters unless the catheter is exchanged frequently [148]. Microbes in the catheter mediate the breakdown of urea, resulting in an increase in the urine pH, [149]

inducing formation of mineral crystals on the catheter surface, leading to the formation of urinary infection stones [149] and blockage of the lumen by encrustation, which can produce kidney and blood stream infections.

Systemic antibiotic therapies, antimicrobial topical ointments, and the use of antimicrobial agents in collection bags are commonly used to treat CUTIs. Silver-impregnated urinary catheters claim 30% reduction in the incidence of CUTI in some studies although this is not a consensus [150]. Several catheters based on silver and silver oxide coatings are commercially available in the United States (SilvaGard®, (I-Flow/Acrymed), KENDALL DOVER® series catheters (Tyco Healthcare), BACTI-GUARD® silver (C.R. Bard)) [75]. A recent UK study involving patients with urethral catheterization for up to 14 days found that silver-coated catheters were ineffective against infection; the incidence of infection is comparable to uncoated PTFE catheters[151].

Ciprofloxacin, gentamicin, norflaxin, nitrofurazone, and combinations of compounds, such as chlorhexidine and protamine sulfate have been successfully incorporated into catheter coatings [152]. Nitrofurazone-coated catheters (Rochester Medical, MN) are an emerging class of antimicrobial urinary catheters shown to be efficacious against E. coli [153] and have exhibited better antimicrobial properties than silver-treated catheters [154] in *in vitro* studies. However, further prospective double-blind powered two-arm clinical studies are required to validate claims for the efficacy of silver-coated and nitrofurazone-coated catheters in CUTIs.

2.4.4 Orthopedic drug-eluting implants

Bone defects from trauma, disease, surgical intervention and congenital deficiencies are among the most challenging orthopedic repair problems faced worldwide. Autologous bone grafts are the gold standard to treat bone defects but are limited, not

always appropriate, with harvesting complications, including infection susceptibility. Bone fractures and joint deficiencies are increasingly treated using a variety of implanted biomaterial stabilization devices including bone cement, hip, knee, shoulder and elbow prosthesis, plates, nails, rods, wires, pins, and screws. Projected market revenues for such orthopedic implants are estimated at $23 billion in 2012 [155]. Bone-implant bonding [156] and long-term stabilization pose significant clinical challenges including implant infection, bone resorption and implant loosening [157-159]. Despite use of advanced stabilization mechanisms and implant instrumentation, some fractures are slow-healing or nonunions, requiring revision surgeries at significant expense and patient morbidity. Recent advances in drug delivery are increasingly used with orthopedic implants as combination devices [160]. Increasing reports document effects from delivery of small molecule osteoinductive agents (drug [161], scaffold [162], gene and cellular delivery [163,164], biologically derived growth factors, anti-osteoporotic agents, and osteo-synthetic genetic materials like DNA transgenes and siRNA to bone defects from a variety of implant devices and vehicles [165-172].

BAI remains a major concern in orthopedic implants [173]. Rates of infection are estimated to be 1% for primary hip implants, 4% for knee implants (higher for secondary revisions), and more than 15% for some trauma-associated open fracture implants [155]. Orthopedic implants carry a lifetime risk of infection (acute and hematogenous sources) and are clinically addressed in most cases by revision surgery involving a further substantial risk of infection [155]. A commonly used clinical approach to manage orthopedic implant infection is the use of antibiotics in bone cement, polymethylmethacrylate (PMMA) or PMMA beads. These nondegradable polymer cements have been used to prevent osteomyelitis for four decades [174-176] using either bulk impregnation by the aminoglycoside antibiotics, gentamicin or tobramycin [6,177], or vancomycin (Europe only). The first antibiotic-blended bone cement to be approved in

the United States was Simplex P (Stryker Howmedica Osteonics) containing tobramycin [6]. The Palacos™ series of bone cements from Biomet, Inc. (Warsaw, USA) contain gentamycin and have been approved shortly after Simplex P. Recently, Depuy 1 gentamycin-releasing bone cement (Depuy Orthopaedics) has been FDA-approved. *In vivo* studies have demonstrated the efficacy of antibiotic-loaded cements in reducing orthopedic implant infections within a short time after implantation [178-180]. However, despite wide enthusiasm, drawbacks limit clinical applications of antibiotic-loaded bone cements. Pharmacokinetics studies show the inefficiencies of gentamicin release from antibiotic-loaded PMMA bone cements or PMMA beads, with less than 50% of the antibiotic release by 4 weeks [181-184]. The primary concerns with the use of antibiotic-loaded bone cements are possible allergic reactions to the antibiotic used, and the development of drug resistance to the antibiotic at the implant site.

An antimicrobial tibial internal fixation nail coated with a degradable polymer containing gentamicin is marketed in Europe. The polymer coated over the metal nail covers the cannulation, enabling antibiotic delivery to the intramedullary canal and releasing antibiotic for ~2 weeks [185,186]. The FDA recently approved a polyurethane sleeve coated with gentamicin (OrthoGuard AB, Smith & Nephew, UK) that can be used for coating pins and wires used for external fixation devices [187].

2.4.5 Antimicrobial sutures

According to the CDC, the overall incidence of surgical site infection is estimated to be 2.8% in the United States [188]. Surgical sutures allow microbial adherence and colonization similar to other biomaterials [189] and contribute to surgical site infection incidence. Microbial colonization to suture materials is highly variable, dependent on specific microbial species, and suture structure, and chemical composition [190]. Braided sutures have been shown to have higher microbial colonization compared to nylon-

based monofilament sutures [191]. Triclosan-coated braided polyglactin 910 suture (Vicryl Plus Ethicon, USA) has been developed to mitigate suture-induced surgical site infections. Several *in vitro* and *in vivo* studies [192,193] have shown that the triclosan-coated Vicryl Plus sutures effectively inhibit growth of normal and methicillin-resistant strains of S. aureus and S. epidermidis [192] while showing no difference in physical (strength, breaking force, etc.) and degradation characteristics compared to uncoated polyglactin 910 sutures [193]. Recent clinical trials have shown that use of triclosan-coated Vicryl Plus sutures in a diverse group of 450 patients resulted in a statistically significant reduction in the incidence of surgical site infection [194]. However, some studies advise caution and the need for larger scale studies [195]. Silver-containing sutures are being developed by X-Static. Another antimicrobial suture being developed by Polymedix (PolyCide^{TM}) contains the antibiotic, polycide, which disrupts microbial cell [75]. New antimicrobial strategies should be developed to overcome the limitations of current technologies.

2.4.6 Vascular grafts with antithrombotic coatings

Synthetic vascular grafts have been used to treat vessel occlusion caused by vascular disease for over four decades. Large diameter grafts have substantially better success rates clinically than those below 5mm diameter, regardless of biomaterials used. Small-diameter vascular graft failure generally occurs as a consequence of acute thrombus formation on the graft luminal surface, anastomotic intimal hyperplasia, or progression of vascular disease [196]. Although anastomotic hyperplasia and disease progression are important factors for failure, reducing the propensity for acute thrombotic failure by improving graft surface blood compatibility has significant potential for improving clinical performance of small-diameter vascular grafts. Small-diameter expanded polytetrafluoroethylene (ePTFE) vascular grafts containing surface-immobilized heparin are FDA-approved for treating vascular occlusion. CBAS-coated

vascular grafts (e.g., Gore® PROPATEN® Vascular Graft, Gore® VIABAHN® Endoprosthesis, W. L. Gore, USA) containing immobilized heparin on the graft luminal surface are commercialized. Studies have shown reduction in thrombogenicity for small-diameter ePTFE vascular grafts containing immobilized heparin compared to uncoated ePTFE grafts [197].

2.4.7 Cerebrospinal shunts

Hydrocephalus is treated using biomaterials-based cerebral shunt implants that drain excess cerebrospinal fluid (CSF) from the cranium to abdomen to relieve intracranial pressure [198]. Infections remain a major clinical complication in using CSF shunt implants and usually require frequent replacement of the shunt system at substantial cost and morbidity (usually in infants and children) [199]. Antibiotic-impregnated CSF shunts demonstrate clinical efficacy in reducing implant infections [200,201]. BACTISEAL® from Depuy and ARES® from Medtronic are two antibiotic-impregnated CSF shunts that contain both clindamycin and rifampicin, released from the shunt surface. Both products demonstrate reduced infection against Gram positive bacteria for at least 31 days after implantation [202,203]. This area however still faces numerous challenges in producing a long-duration product that performs reliabiy and reduces shunt replacement frequency.

2.5 Future Directions

2.5.1 Orthopedic fixation plate sleeves

New biodegradable polymer sleeves formulated with various therapeutics and readily mounted onto orthopedic plates and screw fixation implants intra-operatively prior to implantation provide a patient-specific and implant-specific customizable therapeutics approach to IMD drug delivery. Sleeves must not interfere with device fixation mechanics and healing (typically on periosteum, or in bone) and degrade without

adverse incident. Biodegradable sleeves have been prepared using copolymers of glycolide, caprolactone, trimethylene-carbonate and lactide, containing the antimicrobial agents gentamicin sulfate and triclosan (highly potent bactericidal agents against *S. aureus* [204]). These sleeves slip over metallic internal fixation plates (e.g., limited contact dynamic compression plates) and implanted in sheep tibia with induced bone defects. Local release of antimicrobials to mitigate implant-associated bone infection was shown to kill microbes *in vitro* and produce no observed bone irritation or significant FBR in sheep *in vivo* [205]. A sleeve to deliver bone morphogenetic protein-2 (rhBMP-2) within PLGA microparticles through a porous sleeve made of resorbable polypropylene fumarate has also been tested [206]. The porous sleeve is loaded with desired amounts of drug-loaded microspheres prior to implantation, with possibilities to select from a variety of preloaded, preformulated PLGA microsphere/drug combinations. This strategy provides a case-dependent customized solution to surgeons using these over implants. However, this intra-operative microsphere loading technique may be produce inconsistent results. Multiple variants of sleeves supplied by manufacturers with standardized drug loading and drug delivery mechanisms may result in more standardized results while still allowing surgeons to choose a precise location on the implant to apply it for release.

2.5.2 Customizable drug-releasing adhesive patches and intra-operative custom coatings

Unless performing drug formulation tasks for device addition off-label, surgeons are currently limited to using drug precoated and preloaded implants as received from a device manufacturer. These types of implants have pre-determined amounts of drug, a fixed drug type, and the location of the drug distributed over the implant surface cannot be changed or modified. Such implants are manufactured as “one-size-fits-all” and

generally not customizable to any particular patient or condition, or surgeon preference. Increasingly, combinations of multiple drugs are proving more effective than single drugs in a given application. Flexibility for manipulating the drug type, drug loading and its location over the implant surface can be beneficial to patients receiving certain implant types. New implant coating technologies to address these limitations with the flexibility in design and feasible intra-operative production to be readily customized to patients' needs are desirable. Customizable drug-containing "paints" and patches loaded with desired drugs with a controlled, custom dosing and flexible application locations on a desired implant intra-operatively have been recently proposed [207] to provide a possible solution to such needs. Adhesive drug patches fabricated from resorbable biomaterial laminates or composites in an aseptic environment would be loaded with drugs or drug-loaded degradable microparticles before or during surgery and cut into desired shapes to match the implant, dosing and intended application. Drug-containing polymer coatings could also be sprayed onto implant surfaces directly using computer-controlled calibrated equipment preprogrammed to match the implant specifications with patient needs and surgeon preferences, and applied either pre- or intra-operatively as a validated process. Custom drug-release patches and drug "paintable coatings" would be adhered as thin films to implant sites with surgical glues at desired locations before or during implant surgery.

2.5.3 Shape memory polymeric biomaterials

Many biomedical implants are polymer-based and often require complex surgeries for device implantation and host integration due to their size and shape. Minimally invasive surgeries enable implantations of certain smaller implants with laparoscopes that limit patient risk, procedure cost and morbidity. Use of biocompatible shape-memory polymers further provides new opportunities for improved implantation of

certain medical devices with relative ease and less patient discomfort. Shape memory processing enables specific materials chemistries to “remember” a permanent shape while predeformed into meta-stable temporary shapes that trigger to the permanent shape with a stimulus (mechanical stress, heat, light). This property allows modification of the device shape and size to conform to a catheter or a smaller implant readily inserted through smaller incisions using catheters or laproscopes than required for normal surgery. Nitinol is a shape memory metal commonly used in cardiovascular stent applications due to its ability to be deformed to a small compressed conformation allowing easy insertion on a catheter with minimal implantation trauma, and which regains its intended final shape after mechanical balloon-based deployment. Nickel allergy and final metal mechanical properties limit their utility. As an alternative, thermally induced shape-memory polymers can be used in polymer-based suture applications, especially those requiring complex knots, curve shapes and conformations [208]. Shape-memory polymers have gained increased attention as a proposed biomaterial for minimally invasive surgical devices [208,209]. Medshape (Atlanta, USA) manufactures FDA-approved polymer-based shape-memory implants for suture anchors and soft tissue fasteners. Polymer-based shape memory implants can also be used for drug delivery to implant locations via impregnation of desired drugs into the material and release upon triggering to final shape after deployment [210].

2.5.4 See-and-treat combination imaging/drug delivery theranostic agents

Some creative, new medical nanotechnology enables the possibility to combine the imaging, monitoring and treating of disease condition onto a single platform. Nanoparticles engineered with imaging agents and also containing therapeutic agents permit simultaneous diagnostic and therapeutic functions when circulating *in vivo*.

These so-called “theranostic” agents/devices often incorporate drug conjugates and complexes, dendrimers, liposomes, micelles, core–shell particles, microbubbles, and carbon nanotubes as carriers of either drugs or contrast agents, including optically active small molecules, paramagnetic metals and metal oxides, ultrasonic contrast agents, and radionuclides. This is an emerging area of combination devices, that could significantly contribute to improved disease detection and targeted therapy as well as to personalized medicine [211].

Molecular imaging techniques such as magnetic resonance imaging (MRI), radionuclide-based imaging using computed tomography (CT) or positron emission tomography (PET), and high intensity focused ultrasound allow visualization and distinction of tissue, cellular and subcellular biological processes with the help of contrast agents [211]. These imaging agents, combined into carriers capable of effectively delivering drugs to a biological target will enable a “see and treat” modality to image the disease condition simultaneously with triggers to delivery therapy from the agent, constituting a theranostic device.

Drug conjugates or complexes with soluble polymers like poly[N-(2-hydroxyl propyl) methacrylamide] (polyHPMA) have been well studied [212]. A contrasting agent visualized by magnetic resonance imaging (MRI) such as radioactive I-131, conjugated with the doxorubicin-HPMA polymer anti-cancer prodrug conjugate already synthesized, would enable the complex to be used as a tumor theranostic agent [213]. Dendrimers have been extensively studied and are attractive drug delivery and contrast agent vehicles due to their large number of functional surface chemistry sites on them. Photo-activated drug release using dendrimers with doxorubicin conjugated to a photo-sensitive compound has been accomplished to target cancer [214]. Other researchers have successfully combined dendrimers with various MRI contrast agents like high spin gadolinium and paramagnetic iron oxide [215]. Combination of both of these chemistries

onto a common platform constitutes a theranostic agent. Liposomes are another class of carriers recently studied as theranostic agents encapsulating various drugs and conjugated contrast agents [211]. Multiple studies have been performed with liposomal formulations with targeting, therapeutic, and imaging functionalities [216,217].

Several other colloidal and nanoparticulate carriers like polymersomes, micelles, quantum dots, and carbon nanotubes can be conjugated with drugs and imaging agents for treating a condition simultaneously with detection and diagnosis [211]. While the dual conjugation chemistry is fairly straightforward in many cases, the challenge remains to produce long circulating times to allow these particulate systems to achieve disease site accumulation. The concept of targeting these particles has proven very challenging to date, with very low levels of systemically administered dose (i.e., generally less than 5% of the injected dose) actually reaching the disease site from the blood stream, with the majority of the dose targeting the liver, spleen, kidney and lung in most cases. Imaging requires sensitivity, selectivity and specificity *in vivo* [218]. Therapy requires effective dose delivery without toxic side effects. Building both critical properties onto a single nanoparticle platform is challenging: these two properties are not yet reliably achieved from these nanoparticle systems.

2.6 Acknowledgments

The authors gratefully acknowledge support from a University of Utah SEED grant.

2.7 References

1. Simchi A, Tamjid E, Pishbin F, Boccaccini AR. Recent progress in inorganic and composite coatings with bactericidal capability for orthopaedic applications. *Nanomed.* Feb 2011;7(1):22-39.

2. Raymond Brood LC, Norman Daniels,Gerald C. Davison, et.al. Global Population Ageing: Peril or Promise? In: Bloom D, ed: World Economic Forum; 2012: http://www.icaa.cc/wef/Global-Population-Ageing-Book.pdf. Accessed 09/10/2012.

3. Kramer DB, Xu S, Kesselheim AS. How Does Medical Device Regulation Perform in the United States and the European Union? A Systematic Review. *PLoS Med.* 2012;9(7):e1001276.

4. Lucintel. *Global Medical Device Industry 2012-2017: Trend, Profit, and Forecast Analysis.* July 2012.

5. Trajkovski B, Petersen A, Strube P, Mehta M, Duda GN. Intra-operatively customized implant coating strategies for local and controlled drug delivery to bone. *Adv. Drug Delivery. Rev.* 2012;64(12):1142-1151.

6. Wu P, Grainger DW. Drug/device combinations for local drug therapies and infection prophylaxis. *Biomaterials.* Apr 2006;27(11):2450-2467.

7. Couto DS, Perez-Breva L, Saraiva P, Cooney CL. Lessons from innovation in drug-device combination products. *Adv. Drug Delivery. Rev.* Jan 2012;64(1):69-77.

8. Moses JW, Leon MB, Popma JJ, et al. Sirolimus-eluting stents versus standard stents in patients with stenosis in a native coronary artery. *N. Engl. J. Med.* Oct 2 2003;349(14):1315-1323.

9. Stone GW, Ellis SG, Cox DA, et al. A polymer-based, paclitaxel-eluting stent in patients with coronary artery disease. *N. Engl. J. Med.* Jan 15 2004;350(3):221-231.

10. De Luca G MDPDMTMDSCMD, et al. Drug-eluting vs bare-metal stents in primary angioplasty: A pooled patient-level meta-analysis of randomized trials. *Arch. Intern. Med.* 2012;172(8):611-621.

11. Ansel HC, Popovich NG, Allen LV. *Pharmaceutical dosage forms and drug delivery systems.* 6th ed. Baltimore: Williams & Wilkins; 1995.

12. Liu SJ, Wen-Neng Ueng S, Lin SS, Chan EC. In vivo release of vancomycin from biodegradable beads. *J. Biomed. Mater. Res.* 2002;63(6):807-813.

13. Frost MC, Meyerhoff ME. Implantable chemical sensors for real-time clinical monitoring: progress and challenges. *Curr. Opin. Chem. Biol.* 2002;6(5):633-641.

14. Wilson GS, Gifford R. Biosensors for real-time in vivo measurements. *Biosens. Bioelectron.* 2005;20(12):2388-2403.

15. Anderson JM, Rodriguez A, Chang DT. Foreign body reaction to biomaterials. *Semin. Immunol.* Apr 2008;20(2):86-100.

16. Holt DJ, Grainger DW. Host response to biomaterials. In: Hollinger JO, ed. *An introduction to biomaterials*. 2nd ed. Boca Raton, FL: CRC Press/Taylor & Francis; 2012:91-118.

17. Abbas AK, Lichtman AH, Pillai S. *Cellular and molecular immunology.* 7th ed. Philadelphia: Elsevier/Saunders; 2012.

18. Neuenschwander PF. COAGULATION CASCADE | Intrinsic Factors. In: Geoffrey JL, Steven DS, eds. *Encyclopedia of Respiratory Medicine*. Oxford: Academic Press; 2006:509-514.

19. Janeway C. *Immunobiology 5 : the immune system in health and disease.* 5th ed. New York: Garland Pub.; 2001.

20. Kvist PH, Iburg T, Bielecki M, et al. Biocompatibility of electrochemical glucose sensors implanted in the subcutis of pigs. *Diabetes Technol. Ther.* Aug 2006;8(4):463-475.

21. Wisniewski N, Moussy F, Reichert WM. Characterization of implantable biosensor membrane biofouling. *Fresenius. J. Anal. Chem.* Mar-Apr 2000;366(6-7):611-621.

22. Moussy F. Implantable glucose sensor: progress and problems. Paper presented at: Sensors, 2002. Proceedings of IEEE, 2002.

23. Epstein AE, Kay GN, Plumb VJ, Dailey SM, Anderson PG. Gross and Microscopic Pathological Changes Associated With Nonthoracotomy Implantable Defibrillator Leads. *Circulation.* October 13, 1998 1998;98(15):1517-1524.

24. Zhong Y, Bellamkonda RV. Dexamethasone-coated neural probes elicit attenuated inflammatory response and neuronal loss compared to uncoated neural probes. *Brain Res.* May 7 2007;1148:15-27.

25. Singarayar S, Kistler PM, De Winter C, Mond H. A comparative study of the action of dexamethasone sodium phosphate and dexamethasone acetate in steroid-eluting pacemaker leads. *Pacing Clin. Electrophysiol.* Apr 2005;28(4):311-315.

26. Sharkawy AA, Klitzman B, Truskey GA, Reichert WM. Engineering the tissue which encapsulates subcutaneous implants. I. Diffusion properties. *J. Biomed. Mater. Res.* Dec 5 1997;37(3):401-412.

27. Sharkawy AA, Klitzman B, Truskey GA, Reichert WM. Engineering the tissue which encapsulates subcutaneous implants. III. Effective tissue response times. *J. Biomed. Mater. Res.* Jun 15 1998;40(4):598-605.

28. Sharkawy AA, Klitzman B, Truskey GA, Reichert WM. Engineering the tissue which encapsulates subcutaneous implants. II. Plasma-tissue exchange properties. *J. Biomed. Mater. Res.* Jun 15 1998;40(4):586-597.

29. Mono HG, Stokes KB. The Electrode-Tissue Interface: The Revolutionary Role of Steroid Elution. *Pacing Clin. Electrophysiol.* 1992;15(1):95-107.

30. Radovsky AS, Van Vleet JF. Effects of dexamethasone elution on tissue reaction around stimulating electrodes of endocardial pacing leads in dogs. *Am. Heart J.* 1989;117(6):1288-1298.

31. Gerritsen M, Jansen JA, Lutterman JA. Performance of subcutaneously implanted glucose sensors for continuous monitoring. *Neth. J. Med.* 1999;54(4):167-179.

32. Updike SJ, Shults MC, Rhodes RK, Gilligan BJ, Luebow JO, von Heimburg D. Enzymatic glucose sensors. Improved long-term performance in vitro and in vivo. *ASAIO J.* Apr-Jun 1994;40(2):157-163.

33. Kim DH, Martin DC. Sustained release of dexamethasone from hydrophilic matrices using PLGA nanoparticles for neural drug delivery. *Biomaterials.* May 2006;27(15):3031-3037.

34. Hickey T, Kreutzer D, Burgess DJ, Moussy F. In vivo evaluation of a dexamethasone/PLGA microsphere system designed to suppress the inflammatory tissue response to implantable medical devices. *J. Biomed. Mater. Res.* Aug 2002;61(2):180-187.

35. Masferrer JL, Zweifel BS, Seibert K, Needleman P. Selective regulation of cellular cyclooxygenase by dexamethasone and endotoxin in mice. *The Journal of Clinical Investigation.* 1990;86(4):1375-1379.

36. Chang DF, Wong V. Two clinical trials of an intraocular steroid delivery system for cataract surgery. *Trans. Am. Ophthalmol. Soc.* 1999;97:261-274; discussion 274-269.

37. Chang DF, Garcia IH, Hunkeler JD, Minas T. Phase II results of an intraocular steroid delivery system for cataract surgery. *Ophthalmology.* Jun 1999;106(6):1172-1177.

38. Tan DT, Chee SP, Lim L, Lim AS. Randomized clinical trial of a new dexamethasone delivery system (Surodex) for treatment of post-cataract surgery inflammation. *Ophthalmology.* Feb 1999;106(2):223-231.

39. Kodama M, Numaga J, Yoshida A, et al. Effects of a new dexamethasone-delivery system (Surodex) on experimental intraocular inflammation models. *Graefes Arch. Clin. Exp. Ophthalmol.* Nov 2003;241(11):927-933.

40. Kagaya F, Usui T, Kamiya K, et al. Intraocular dexamethasone delivery system for corneal transplantation in an animal model. *Cornea.* Mar 2002;21(2):200-202.

41. Khardori N, Yassien M. Biofilms in device-related infections. *J. Ind. Microbiol.* Sep 1995;15(3):141-147.

42. Dev V, Eigler N, Fishbein MC, et al. Sustained local drug delivery to the arterial wall via biodegradable microspheres. *Cathet. Cardiovasc. Diagn.* Jul 1997;41(3):324-332.

43. Guzman LA, Labhasetwar V, Song C, et al. Local intraluminal infusion of biodegradable polymeric nanoparticles. A novel approach for prolonged drug delivery after balloon angioplasty. *Circulation.* Sep 15 1996;94(6):1441-1448.

44. Lincoff AM, Furst JG, Ellis SG, Tuch RJ, Topol EJ. Sustained local delivery of dexamethasone by a novel intravascular eluting stent to prevent restenosis in the porcine coronary injury model. *J. Am. Coll. Cardiol.* Mar 15 1997;29(4):808-816.

45. Timmis GC, Helland J, Westveer DC, Stewart J, Gordon S. The Evolution of Low Threshold Leads. *J. Cardiovasc. Electrophysiol.* 1990;1(4):313-334.

46. Hickey T, Kreutzer D, Burgess DJ, Moussy F. In vivo evaluation of a dexamethasone/PLGA microsphere system designed to suppress the inflammatory tissue response to implantable medical devices. *J. Biomed. Mater. Res.* 2002;61(2):180-187.

47. Patil SD, Papadmitrakopoulos F, Burgess DJ. Concurrent delivery of dexamethasone and VEGF for localized inflammation control and angiogenesis. *J. Control. Release.* Jan 22 2007;117(1):68-79.

48. Tilakaratne HK, Hunter SK, Andracki ME, Benda JA, Rodgers VG. Characterizing short-term release and neovascularization potential of multi-protein growth supplement delivered via alginate hollow fiber devices. *Biomaterials.* Jan 2007;28(1):89-98.

49. Norton LW, Tegnell E, Toporek SS, Reichert WM. In vitro characterization of vascular endothelial growth factor and dexamethasone releasing hydrogels for implantable probe coatings. *Biomaterials.* Jun 2005;26(16):3285-3297.

50. Jain NK, Vegad JL, Katiyar AK, Awadhiya RP. Effects of anti-inflammatory drugs on increased vascular permeability in acute inflammatory response in the chicken. *Avian Pathol.* Dec 1995;24(4):723-729.

51. Sung J, Barone PW, Kong H, Strano MS. Sequential delivery of dexamethasone and VEGF to control local tissue response for carbon nanotube fluorescence based micro-capillary implantable sensors. *Biomaterials.* Feb 2009;30(4):622-631.

52. Chan S. Targeting the mammalian target of rapamycin (mTOR): A new approach to treating cancer. *Br. J. Cancer.* 2004;91(8):1420-1424.

53. Gingras AC, Raught B, Sonenberg N. mTOR signaling to translation. *Curr. Top. Microbiol. Immunol.* 2004;279:169-197.

54. Poon M, Badimon JJ, Fuster V. Viewpoint Overcoming restenosis with sirolimus: from alphabet soup to clinical reality. *Lancet.* 2002;359(9306):619-622.

55. Garcia-Garcia HM, Vaina S, Tsuchida K, Serruys PW. Drug-eluting stents. *Arch. Cardiol. Mex.* Jul-Sep 2006;76(3):297-319.

56. Weinbaum S, Tarbell JM, Damiano ER. The structure and function of the endothelial glycocalyx layer. *Annu. Rev. Biomed. Eng.* 2007;9:121-167.

57. Li S, Henry JJ. Nonthrombogenic approaches to cardiovascular bioengineering. *Annu. Rev. Biomed. Eng.* Aug 15 2011;13:451-475.

58. Best LC, Martin TJ, Russell RG, Preston FE. Prostacyclin increases cyclic AMP levels and adenylate cyclase activity in platelets. *Nature.* Jun 30 1977;267(5614):850-852.

59. de Graaf JC, Banga JD, Moncada S, Palmer RM, de Groot PG, Sixma JJ. Nitric oxide functions as an inhibitor of platelet adhesion under flow conditions. *Circulation.* Jun 1992;85(6):2284-2290.

60. Hashi CK, Zhu Y, Yang GY, et al. Antithrombogenic property of bone marrow mesenchymal stem cells in nanofibrous vascular grafts. *Proc. Natl. Acad. Sci. U. S. A.* Jul 17 2007;104(29):11915-11920.

61. Bernfield M, Gotte M, Park PW, et al. Functions of cell surface heparan sulfate proteoglycans. *Annu. Rev. Biochem.* 1999;68:729-777.

62. Bernfield M, Kokenyesi R, Kato M, et al. Biology of the syndecans: a family of transmembrane heparan sulfate proteoglycans. *Annu. Rev. Cell Biol.* 1992;8:365-393.

63. Matsuno H, Kozawa O, Niwa M, et al. Differential role of components of the fibrinolytic system in the formation and removal of thrombus induced by endothelial injury. *Thromb. Haemost.* Apr 1999;81(4):601-604.

64. Fay WP, Garg N, Sunkar M. Vascular functions of the plasminogen activation system. *Arterioscler. Thromb. Vasc. Biol.* Jun 2007;27(6):1231-1237.

65. Schneiderman J, Sawdey MS, Keeton MR, et al. Increased type 1 plasminogen activator inhibitor gene expression in atherosclerotic human arteries. *Proc. Natl. Acad. Sci. U. S. A.* Aug 1 1992;89(15):6998-7002.

66. Bajou K, Noel A, Gerard RD, et al. Absence of host plasminogen activator inhibitor 1 prevents cancer invasion and vascularization. *Nat. Med.* Aug 1998;4(8):923-928.

67. Fay WP. Plasminogen activator inhibitor 1, fibrin, and the vascular response to injury. *Trends Cardiovasc. Med.* Jul 2004;14(5):196-202.

68. Hitz F, Klingbiel D, Omlin A, Riniker S, Zerz A, Cerny T. Athrombogenic coating of long-term venous catheter for cancer patients: a prospective, randomised, double-blind trial. *Ann. Hematol.* Apr 2012;91(4):613-620.

69. Frost MC, Reynolds MM, Meyerhoff ME. Polymers incorporating nitric oxide releasing/generating substances for improved biocompatibility of blood-contacting medical devices. *Biomaterials.* 2005;26(14):1685-1693.

70. Mason KD, Carpinelli MR, Fletcher JI, et al. Programmed anuclear cell death delimits platelet life span. *Cell.* Mar 23 2007;128(6):1173-1186.

71. Engberg AE, Rosengren-Holmberg JP, Chen H, et al. Blood protein-polymer adsorption: Implications for understanding complement-mediated hemoincompatibility. *J. Biomed. Mater. Res. A.* Feb 11 2011.

72. Andersson J, Ekdahl KN, Larsson R, Nilsson UR, Nilsson B. C3 adsorbed to a polymer surface can form an initiating alternative pathway convertase. *J. Immunol.* Jun 1 2002;168(11):5786-5791.

73. Wettero J, Bengtsson T, Tengvall P. C1q-independent activation of neutrophils by immunoglobulin M-coated surfaces. *J. Biomed. Mater. Res.* Dec 15 2001;57(4):550-558.

74. Back J, Lang MH, Elgue G, et al. Distinctive regulation of contact activation by antithrombin and C1-inhibitor on activated platelets and material surfaces. *Biomaterials.* Dec 2009;30(34):6573-6580.

75. Brooks BD, Brooks AE, Grainger DW. Antimicrobial medical devices in preclinical development and use. In: Moriarty TF, Zaat SAJ, Busscher HJ, eds. *Biomaterials associated infection*: Springer; 2013:307-354.

76. Schierholz JM, Beuth J. Implant infections: a haven for opportunistic bacteria. *J. Hosp. Infect.* Oct 2001;49(2):87-93.

77. Bryers JD. Medical biofilms. *Biotechnol. Bioeng.* May 1 2008;100(1):1-18.

78. Widmer AF. New Developments in Diagnosis and Treatment of Infection in Orthopedic Implants. *Clin. Infect. Dis.* September 1, 2001 2001;33(Supplement 2):S94-S106.

79. Zimmerli W, Widmer AF, Blatter M, Frei R, Ochsner PE. Role of rifampin for treatment of orthopedic implant-related staphylococcal infections: a randomized controlled trial. Foreign-Body Infection (FBI) Study Group. *JAMA*. May 20 1998;279(19):1537-1541.

80. Tanner A, Maiden MFJ, Lee K, Shulman LB, Weber HP. Dental Implant Infections. *Clin. Infect. Dis.* September 1, 1997 1997;25(Supplement 2):S213-S217.

81. John MD, Hibberd PL, Karchmer AW, Sleeper LA, Calderwood SB. Staphylococcus aureus prosthetic valve endocarditis: optimal management and risk factors for death. *Clin. Infect. Dis.* Jun 1998;26(6):1302-1309.

82. Vongpatanasin W, Hillis LD, Lange RA. Prosthetic heart valves. *N. Engl. J. Med.* Aug 8 1996;335(6):407-416.

83. Gassel HJ, Klein I, Steger U, et al. Surgical management of prosthetic vascular graft infection: comparative retrospective analysis of 30 consecutive cases. *VASA. Zeitschrift fur Gefasskrankheiten. Journal for vascular diseases.* Feb 2002;31(1):48-55.

84. von Eiff C, Jansen B, Kohnen W, Becker K. Infections associated with medical devices: pathogenesis, management and prophylaxis. *Drugs.* 2005;65(2):179-214.

85. Dart JK, Stapleton F, Minassian D. Contact lenses and other risk factors in microbial keratitis. *Lancet.* Sep 14 1991;338(8768):650-653.

86. Elek SD, Conen PE. The virulence of Staphylococcus pyogenes for man; a study of the problems of wound infection. *Br. J. Exp. Pathol.* Dec 1957;38(6):573-586.

87. Busscher HJ, van der Mei HC, Subbiahdoss G, et al. Biomaterial-associated infection: locating the finish line in the race for the surface. *Sci. Transl. Med.* Sep 26 2012;4(153):153rv110.

88. Gruntzig A. Transluminal dilatation of coronary-artery stenosis. *Lancet.* Feb 4 1978;1(8058):263.

89. Fischman DL, Leon MB, Baim DS, et al. A randomized comparison of coronary-stent placement and balloon angioplasty in the treatment of coronary artery disease. Stent Restenosis Study Investigators. *N. Engl. J. Med.* Aug 25 1994;331(8):496-501.

90. Serruys PW, de Jaegere P, Kiemeneij F, et al. A comparison of balloon-expandable-stent implantation with balloon angioplasty in patients with coronary artery disease. Benestent Study Group. *N. Engl. J. Med.* Aug 25 1994;331(8):489-495.

91. Meads C, Cummins C, Jolly K, Stevens A, Burls A, Hyde C. Coronary artery stents in the treatment of ischaemic heart disease: a rapid and systematic review. *Health Technol. Assess.* 2000;4(23):1-153.

92. Indolfi C, Mongiardo A, Curcio A, Torella D. Molecular mechanisms of in-stent restenosis and approach to therapy with eluting stents. *Trends Cardiovasc. Med.* May 2003;13(4):142-148.

93. Serruys PW, Foley DP, Jackson G, et al. A randomized placebo-controlled trial of fluvastatin for prevention of restenosis after successful coronary balloon angioplasty; final results of the fluvastatin angiographic restenosis (FLARE) trial. *Eur. Heart J.* Jan 1999;20(1):58-69.

94. Serruys PW, Foley DP, Pieper M, Kleijne JA, de Feyter PJ. The TRAPIST Study. A multicentre randomized placebo controlled clinical trial of trapidil for prevention of restenosis after coronary stenting, measured by 3-D intravascular ultrasound. *Eur. Heart J.* Oct 2001;22(20):1938-1947.

95. Holmes DR, Jr., Savage M, LaBlanche JM, et al. Results of Prevention of REStenosis with Tranilast and its Outcomes (PRESTO) trial. *Circulation.* Sep 3 2002;106(10):1243-1250.

96. Morice MC, Serruys PW, Sousa JE, et al. A randomized comparison of a sirolimus-eluting stent with a standard stent for coronary revascularization. *N. Engl. J. Med.* Jun 6 2002;346(23):1773-1780.

97. Stone GW, Ellis SG, Cox DA, et al. One-year clinical results with the slow-release, polymer-based, paclitaxel-eluting TAXUS stent: the TAXUS-IV trial. *Circulation.* Apr 27 2004;109(16):1942-1947.

98. Takahashi H, Letourneur D, Grainger DW. Delivery of Large Biopharmaceuticals from Cardiovascular Stents: A Review. *Biomacromolecules.* 2007/11/01 2007;8(11):3281-3293.

99. Fattori R, Piva T. Drug-eluting stents in vascular intervention. *Lancet.* 2003;361(9353):247-249.

100. Liistro F, Bolognese L. Drug-Eluting Stents. *HeartDrug.* 2003;3(4):203-213.

101. McLean DR, Eiger NL. Stent design: implications for restenosis. *Rev. Cardiovasc. Med.* 2002;3 Suppl 5:S16-22.

102. Finkelstein A, McClean D, Kar S, et al. Local drug delivery via a coronary stent with programmable release pharmacokinetics. *Circulation.* Feb 11 2003;107(5):777-784.

103. Song S-J, Kim KS, Park YJ, Jeong MH, Ko Y-M, Cho DL. Preparation of a dual-drug-eluting stent by grafting of ALA with abciximab on a bare metal stent. *J. Mater. Chem.* 2009;19(43):8135-8141.

104. Venkatraman S, Boey F. Release profiles in drug-eluting stents: issues and uncertainties. *J. Control. Release.* Jul 31 2007;120(3):149-160.

105. Sousa JE, Costa MA, Abizaid A, et al. Lack of neointimal proliferation after implantation of sirolimus-coated stents in human coronary arteries: a quantitative coronary angiography and three-dimensional intravascular ultrasound study. *Circulation.* Jan 16 2001;103(2):192-195.

106. Birkenhauer P, Yang Z, Gander B. Preventing restenosis in early drug-eluting stent era: recent developments and future perspectives. *J. Pharm. Pharmacol.* Nov 2004;56(11):1339-1356.

107. Serruys PW, Daemen J. Late Stent Thrombosis. *Circulation.* March 20, 2007 2007;115(11):1433-1439.

108. McFadden EP, Stabile E, Regar E, et al. Late thrombosis in drug-eluting coronary stents after discontinuation of antiplatelet therapy. *Lancet.*;364(9444):1519-1521.

109. Bertrand OF, Sipehia R, Mongrain R, et al. Biocompatibility aspects of new stent technology. *J. Am. Coll. Cardiol.* Sep 1998;32(3):562-571.

110. Nakazawa G, Finn AV, Ladich E, et al. Drug-eluting stent safety: findings from preclinical studies. *Expert Rev. Cardiovasc. Ther.* Nov 2008;6(10):1379-1391.

111. Nakazawa G, Finn AV, Joner M, et al. Delayed arterial healing and increased late stent thrombosis at culprit sites after drug-eluting stent placement for acute myocardial infarction patients: an autopsy study. *Circulation.* Sep 9 2008;118(11):1138-1145.

112. Feres F, Costa JR, Jr., Abizaid A. Very late thrombosis after drug-eluting stents. *Catheter. Cardiovasc. Interv.* Jul 2006;68(1):83-88.

113. Kounis NG, Hahalis G, Theoharides TC. Coronary stents, hypersensitivity reactions, and the Kounis syndrome. *J. Interv. Cardiol.* Oct 2007;20(5):314-323.

114. Pendyala LK, Li J, Shinke T, et al. Endothelium-dependent vasomotor dysfunction in pig coronary arteries with Paclitaxel-eluting stents is associated with inflammation and oxidative stress. *JACC Cardiovasc. Interv.* Mar 2009;2(3):253-262.

115. Luscher TF, Steffel J, Eberli FR, et al. Drug-eluting stent and coronary thrombosis: biological mechanisms and clinical implications. *Circulation.* Feb 27 2007;115(8):1051-1058.

116. Mauri L, Hsieh WH, Massaro JM, Ho KK, D'Agostino R, Cutlip DE. Stent thrombosis in randomized clinical trials of drug-eluting stents. *N. Engl. J. Med.* Mar 8 2007;356(10):1020-1029.

117. Grube E, Buellesfeld L. BioMatrix® Biolimus A9®-eluting coronary stent: a next-generation drug-eluting stent for coronary artery disease. *Expert Rev. Med. Devices.* 2006/11/01 2006;3(6):731-741.

118. Raad I. Intravascular-catheter-related infections. *Lancet.* Mar 21 1998;351(9106):893-898.

119. Schwab SJ, Beathard G. The hemodialysis catheter conundrum: hate living with them, but can't live without them. *Kidney Int.* Jul 1999;56(1):1-17.

120. Raad I, Darouiche R, Dupuis J, et al. Central venous catheters coated with minocycline and rifampin for the prevention of catheter-related colonization and bloodstream infections. A randomized, double-blind trial. The Texas Medical Center Catheter Study Group. *Ann. Intern. Med.* 1997;127(4):267-274.

121. Maki DG, Kluger DM, Crnich CJ. The risk of bloodstream infection in adults with different intravascular devices: a systematic review of 200 published prospective studies. *Mayo Clin. Proc.* Sep 2006;81(9):1159-1171.

122. Raad I, Hanna H, Maki D. Intravascular catheter-related infections: advances in diagnosis, prevention, and management. *The Lancet infectious diseases.* Oct 2007;7(10):645-657.

123. Chatzinikolaou I, Raad II. Central Venous Catheter Related Infections: The Role of Antimicrobial Catheters
Immunology and Infectious Disease. In: Doughty LA, Linden P, eds. Vol 3: Springer US; 2003:187-215.

124. Viot M. Intravenous access: related problems in oncology. *Int. J. Antimicrob. Agents.* Oct 2000;16(2):165-168.

125. Jaffer Y, Selby NM, Taal MW, Fluck RJ, McIntyre CW. A meta-analysis of hemodialysis catheter locking solutions in the prevention of catheter-related infection. *Am. J. Kidney Dis.* Feb 2008;51(2):233-241.

126. Hockenhull JC, Dwan KM, Smith GW, et al. The clinical effectiveness of central venous catheters treated with anti-infective agents in preventing catheter-related bloodstream infections: a systematic review. *Crit. Care Med.* Feb 2009;37(2):702-712.

127. Ramritu P, Halton K, Collignon P, et al. A systematic review comparing the relative effectiveness of antimicrobial-coated catheters in intensive care units. *Am. J. Infect. Control.* Mar 2008;36(2):104-117.

128. Zhang X. Anti-infective coatings reduce device-related infections. *Antimicrobial/Anti-Infective Materials: Principles and Applications*: CRC Press; 2000:149-180.

129. Greco RS, Harvey RA. The role of antibiotic bonding in the prevention of vascular prosthetic infections. *Ann. Surg.* Feb 1982;195(2):168-171.

130. Kamal GD, Pfaller MA, Rempe LE, Jebson PJ. Reduced intravascular catheter infection by antibiotic bonding. A prospective, randomized, controlled trial. *JAMA.* May 8 1991;265(18):2364-2368.

131. Cheng G, Li G, Xue H, Chen S, Bryers JD, Jiang S. Zwitterionic carboxybetaine polymer surfaces and their resistance to long-term biofilm formation. *Biomaterials.* 2009;30(28):5234-5240.

132. Smith RS, Zhang Z, Bouchard M, et al. Vascular catheters with a nonleaching poly-sulfobetaine surface modification reduce thrombus formation and microbial attachment. *Sci. Transl. Med.* Sep 26 2012;4(153):153ra132.

133. Schierholz JM, Rump AF, Pulverer G, Beuth J. Anti-infective catheters: novel strategies to prevent nosocomial infections in oncology. *Anticancer Res.* 1998;18(5B):3629-3638.

134. Pai MP, Pendland SL, Danziger LH. Antimicrobial-coated/bonded and -impregnated intravascular catheters. *Ann. Pharmacother.* Oct 2001;35(10):1255-1263.

135. Darouiche RO, Raad, II, Heard SO, et al. A comparison of two antimicrobial-impregnated central venous catheters. Catheter Study Group. *N. Engl. J. Med.* Jan 7 1999;340(1):1-8.

136. Marik PE, Abraham G, Careau P, Varon J, Fromm RE, Jr. The ex vivo antimicrobial activity and colonization rate of two antimicrobial-bonded central venous catheters. *Crit. Care Med.* Jun 1999;27(6):1128-1131.

137. Darouiche RO, Berger DH, Khardori N, et al. Comparison of antimicrobial impregnation with tunneling of long-term central venous catheters: a randomized controlled trial. *Ann. Surg.* Aug 2005;242(2):193-200.

138. Raad I, Reitzel R, Jiang Y, Chemaly RF, Dvorak T, Hachem R. Anti-adherence activity and antimicrobial durability of anti-infective-coated catheters against multidrug-resistant bacteria. *J. Antimicrob. Chemother.* Oct 2008;62(4):746-750.

139. Raad I, Mohamed JA, Reitzel RA, et al. Improved Antibiotic-Impregnated Catheters with Extended-Spectrum Activity against Resistant Bacteria and Fungi. *Antimicrob. Agents Chemother.* February 1, 2012 2012;56(2):935-941.

140. Khare S, Hondalus MK, Nunes J, Bloom BR, Garry Adams L. Mycobacterium bovis DeltaleuD auxotroph-induced protective immunity against tissue colonization, burden and distribution in cattle intranasally challenged with Mycobacterium bovis Ravenel S. *Vaccine.* Feb 26 2007;25(10):1743-1755.

141. Stevens KN, Crespo-Biel O, van den Bosch EE, et al. The relationship between the antimicrobial effect of catheter coatings containing silver nanoparticles and the coagulation of contacting blood. *Biomaterials.* Aug 2009;30(22):3682-3690.

142. Hirsh J, Anand SS, Halperin JL, Fuster V. Guide to anticoagulant therapy: Heparin : a statement for healthcare professionals from the American Heart Association. *Circulation.* Jun 19 2001;103(24):2994-3018.

143. Tevaearai HT, Mueller XM, Seigneul I, et al. Trillium coating of cardiopulmonary bypass circuits improves biocompatibility. *Int. J. Artif. Organs.* Sep 1999;22(9):629-634.

144. Daeihagh P, Jordan J, Chen J, Rocco M. Efficacy of tissue plasminogen activator administration on patency of hemodialysis access catheters. *Am. J. Kidney Dis.* Jul 2000;36(1):75-79.

145. Mokrzycki MH, Jean-Jerome K, Rush H, Zdunek MP, Rosenberg SO. A randomized trial of minidose warfarin for the prevention of late malfunction in tunneled, cuffed hemodialysis catheters. *Kidney Int.* May 2001;59(5):1935-1942.

146. Reddy ST, Chung KK, McDaniel CJ, Darouiche RO, Landman J, Brennan AB. Micropatterned surfaces for reducing the risk of catheter-associated urinary tract

infection: an in vitro study on the effect of sharklet micropatterned surfaces to inhibit bacterial colonization and migration of uropathogenic Escherichia coli. *J. Endourol.* Sep 2011;25(9):1547-1552.

147. Wald Hl KAM. Nonpayment for harms resulting from medical care: Catheter-associated urinary tract infections. *JAMA.* 2007;298(23):2782-2784.

148. Warren JW. Catheter-associated urinary tract infections. *Infect. Dis. Clin. North Am.* Sep 1997;11(3):609-622.

149. Bichler KH, Eipper E, Naber K, Braun V, Zimmermann R, Lahme S. Urinary infection stones. *Int. J. Antimicrob. Agents.* 2002;19(6):488-498.

150. Donlan RM, Costerton JW. Biofilms: survival mechanisms of clinically relevant microorganisms. *Clin. Microbiol. Rev.* Apr 2002;15(2):167-193.

151. Pickard R, Lam T, MacLennan G, et al. Antimicrobial catheters for reduction of symptomatic urinary tract infection in adults requiring short-term catheterisation in hospital: a multicentre randomised controlled trial. *Lancet.* In press, Available online November 4 2012(0).

152. Jacobsen SM, Stickler DJ, Mobley HLT, Shirtliff ME. Complicated catheter-associated urinary tract infections due to Escherichia coli and Proteus mirabilis. *Clin. Microbiol. Rev.* 2008;21(1):26-59.

153. Regev-Shoshani G, Ko M, Crowe A, Av-Gay Y. Comparative Efficacy of Commercially Available and Emerging Antimicrobial Urinary Catheters Against Bacteriuria Caused by E. coli In Vitro. *Urology.* 2011;78(2):334-339.

154. Bjarnsholt T, Kirketerp-Moller K, Kristiansen S, et al. Silver against Pseudomonas aeruginosa biofilms. *APMIS.* Aug 2007;115(8):921-928.

155. Trampuz A, Widmer AF. Infections associated with orthopedic implants. *Curr. Opin. Infect. Dis.* Aug 2006;19(4):349-356.

156. Nishiguchi S, Kato H, Fujita H, et al. Titanium metals form direct bonding to bone after alkali and heat treatments. *Biomaterials.* Sep 2001;22(18):2525-2533.

157. Sporer SM, Paprosky WG. Biologic fixation and bone ingrowth. *Orthop. Clin. North Am.* Jan 2005;36(1):105-111, vii.

158. Hirakawa K, Jacobs JJ, Urban R, Saito T. Mechanisms of failure of total hip replacements: lessons learned from retrieval studies. *Clin. Orthop. Relat. Res.* Mar 2004(420):10-17.

159. Morscher EW. Failures and successes in total hip replacement--why good ideas may not work. *Scand. J. Surg.* 2003;92(2):113-120.

160. Grainger DW. Targeted delivery of therapeutics to bone and connective tissues. *Adv. Drug Delivery. Rev.* 2012;64(12):1061-1062.

161. Verron E, Khairoun I, Guicheux J, Bouler J-M. Calcium phosphate biomaterials as bone drug delivery systems: a review. *Drug Discov. Today.* 2010;15(13–14):547-552.

162. Doll B, Sfeir C, Winn SR, Huard J, Hollinger J. Critical aspects of tissue-engineered therapy for bone regeneration. *Crit. Rev. Eukaryot. Gene Expr.* 2001;11(1-3):173-198.

163. Leach JK, Mooney DJ. Bone engineering by controlled delivery of osteoinductive molecules and cells. *Expert Opin. Biol. Ther.* 2004;4(7):1015-1027.

164. Gamradt SC, Lieberman JR. Genetic modification of stem cells to enhance bone repair. *Ann. Biomed. Eng.* 2004;32(1):136-147.

165. Samartzis D, Khanna N, Shen FH, An HS. Update on bone morphogenetic proteins and their application in spine surgery. *J. Am. Coll. Surg.* Feb 2005;200(2):236-248.

166. Luginbuehl V, Meinel L, Merkle HP, Gander B. Localized delivery of growth factors for bone repair. *Eur. J. Pharm. Biopharm.* Sep 2004;58(2):197-208.

167. Leach JK, Mooney DJ. Bone engineering by controlled delivery of osteoinductive molecules and cells. *Expert Opin. Biol. Ther.* Jul 2004;4(7):1015-1027.

168. Kandziora F, Bail H, Schmidmaier G, et al. Bone morphogenetic protein-2 application by a poly(D,L-lactide)-coated interbody cage: in vivo results of a new carrier for growth factors. *J. Neurosurg.* Jul 2002;97(1 Suppl):40-48.

169. Wang Y, Grainger DW. RNA therapeutics targeting osteoclast-mediated excessive bone resorption. *Adv. Drug Delivery. Rev.* 2012;64(12):1341-1357.

170. Holt DJ, Grainger DW. Demineralized bone matrix as a vehicle for delivering endogenous and exogenous therapeutics in bone repair. *Adv. Drug Delivery. Rev.* 2012;64(12):1123-1128.

171. Kofron MD, Laurencin CT. Bone tissue engineering by gene delivery. *Adv. Drug Delivery. Rev.* 2006;58(4):555-576.

172. Evans CH. Gene delivery to bone. *Adv. Drug Delivery. Rev.* 2012;64(12):1331-1340.

173. Del Pozo JL, Patel R. Infection Associated with Prosthetic Joints. *N. Engl. J. Med.* 2009;361(8):787-794.

174. Trippel SB. Antibiotic-impregnated cement in total joint arthroplasty. *J. Bone Joint Surg. Am.* Oct 1986;68(8):1297-1302.

175. Huang YY, Chung TW. Microencapsulation of gentamicin in biodegradable PLA and/or PLA/PEG copolymer. *J. Microencapsul.* Jul-Aug 2001;18(4):457-465.

176. Yu D, Wong J, Matsuda Y, Fox JL, Higuchi WI, Otsuka M. Self-setting hydroxyapatite cement: a novel skeletal drug-delivery system for antibiotics. *J. Pharm. Sci.* Jun 1992;81(6):529-531.

177. Espehaug B, Engesaeter LB, Vollset SE, Havelin LI, Langeland N. Antibiotic prophylaxis in total hip arthroplasty. Review of 10,905 primary cemented total hip replacements reported to the Norwegian arthroplasty register, 1987 to 1995. *J. Bone Joint Surg. Br.* Jul 1997;79(4):590-595.

178. Picknell B, Mizen L, Sutherland R. Antibacterial activity of antibiotics in acrylic bone cement. *J. Bone Joint Surg. Br.* Aug 1977;59(3):302-307.

179. Elson RA, Jephcott AE, McGechie DB, Verettas D. Bacterial infection and acrylic cement in the rat. *J. Bone Joint Surg. Br.* Nov 1977;59-B(4):452-457.

180. Nijhof MW, Stallmann HP, Vogely HC, et al. Prevention of infection with tobramycin-containing bone cement or systemic cefazolin in an animal model. *J. Biomed. Mater. Res.* Dec 15 2000;52(4):709-715.

181. Wahlig H, Dingeldein E, Bergmann R, Reuss K. The release of gentamicin from polymethylmethacrylate beads. An experimental and pharmacokinetic study. *J. Bone Joint Surg. Br.* May 1978;60-B(2):270-275.

182. Hoff SF, Fitzgerald RH, Jr., Kelly PJ. The depot administration of penicillin G and gentamicin in acrylic bone cement. *J. Bone Joint Surg. Am.* Jun 1981;63(5):798-804.

183. Bunetel L, Segui A, Cormier M, Percheron E, Langlais F. Release of gentamicin from acrylic bone cement. *Clin. Pharmacokinet.* Oct 1989;17(4):291-297.

184. Walenkamp GH, Vree TB, van Rens TJ. Gentamicin-PMMA beads. Pharmacokinetic and nephrotoxicological study. *Clin. Orthop. Relat. Res.* Apr 1986(205):171-183.

185. Lucke M, Schmidmaier G, Sadoni S, et al. Gentamicin coating of metallic implants reduces implant-related osteomyelitis in rats. *Bone.* May 2003;32(5):521-531.

186. Schmidmaier G, Lucke M, Wildemann B, Haas NP, Raschke M. Prophylaxis and treatment of implant-related infections by antibiotic-coated implants: a review. *Injury.* May 2006;37 Suppl 2:S105-112.

187. Forster H, Marotta JS, Heseltine K, Milner R, Jani S. Bactericidal activity of antimicrobial coated polyurethane sleeves for external fixation pins. *J. Orthop. Res.* May 2004;22(3):671-677.

188. Barie PS. Surgical site infections: epidemiology and prevention. *Surg Infect (Larchmt).* 2002;3 Suppl 1:S9-21.

189. Edmiston CE, Seabrook GR, Goheen MP, et al. Bacterial adherence to surgical sutures: can antibacterial-coated sutures reduce the risk of microbial contamination? *J. Am. Coll. Surg.* Oct 2006;203(4):481-489.

190. Osterberg B, Blomstedt B. Effect of suture materials on bacterial survival in infected wounds. An experimental study. *Acta Chir. Scand.* 1979;145(7):431-434.

191. Katz S, Izhar M, Mirelman D. Bacterial adherence to surgical sutures. A possible factor in suture induced infection. *Ann. Surg.* Jul 1981;194(1):35-41.

192. Rothenburger S, Spangler D, Bhende S, Burkley D. In vitro antimicrobial evaluation of Coated VICRYL* Plus Antibacterial Suture (coated polyglactin 910 with triclosan) using zone of inhibition assays. *Surg Infect (Larchmt).* 2002;3 Suppl 1:S79-87.

193. Storch M, Perry LC, Davidson JM, Ward JJ. A 28-day study of the effect of Coated VICRYL* Plus Antibacterial Suture (coated polyglactin 910 suture with triclosan) on wound healing in guinea pig linear incisional skin wounds. *Surg Infect (Larchmt).* 2002;3 Suppl 1:S89-98.

194. Galal I, El-Hindawy K. Impact of using triclosan-antibacterial sutures on incidence of surgical site infection. *Am. J. Surg.* Aug 2011;202(2):133-138.

195. Deliaert AE, Van den Kerckhove E, Tuinder S, et al. The effect of triclosan-coated sutures in wound healing. A double blind randomised prospective pilot study. *J. Plast. Reconstr. Aesthet. Surg.* Jun 2009;62(6):771-773.

196. Moneta GL, Porter JM. Arterial substitutes in peripheral vascular surgery: a review. *J. Long. Term Eff. Med. Implants.* 1995;5(1):47-67.

197. Heyligers JM, Verhagen HJ, Rotmans JI, et al. Heparin immobilization reduces thrombogenicity of small-caliber expanded polytetrafluoroethylene grafts. *J. Vasc. Surg.* Mar 2006;43(3):587-591.

198. Drake JM, Kestle JR, Tuli S. CSF shunts 50 years on--past, present and future. *Childs Nerv. Syst.* Nov 2000;16(10-11):800-804.

199. Pople IK, Bayston R, Hayward RD. Infection of cerebrospinal fluid shunts in infants: a study of etiological factors. *J. Neurosurg.* 1992;77(1):29-36.

200. Farber SH, Parker SL, Adogwa O, Rigamonti D, McGirt MJ. Cost analysis of antibiotic-impregnated catheters in the treatment of hydrocephalus in adult patients. *World Neurosurgery.* Oct-Nov 2010;74(4-5):528-531.

201. Eymann R, Chehab S, Strowitzki M, Steudel WI, Kiefer M. Clinical and economic consequences of antibiotic-impregnated cerebrospinal fluid shunt catheters. *J. Neurosurg. Pediatr.* Jun 2008;1(6):444-450.

202. Wong GK, Ip M, Poon WS, Mak CW, Ng RY. Antibiotics-impregnated ventricular catheter versus systemic antibiotics for prevention of nosocomial CSF and non-

CSF infections: a prospective randomised clinical trial. *J. Neurol. Neurosurg. Psychiatry.* Oct 2010;81(10):1064-1067.

203. Pattavilakom A, Kotasnas D, Korman TM, Xenos C, Danks A. Duration of in vivo antimicrobial activity of antibiotic-impregnated cerebrospinal fluid catheters. *Neurosurgery.* May 2006;58(5):930-935; discussion 930-935.

204. Webster J. Handwashing in a neonatal intensive care nursery: product acceptability and effectiveness of chlorhexidine gluconate 4% and triclosan 1%. *J. Hosp. Infect.* Jun 1992;21(2):137-141.

205. von Plocki SC, Armbruster D, Klein K, et al. Biodegradable Sleeves for Metal Implants to Prevent Implant-Associated Infection: An Experimental In Vivo Study in Sheep. *Vet. Surg.* 2012;41(3):410-421.

206. Henslee AM, Spicer PP, Yoon DM, et al. Biodegradable composite scaffolds incorporating an intramedullary rod and delivering bone morphogenetic protein-2 for stabilization and bone regeneration in segmental long bone defects. *Acta Biomater.* Oct 2011;7(10):3627-3637.

207. Trajkovski B, Petersen A, Strube P, Mehta M, Duda GN. Intra-operatively customized implant coating strategies for local and controlled drug delivery to bone. *Adv. Drug Delivery. Rev.* Sep 2012;64(12):1142-1151.

208. Lendlein A, Langer R. Biodegradable, elastic shape-memory polymers for potential biomedical applications. *Science.* May 31 2002;296(5573):1673-1676.

209. Shmulewitz A, Langer R, Patton J. Convergence in biomedical technology. *Nat Biotech.* 2006;24(3):277-277.

210. Yakacki CM, Shandas R, Lanning C, Rech B, Eckstein A, Gall K. Unconstrained recovery characterization of shape-memory polymer networks for cardiovascular applications. *Biomaterials.* 2007;28(14):2255-2263.

211. Janib SM, Moses AS, MacKay JA. Imaging and drug delivery using theranostic nanoparticles. *Adv. Drug Delivery. Rev.* 2010;62(11):1052-1063.

212. Kopecek J, Kopeckova P. HPMA copolymers: origins, early developments, present, and future. *Adv. Drug Delivery. Rev.* Feb 17 2010;62(2):122-149.

213. Lu ZR. Molecular imaging of HPMA copolymers: Visualizing drug delivery in cell, mouse and man. *Adv. Drug Delivery. Rev.* 2010;62(2):246-257.

214. Choi SK, Thomas T, Li MH, Kotlyar A, Desai A, Baker JR, Jr. Light-controlled release of caged doxorubicin from folate receptor-targeting PAMAM dendrimer nanoconjugate. *Chem. Commun.* Apr 21 2010;46(15):2632-2634.

215. Konda SD, Aref M, Wang S, Brechbiel M, Wiener EC. Specific targeting of folate–dendrimer MRI contrast agents to the high affinity folate receptor expressed in ovarian tumor xenografts. *Magnetic Resonance Materials in Physics, Biology and Medicine.* 2001;12(2–3):104-113.

216. Erdogan S, Torchilin VP. Gadolinium-loaded polychelating polymer-containing tumor-targeted liposomes. *Methods Mol. Biol.* 2010;605:321-334.

217. Al-Jamal W, Al-Jamal KT, Tian B, Cakebread A, Halket JM, Kostarelos K. Tumor targeting of functionalized quantum dot liposome hybrids by intravenous administration. *Mol. Pharm.* 2009;6(2):520-530.

218. Kwon IK, Lee SC, Han B, Park K. Analysis on the current status of targeted drug delivery to tumors. *J. Control. Release.* Jul 16 2012.

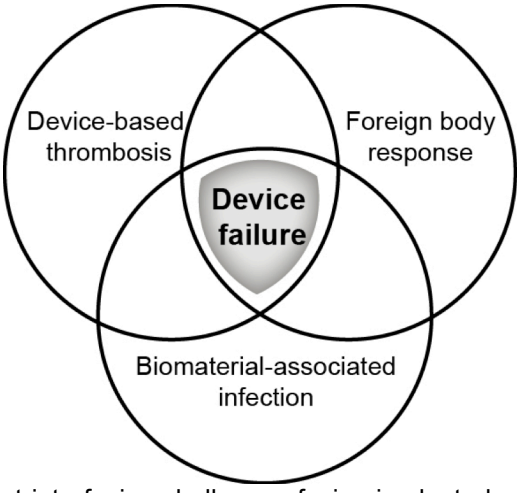

Figure 2.1: General host-interfacing challenges facing implanted medical devices.

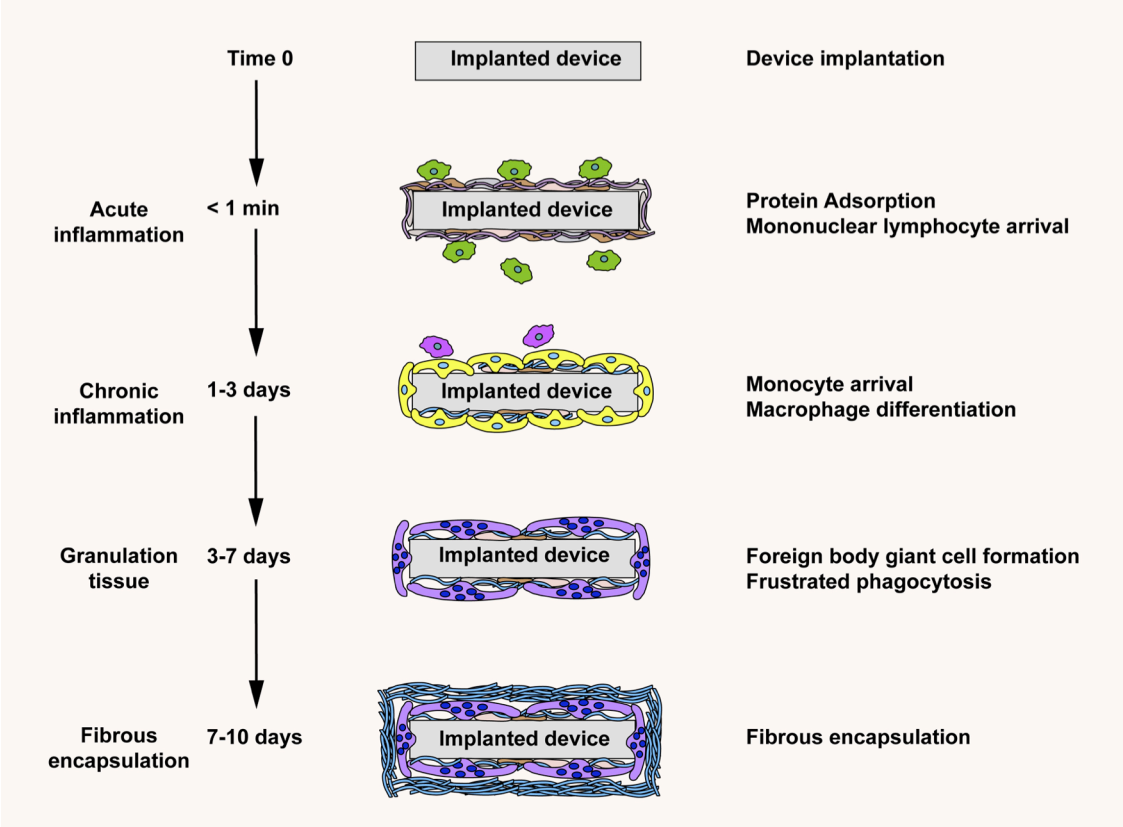

Figure 2.2: Illustration of the temporal series of host biological events during the host foreign body response following biomaterial implantation.

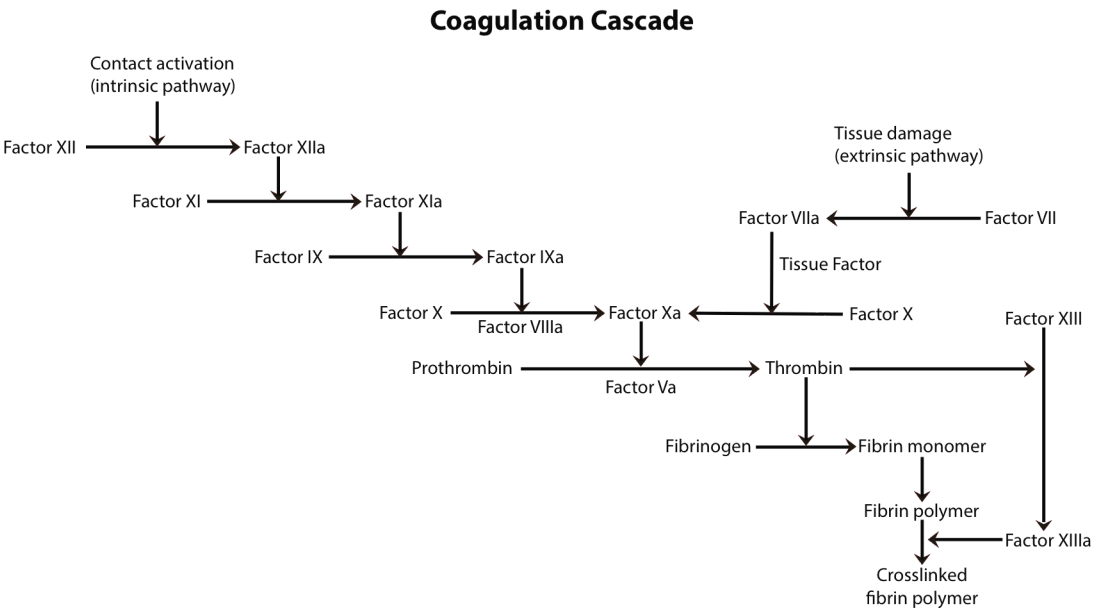

Figure 2.3: Extrinsic and intrinsic cascades for the zymogens, active proteins, and clotting factors mediating clot formation after procoagulant stimulus.

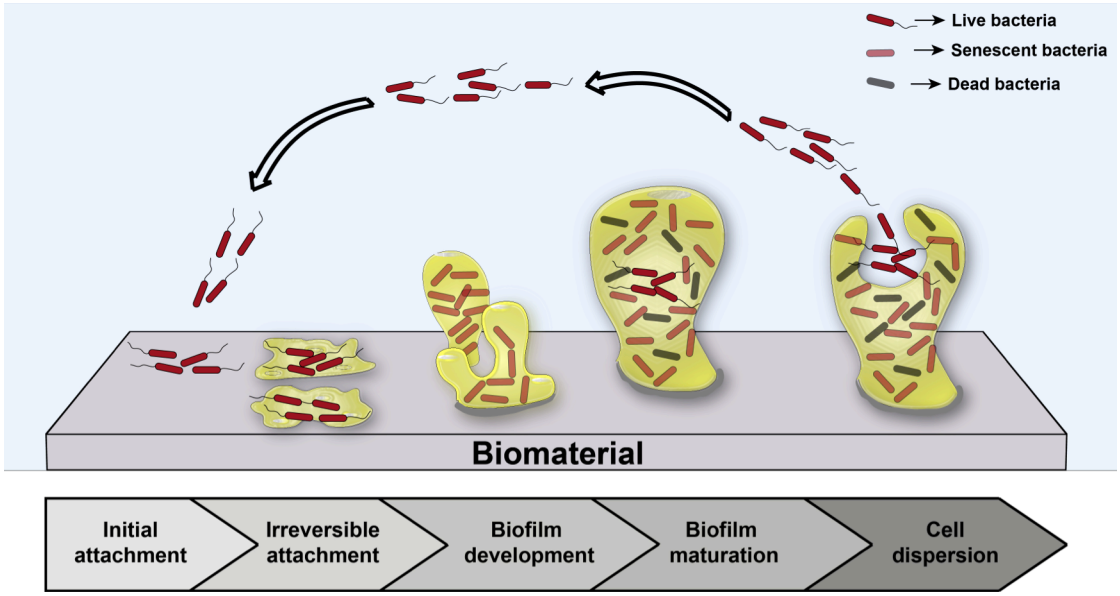

Figure 2.4: Bacterial seeding, colonization, biofilm transformation, differentiation, maturation, and further dissemination producing following biomaterial-associated contamination and infection.

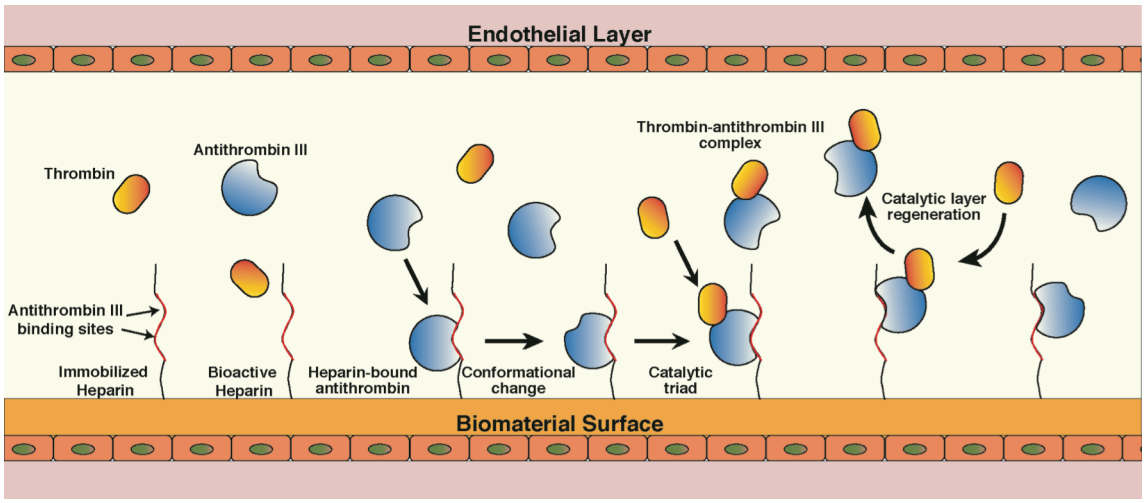

Figure 2.5: Bioactive heparin-immobilized surface capable of inhibiting thrombin activation, a key mediator in clot formation. The strategy is used for blood-contacting devices to limit complications from device-based thrombosis. (adapted from illustration of Carmeda™ coating, W.L. Gore & Associates, USA)

Table 2.1: Diversity of combination medical products used in physical or chemical combinations, or co-packaged as a kit, or as separate cross-labeled products.

Combination product type	Clinical examples
Drug and device	Drug-eluting stents, antimicrobial catheters, tibial nail, and sutures
Drug and biologic	Autologous platelet concentrate delivery of gentamycin to a open fracture; demineralized bone matrix delivery of statins to bone defect
Biologic and device	Heparin-coated vascular grafts, insulin infusion pumps, spinal cages with rhBMP-2
Drug and biologic and device	(No precedents approved); fictional example: adenoviral NfkB transgene delivery from Taxol-eluting vascular stent.

CHAPTER 3

MODULATION OF THE FOREIGN BODY RESPONSE TO IMPLANTED SENSOR MODELS THROUGH DEVICE-BASED DELIVERY OF THE TYROSINE KINASE INHIBITOR, MASITINIB

M. Avula[1], A.N. Rao[2], L.D. McGill[3], D.W. Grainger[1,2*], F. Solzbacher[1,4]

[1]Department of Bioengineering, University of Utah, Salt Lake City, UT 84112 USA

[2]Department of Pharmaceutics and Pharmaceutical Chemistry, University of Utah, Salt Lake City, UT 84112 USA

[3]Associated Regional and University Pathologist Laboratories, University of Utah, Salt Lake City, UT 84112 USA

[4]Department of Electrical and Computer Engineering, University of Utah, Salt Lake City, UT 84112 USA

[*]corresponding author – David W. Grainger, david.grainger@utah.edu

Keywords: foreign body response, continuous glucose monitoring, sensors, mast cells, tyrosine kinase inhibitor, local drug delivery, PLGA microspheres, biomedical implants

---

Reprinted with permission from: Biomaterials. 2013; 34: 9737-46

Biomaterials 34 (2013) 9737–9746

Contents lists available at ScienceDirect

Biomaterials

journal homepage: www.elsevier.com/locate/biomaterials

Modulation of the foreign body response to implanted sensor models through device-based delivery of the tyrosine kinase inhibitor, masitinib

Mahender Nath Avula [a], Archana Nagaraja Rao [b], Lawrence D. McGill [c], David William Grainger [a, b, *], Florian Solzbacher [a, d]

[a] Department of Bioengineering, University of Utah, Salt Lake City, UT 84112, USA
[b] Department of Pharmaceutics and Pharmaceutical Chemistry, University of Utah, Salt Lake City, UT 84112, USA
[c] Associated Regional and University Pathologist Laboratories, University of Utah, Salt Lake City, UT 84112, USA
[d] Department of Electrical and Computer Engineering, University of Utah, Salt Lake City, UT 84112, USA

ARTICLE INFO

Article history:
Received 5 July 2013
Accepted 30 August 2013
Available online 20 September 2013

Keywords:
Foreign body response
Continuous glucose monitoring sensors
Mast cells
Tyrosine kinase inhibitor
Local drug delivery
Biomedical implants

ABSTRACT

The host foreign body response (FBR) adversely effects the performance of numerous implanted biomaterials especially biosensors, including clinically popular glucose-monitoring sensors. Reactive formation of a fibrous capsule around implanted sensors hinders the transport of essential analytes to the sensor from the surrounding tissue, resulting in loss of glucose response sensitivity and eventual sensor failure. Several strategies have sought to mitigate the foreign body response's effects on CGM sensors through the use of local delivery of pharmaceuticals and biomolecules with limited success. This study describes release of a tyrosine kinase inhibitor – masitinib – from the sensor implant to target tissue resident mast cells as key mediators of the FBR. Model implants are coated with a composite polymer hydrophilic matrix that rapidly dissolves upon tissue implantation to deposit slower-degrading polymer microparticles containing masitinib. Matrix dissolution limits coating interference with sensor function while establishing a local controlled-release delivery depot formulation to alter implant tissue pharmacology and addressing the FBR. Drug efficacy was evaluated in a murine subcutaneous pocket implant model. Drug release extends to more than 30 days *in vitro*. The resulting FBR *in vivo*, evaluated by implant capsule thickness and inflammatory cell densities at 14, 21, and 28 days, displays statistically significant reduction in capsule thickness around masitinib-releasing implant sites compared to control implant sites.

1. Introduction

The host's acute and chronic foreign body response (FBR) remains an important, unsolved challenge for many implantable medical devices (IMDs). As the implantation of almost every medical device creates a wound (e.g., knee arthroplasty, pacemaker), or local disturbance in a tissue bed (e.g., contact lens, catheter needle), a normal host tissue wounding response is spontaneously initiated. This reaction begins normally but is quickly and irreversibly altered in acute and chronic wound healing phases in the presence of an implant, producing the FBR. This is primarily a chronic, unresolved tissue healing response, often resulting in extended inflammation, granulomatous tissue and eventually excessive fibrosis. In particular, sensor implants like continuous glucose monitoring sensors (CGM), pacemaker electrical leads [1], and neural deep brain stimulation arrays [2] undergo fibrosis that hinders device feedback and function. Clinically common CGM exploits implanted glucose-sensitive sensor technologies [3–6], subcutaneous fibrosis around the CGM compromises glucose and co-analyte (e.g., oxygen) diffusion, altering the CGM reporting response. Clinically, this reduces implant lifetimes for these expensive CGM devices in humans [7–9], resulting in regulatory mandates that restrict their *in vivo* use to a few days. Resulting avascular fibrous tissue surrounding the implant impedes the implant's electrical [10] and chemical contact with the surrounding tissue while also depriving it of essential analytes [10] and nutrients, rendering implants unreliable. Extending the functional clinical lifetime of CGMs specifically and IMDs generally,

* Corresponding author. Department of Pharmaceutics and Pharmaceutical Chemistry, University of Utah, Salt Lake City, UT 84112, USA.
E-mail address: david.grainger@utah.edu (D.W. Grainger).

0142-9612/$ – see front matter © 2013 Elsevier Ltd. All rights reserved.
http://dx.doi.org/10.1016/j.biomaterials.2013.08.090

while reducing their adverse events *in vivo*, remains an important goal that can profoundly impact the use of current device technologies *in vivo*. Nonetheless, despite many CGM device improvements and design changes, this goal remains elusive.

Many CGMs are placed subcutaneously where normal sensor fouling, including protein adsorption onto or penetration into the implanted sensors, as well as inflammatory wound-site cellular reactions, eventually hinder analyte diffusion (i.e., glucose and oxygen primarily) into the sensing element, and contribute to the observed continual decreased analyte sensitivity with prolonged implantation [4,8,11]. In addition to ubiquitous sensor fouling and encapsulation, the host's acute inflammatory response to the implanted foreign body produces an immediate, sustained cascade of local tissue cellular reactions that alter the local environment around the implant, substantially modifying local metabolism and homeostasis, some that alter analyte levels. This triggers a departure from normal tissue analyte levels and causes the sensors to produce highly altered analyte levels solely from acute inflammation – an acute reporting phenomenon called "break-in" [12]. Return to normal tissue homeostasis after break-in is critical to reliable sensor function and CGM and other sensor reporting fidelity.

As the FBR in soft and hard tissue sites typically produces device-based challenges associated with excess or unresolved tissue inflammation, fibrosis, and infection, combination device strategies seeking to address this issue have used drugs with known pharmacological actions against these specific problems [13,14]. In this regard, several strategies employ various drugs and biomolecules to specifically mitigate FBR to soft tissue implants with limited success. These include targeting local inflammation around the implant, targeting collagen production from recruited wound healing fibroblasts, and/or stimulating the local growth of new vasculature using vascular endothelial growth factor (VEGF). Diverse past efforts for local drug release from sensor implants *in vivo* to improve device performance are shown in Table 1.

Mast cells (MC) play critical roles in mediating acute phases of the tissue inflammatory response following sensor implantation: they are located perivascularly throughout all tissues and are mobilized during any inflammatory stimuli. MC degranulation of histamine and other pro-inflammatory mediators including heparin, cytokines (TNF-alpha), chemokines, and many proteases together with fibrinogen adsorption are recognized as powerful inducers of acute inflammatory responses to implanted biomaterials [21,22]. MC-released cytokines produce cell chemotaxis along with histamine and serotonin prompting vasodilation and increased recruitment of phagocytes to the implant site. Their role in FBR has long been recognized [23–25].

Specific to CGMs, Klueh et al. [26] have recently compared *in vivo* CGM subcutaneous implant performance in both wild-type and mutant MC-deficient (W-sash) mice. Significantly, they confirmed, based on changing CGM signal-to-noise ratio (S/N) and analyte response time as a function of implant time, that MCs play a major role in the host FBR around CGMs. Importantly, this was linked to subsequent fibrous capsule formation around the CGM that impedes sensor function [26].

The operative mechanism behind apparent MC regulation of the host FBR has been elusive. One recent finding is that stem cell factor (SCF), the ligand of the MC-specific c-KIT tyrosine kinase receptor, is an important growth factor for MC survival, proliferation, differentiation, and degranulation processes [27]. The correlation between the MC-specific SCF/MC c-KIT pathway and the intensity of the acute inflammatory response is critical in MC function and degranulation reactions [27]. Recent work shows that masitinib, a newly screened tyrosine kinase inhibitor, effectively inhibits the mast cell SCF receptor, c-KIT, and is a potent inducer controlling MC reactivity [28,29] by binding competitively to the ATP-binding c-KIT receptor, and blocks its critical tyrosine kinase signaling activity. Importantly, this action stabilizes MCs from degranulating or activating. A recent study [28] concludes that masitinib is a potent TKI that stabilizes MC reactivity both *in vitro* and *in vivo* when compared to imatinib mesylate, another widely used TKI to inhibit c-KIT [30]. As an indicator of common TKI bioactivity pathways, imatinib mesylate has already been shown to reduce production of extracellular matrix and prevent development of experimental non-implant fibrosis [31]. Masitinib is selective at inhibiting recombinant human c-KIT receptor [28], as well as platelet derived growth factor receptor (PDGFR), while weakly inhibiting other type III tyrosine kinase receptors, including fibroblast growth factor receptor 3 (FGFR3) and FCεRI receptor. The clinically approved TKI imatinib by contrast inhibits a broader range of receptors [28]. These receptors, when bound to stimulatory ligands like IgE, SCF, C3a, and PAMPs, result in mast cell activity and degranulation [32] leading to increased inflammatory cell activity. Masitinib is currently in clinical trials as an oral therapeutic for Alzheimer's disease [33], pancreatic cancer [34], canine mastocytosis [29], gastro-intestinal stromal tumors [35], and rheumatoid arthritis [36].

In this study, we hypothesized that targeting MCs recruited to implant sites with the TKI masitinib to inhibit MC degranulation will result in reduced FBR to soft tissue implants such as CGMs. This hypothesis was tested using implanted model non-functional polymer fiber implants as mimics for the geometry of commercially available CGMs, coated with a masitinib-releasing formulation subcutaneously in wild-type C57BL\6J mice. Drug-loaded poly(lactic-co-glycolic acid) (PLGA) microspheres loaded into coatings on implanted fibers delivered masitinib locally to the implant tissue. These masitinib-loaded PLGA microspheres were coated around the fiber implants using a blended polyethylene glycol/polyethylene oxide (PEG/PEO) soluble matrix used transiently only to carry the drug microspheres to the wound site during the implantation process. This polymer matrix was designed to rapidly dissolve in wound bed fluids within a few minutes of

Table 1
Summary of published outcomes for locally released drugs and bioactive agents to enhance the performance of combination CGM sensor implants in the context of the foreign body response.

Investigator	Drug release	Key findings
Klueh et al. [15]	VEGF	Significant neovascularization surrounding the implanted sensor resulting in enhanced glucose sensor function *in vivo*
Moussy et al. [16]	Dexamethasone/PLGA microspheres	Reduced inflammation at the site and implanted suture for more than a month
Reichert et al. [17]	Dexamethasone and VEGF co-release	Reduced inflammation at 2 weeks after implantation; however, no enhanced vessel formation was observed indicating that dexamethasone diminished VEGF effects
Schoenfisch et al. [18]	Nitric oxide	Reduced foreign body response at nitric oxide-releasing subcutaneous implants
Ward et al. [19]	VEGF infusion	Vascularization of foreign body capsule surrounding subcutaneous biosensor to extend sensor life
Takahashi et al. [20]	mTOR siRNA	Reduction of mTOR and collagen in fibroblasts; no difference *in vivo* in capsule thickness

implantation, eliminating any barrier interference to sensor function and leaving the drug-loaded PLGA microspheres behind adjacent to the implant. These implants were evaluated for drug release and inflammatory modulation in a standard murine subcutaneous implant model to 4 weeks and evaluated histologically for FBR markers.

2. Materials and methods

2.1. Materials

Poly(lactic-co-glycolic acid) (PLGA) of 3 different intrinsic viscosities (PLGA 1A: 0.05–0.15 dL/g, 2A: 0.15–0.25 dL/g, and 4A: 0.35–0.45 dL/g) was purchased from Lakeshore Biomaterials (now Evonik Biomaterials, USA). Polyethylene glycol (PEG), polyethylene oxide (PEO), poly(vinyl alcohol) (PVA), and solvents – dichloromethane (DCM), dimethyl sulfoxide (DMSO), chloroform, ethanol, methanol, and acetonitrile – were purchased from Sigma Aldrich, USA. Masitinib drug was purchased from Selleck Chemicals, USA. Commercial polyester fiber (Trilene, 300 μm diameter, Berkley Fishing, USA) was cleaned using 70% ethanol. Ultrapure water (Millipore filtered ASTM Grade II) was used for all experiments.

2.2. Fabrication of masitinib-loaded PLGA microspheres

Drug-loaded PLGA microspheres comprising PLGA 1A, 2A, and 4A were synthesized separately using an established solvent-evaporation technique [37]. A solution of 500 μg/ml masitinib in DCM was sonicated for 30 min to allow complete dissolution. Then 100 mg of PLGA was mixed into 2 ml of drug-DCM solution and allowed to dissolve for 30 min, yielding a polymer-drug solution. PVA (10 ml of 5% w/v) in water was mechanically stirred in a 100-ml beaker at 800 rpm while slowly adding the polymer-drug solution drop-wise through a separatory funnel. The resulting oil-in-water emulsion was stirred at 800 rpm for 5 h to evaporate DCM. The emulsion was collected and centrifuged at 10,000 rpm for 10 min at −4 °C to remove free drug and PLGA in solution before re-suspending the product microspheres in 2 ml water. The final suspension was stored at −80 °C and the frozen sample was lyophilized for 24 h at −50 °C and 0.02 bar pressure. The product microspheres were characterized using scanning electron microscopy (SEM) for morphology and size analysis. Drug loading efficiency in PLGA microspheres was calculated using HPLC of product microspheres dissolved in chloroform at 5 mg/ml, known drug concentration standards, and equation (1):

$$\text{Drug loading efficiency} = \frac{\text{Drug obtained per mg of PLGA microspheres}}{\text{Drug added per mg of PLGA polymer}} \times 100\% \quad (1)$$

Control microspheres without drug in DCM were fabricated using the same process.

2.3. Drug release in vitro

Drug-loaded PLGA 1A, 2A and 4A microspheres ($n = 3$, 5 mg each) were suspended in separate vials with 1.5 ml of phosphate buffered saline (PBS) at pH 7.4 and placed in a shaker maintained at 150 rpm and 37 °C for 30 days in sink release conditions. Aliquots of PBS were collected periodically to quantify drug release. Vials were placed in a centrifuge at 1000 rpm for 3 min. Aliquots (1 ml) of the supernatant were collected for drug quantification and the release study vials were then replenished with equal amounts of fresh PBS solution and placed back in the shaker for later time points.

Samples were collected at regular intervals over a 30-day period and analyzed using HPLC to quantify the amount of released masitinib. An HPLC standard curve for masitinib calibration was prepared and area under the curve from the characteristic HPLC drug peak was calculated and drug loading in the microspheres was quantified using the standard curve.

2.4. PEG–PLGA composite coatings on model sensor fiber implants

PLGA microspheres were coated over fiber model implants using a PEG/PEO uncrosslinked blended matrix. The water-soluble matrix was designed using GRAS ingredients to facilitate rapid PEG/PEO dissolution within a few minutes after implantation in the surrounding wound interstitial fluid, depositing PLGA-drug particles remain in the vicinity of the implant for local drug release while not hindering sensor function. An illustration of the coating design and strategy is shown in Fig. 1.

PEG/PEO coating compositions with 20,000 MW PEG and 100,000 MW PEO in the ratio of 1:9 were mixed in water at a concentration of 200 mg/ml. A polyester fiber (300 μm in diameter) was selected as a non-functional model implant to mimic a commercial CGM in implant dimensions. A 2-part aluminum 6061 mold was manufactured to coat the fiber with a resulting coating thickness of 350 μm on the model implant surface resulting in a 1 mm-thick (diameter) coated implant. Parylene C was first vapor-deposited onto the molds to act as a release agent. Equal amounts of PLGA 1A, 2A and 4A particles were added to the PEG/PEO aqueous solution at a concentration of 350 mg/ml. The resulting mixture was mixed thoroughly, forming a PEG–PLGA suspension. This suspension (30 μl) was dispensed into each cavity of the 2-part aluminum mold to coat the model fiber implants. After filling the cavities in the mold, the mold was closed tightly with screws and the polyester fiber model implants were then inserted into each PEG–PLGA suspension-filled cavity. The assembled mold with the model implants was then submerged into liquid nitrogen for flash freezing for 3 min. The frozen mold was then opened using a built-in release mechanism, and the 2 halves placed in glass jars and lyophilized for 12 h at −50 °C and 0.02 bar pressure. The final fiber implants, complete with PEG–PLGA composite coating, are gently released from the molds and a few random samples

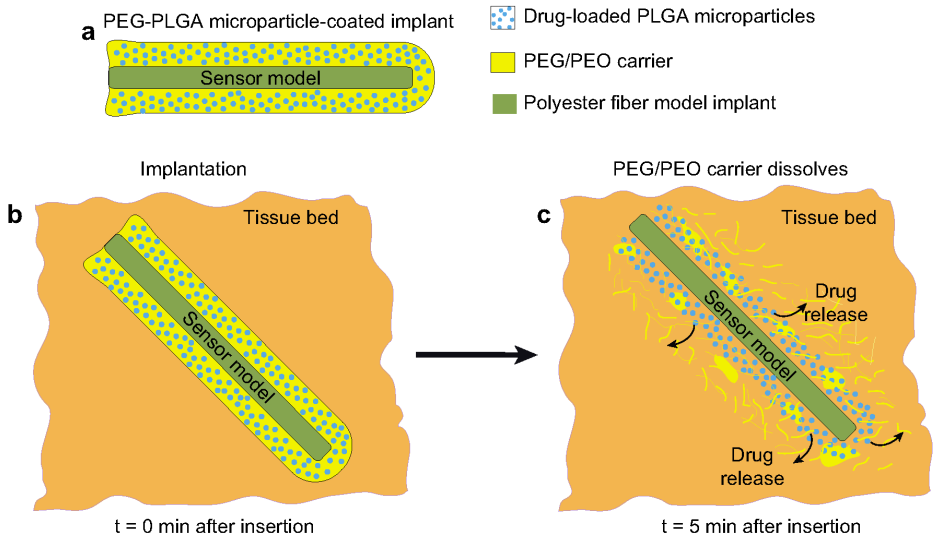

Fig. 1. Illustration of rapidly dissolving PEG–PLGA microsphere scaffold coating. a) Polyester fiber model sensor implant coated with PEG–PLGA microsphere coating, b) and c) Desired coating performance post-implantation *in vivo*.

were dissolved in chloroform to calculate the coating drug-loading efficiency using HPLC.

Intended masitinib load within each implant was calculated based on drug dosing values from Dubreuil et al. [28] and assumptions about the intended tissue delivery volume surrounding the implant. A tissue thickness of 200 μm was considered the target zone around each implant, and the potent dosing values were extrapolated for a 30-day release as the drug loading/implant. A margin of 1.5× was used in calculating the drug loading/implant to accommodate this required drug load. Implants were tested for viable bacterial contamination using blood agar cultures for a 24-hour incubation period. USP chromogenic LAL assay (Lonza, USA) was used to test for endotoxin content on the final implants. Implants ($n = 3$) coatings were dissolved in 1 ml water for 4 h and a 50 μl sample was analyzed for endotoxin (UV absorbance wavelength = 410 nm).

Polymer composite-coated implants containing the drug-loaded PLGA microspheres or control (PLGA, no-drug) microspheres were fabricated using the process described above. Dissolution tests were conducted to measure the time elapsed for PEG/PEO matrix dissolution observed visually. PEG–PLGA microsphere-coated implants were placed in 150 μl HPLC vial inserts containing 100 μl PBS solution. The time elapsed between matrix immersion in PBS and its dissolution from the fiber was noted.

2.5. In vivo implant studies

Male wild-type C57BL/6 mice (12–14 weeks) were purchased from Jackson Laboratories (USA). Animals were divided into 3 cohorts of 2, 3, and 4 weeks study time points with $n = 5$ for each time point. Each animal was implanted subcutaneously with one control and one masitinib-loaded fiber implant bilaterally across the spine in the dorsal regions.

2.5.1. Surgical implantation procedures

All procedures performed were approved by the institutional animal care and use committee, University of Utah. The surgical implant procedure was adapted with slight modifications from that published in a similar context by Klueh et al. [38]. Each animal was anesthetized using 1–2.5% isofluorane administered through a nose cap throughout the procedure. Each animal was placed on a warming water pad to maintain body temperature for the duration of surgery and recovery. An area of 6 × 4 cm^2 on the back of the animal was shaved and the exposed skin treated with betadine solution to create an aseptic environment at the surgical site. A sterile 18G needle was used to gently puncture the skin and to inject the wound site with 100 μl of pyrogen-free 0.9% NaCl solution to create a subcutaneous "pocket" for the implantation procedure. The needle was then removed and the implant was gently inserted through the puncture into the subcutaneous pocket created with the NaCl solution such that the entire implant is placed subcutaneously with no fiber protrusions through the animal's skin, and the perforated skin was then sealed with skin glue (Nexcare Skin Care, USA). The animal was then removed from anesthesia and monitored to complete recovery before placing it into a cage in 12-hour dark/light cycles for the duration of the study under normal food/water diet. Animals were housed in individual cages to prevent biting of each other's implant sites. They were divided into 3 cohorts with different study end points of 14, 21 and 28 days.

2.5.2. Explant histological analysis

At each time point, animals were euthanized using 100% CO_2 in a bell jar and the entire tissue bed surrounding the implant including the implant was harvested intact for histology. Harvested tissue was fixed in 10% neutral buffered formalin (Fisher Scientific) for 48 h with the formalin being replaced after 24 h. The fixed tissue was then sent to Associated Regional and University Pathologists (ARUP, USA) Laboratories for further processing and histological analytical guidance. Tissue samples were sectioned and stained with hematoxylin and eosin (H&E) stain to identify cell nuclei and to quantify inflammatory cell densities, and with Masson's trichrome stain to identify fibrosis and to quantify capsule thicknesses around implants. Toluidine blue staining was performed on the explant tissue samples to identify mast cells [39].

2.6. Inflammatory cell densities measurement

Cell densities on H&E-stained sections of implant tissue were determined microscopically by scoring the number of cells surrounding each implant in five representative 40× fields per sample. Cell density was expressed as a score of the number of cells present per field. Neutrophils and plasma cells, macrophages and foreign body giant cells, and fibroblasts were identified visually by morphology and scored at radial distances of 50 μm, 150 μm, and 300 μm implant interface for both control and masitinib-releasing implants. These cells were chosen to represent those typical of the foreign body response, with neutrophils representing the acute wound stage infiltrates, while macrophages and fibroblasts represent more chronic FBR and tissue resolution stages, respectively [9].

2.7. Capsule thickness measurement

Tissue sections stained with both H&E and Masson's trichrome were observed under bright field microscopy using a 10× objective, and images were captured and analyzed. Capsule thickness from fibrosis around each implant was measured at the interface of the implant and adipose tissue on the apical side, and also the interface of the implant and muscle tissue on the basal side. Multiple random locations ($n = 5$ per implant site, $N = 5$ implants) at these interfaces were chosen for the capsule thickness measurements using ImageJ software.

2.8. Statistical significance

All data are expressed as the mean ± 1 standard deviation and compared with an ANOVA test. Capsule thickness data for control implants were compared with masitinib-releasing implants for identical time points using Student's *T*-test assuming equal variance. Data were considered statistically significant for $p < 0.05$.

3. Results

3.1. Implant fabrication and characterization

PLGA microspheres with diameters in the range of 5–20 μm were obtained as characterized using SEM. Fig. 2A and B shows

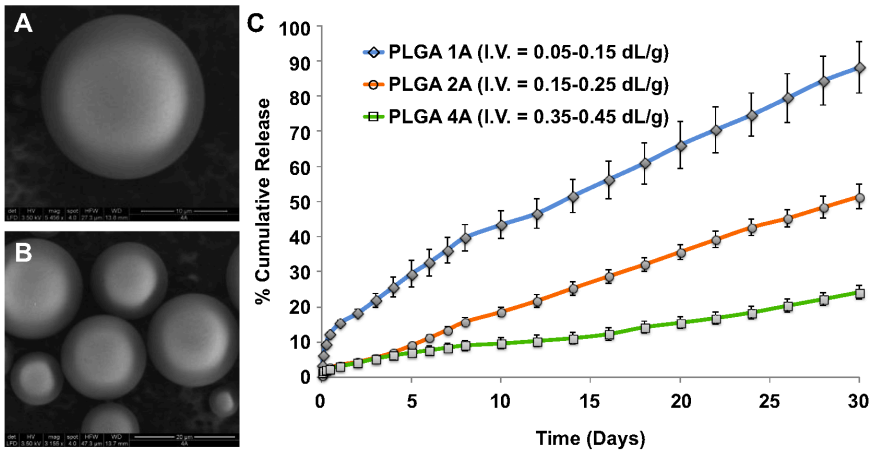

Fig. 2. PLGA microspheres synthesized using solvent-evaporation technique. A) and B) SEM micrographs of the PLGA microspheres, and C) Release profiles of the drug from PLGA microspheres synthesized from different molecular weight PLGAF.

electron micrographs of the microspheres. This size range is beyond the phagocytosable range of tissue site phagocytes, eliminating confounding effects of undesired cell particle uptake.

Drug-loading efficiency of the microspheres was calculated using equation (1) to be ~34% for PLGA 4A, ~55% for PLGA 2A and ~60% for PLGA 1A. During the first day of the *in vitro* drug release study, PLGA 1A exhibited a burst release of 15.4 ± 0.8% (mean ± standard deviation, $n = 3$) of total drug loading while PLGA 2A and 4A exhibited initial burst releases of 3.5 ± 0.3% and 3.2 ± 0.6%, respectively. Over 30 days, 88% of drug was released from PLGA 1A microspheres, while 51% and 25% drug released from PLGA 2A and 4A microspheres, respectively for the same time period. The *in vitro* release study results show an inverse relationship between the release rate and PLGA molecular weight (intrinsic viscosity) as shown in Fig. 2C.

A water-soluble PEG/PEO composition was used to coat implants using the 2-part aluminum molds (shown in Fig. 3A) and to produce the resulting implant matrices shown in Fig. 3B with the PEG–PLGA composite coating. These coatings were visually observed to dissolve *in vitro* in less than 3 min. These were characterized for drug-loading using HPLC analysis of release media *in vitro*. Masitinib loading in the PEG/PEO-PLGA microsphere composite coating on the implants was determined to be 11.2 ± 1.2 μg/implant (mean ± standard deviation, $n = 3$) using HPLC analysis. This dosing is ~1.5× the theoretically calculated dose required to target MCs in 200 μm-thick tissue volume surrounding the implant site at a desired concentration of 7.5 μg/implant, assuming complete clearance each day over the dosing interval. Dissolution tests for the matrix (Fig. 3C) show that the PEG/PEO-PLGA composite coating completely dissolves within 3 minutes upon exposure to release media. Blood agar cultures with the implants showed no bacterial colony formation after 24 hours of culture. LAL assay results show endotoxin content of 0.1 ng/implant which is negligible compared to the reported endotoxin clearance rate of 5 ng/kg/hr [40].

3.2. Inflammatory cell densities around implants in vivo

H&E-stained tissue preparations exhibit variable distributions of different inflammatory and wound-recruited cell densities for both control and masitinib-releasing implant sites at each time point as shown in Fig. 4. Densities of PMNs, macrophages, FBGCs, and fibroblasts were quantified as a function of distance from the implant surfaces. Cell densities up to distances of 300 μm from implant interfaces were considered in this analysis.

PLGA microspheres were observed (as shown in Fig. 5A) in a region between 100 μm and 300 μm distance from the implant edge for both the control and masitinib-releasing implants in the tissue sections. The presence of these microspheres validates the performance of the composite matrix designed to dissolve rapidly *in situ* to deposit masitinib-releasing or control PLGA microspheres in areas surrounding the implant. Most tissue inflammation markers were observed to be localized around PLGA microspheres located at implant sites, not at the fiber surfaces.

Implant-cell density responses shown in histology at the 14-day time point are shown in Fig. 5B for PMNs, macrophages, FBGCs, and fibroblasts. PMNs were observed in roughly equal, normal numbers around both control and masitinib-releasing implant sites. Macrophages and FBGCs were found in higher numbers closer to the implant sites (i.e., 50 μm and 150 μm) compared to these cell densities at 300 μm for control implants, while masitinib-releasing implant sites show higher macrophage densities at 150–200 μm distance from the implant site. Both control and masitinib-releasing implant sites show higher numbers of fibroblasts closer to the implant with decreasing fibroblast densities more distant from the implant site.

The same cell density analysis for the 21-day implant time point is shown in Fig. 5C. Noticeable differences are seen compared to the 14-day time point (i.e., in Fig. 5B) among the various cell types. PMN cell density around masitinib-releasing implant sites is higher than

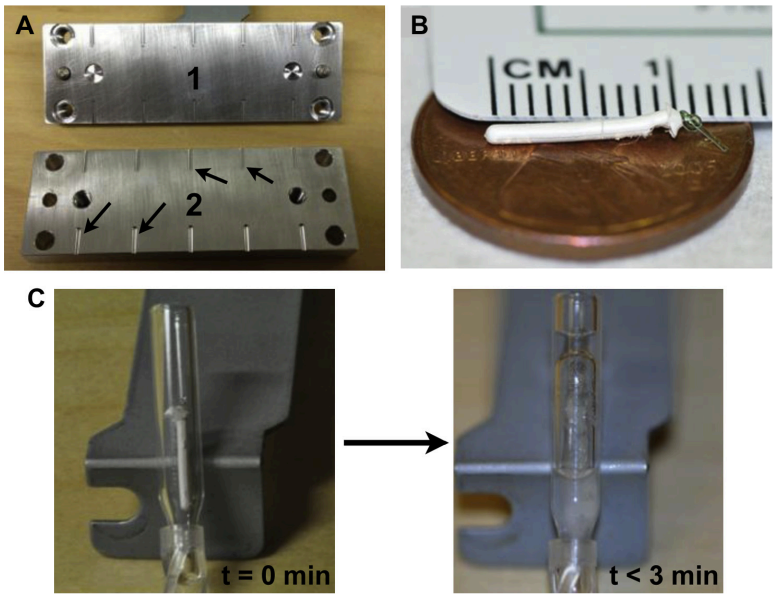

Fig. 3. PEG–PLGA scaffold-coated implants: A) Two-part aluminum mold used for the fabrication of the scaffold coating (arrows showing the cavities), B) A scaffold-coated polyester fiber model sensor implant (seen at the right in green), and C) Dissolution test showing the complete dissolution of the coating in less than 3 min. (For interpretation of the references to color in this figure legend, the reader is referred to the web version of this article.)

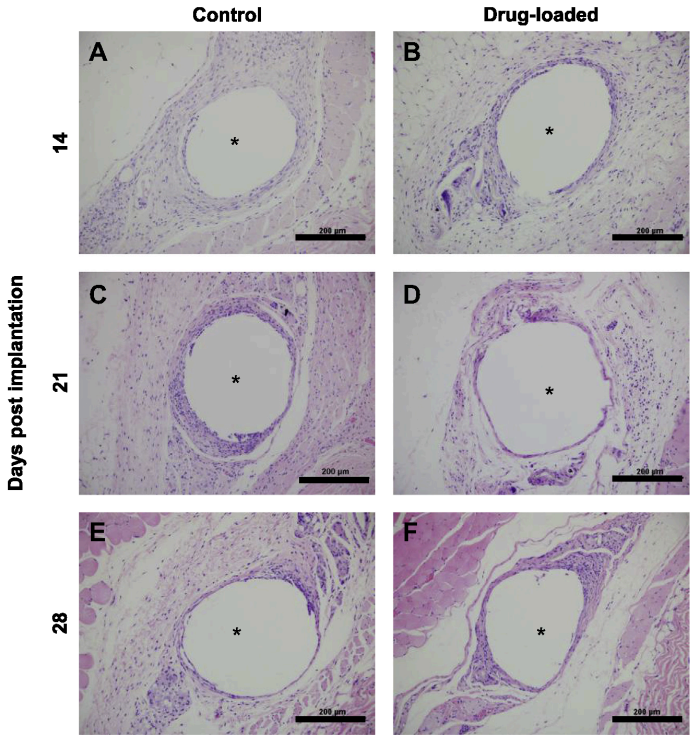

Fig. 4. H&E stained histology slides of A), C), and E) control implants and B), D), and F) drug-loaded implants for 14, 21 and 28 day time points respectively. Location of the implants is denoted by the asterisk '*'. Scale bar: 200 μm.

that around control implants. Macrophages and FBGCs are observed in higher numbers around the control implants compared to masitinib-releasing implant sites. Fibroblast cell densities decrease with increasing distance for control implant sites. Fibroblasts were observed in high numbers around PLGA microspheres 150–200 μm distance from masitinib-releasing implants.

Analogous cell density analysis for the 28-day time point (Fig. 5D) shows that PMNs are observed around both control and masitinib-releasing implant sites. High numbers of macrophages are observed around masitinib-releasing implant sites compared to control implants. Fibroblasts are also observed in higher numbers around masitinib-releasing implant sites compared to those around control implants. Mast cells seen in toluidine blue-stained explant tissue samples exhibited no discernable differences in their density or numbers between masitinib-releasing and control implant sites (shown in Fig. S1).

3.3. Implant capsule thickness

Masson's trichrome-stained (MTC) histology preparations were used to measure fibrous capsule thickness formed around implants at the different time points. Capsule thicknesses were measured at multiple locations between the arrows shown in Fig. 6. Fig. 7 plots capsule thicknesses for both implant types at respective time points. Capsule thickness values are averaged for measurements taken from 5 random locations on each implant site in 5 individual implant sites (i.e., $n = 5$ for $N = 5$). Capsule thickness values for control implant sites were found to be 42.16 ± 4.03 μm, 60.17 ± 6.91 μm, and 53.19 ± 17.39 μm for 14-, 21-, and 28-day time points, respectively, whereas they were 11.68 ± 1.12 μm, 14.46 ± 4.75 μm, and 14.95 ± 6.32 μm for tissue around the masitinib-releasing implant sites for these same respective time points. Capsule thickness measurements among control and masitinib-releasing implant groups show statistically significant difference ($p < 0.05$) for all time points as shown in Fig. 7.

4. Discussion

The host FBR poses a serious challenge to long-term performance of implantable sensors, now clinically important for CGM performance and effective diabetes management [41,42]. Fibrous capsule formation mediated by a complex series of cellular activities around the implant site results in the loss of CGM sensitivity [26]. Hence, improved strategies to mitigate the FBR to improve long-term sensing must be developed to make these devices effective, reliable and economical (summarized in Table 1). The new approach described here targets tissue MCs involved with the FBR using local therapeutic delivery of a known TKI-based MC inhibitor from the implanted sensor surface. Local delivery of masitinib exploits a combination device approach using locally delivered, microsphere controlled drug release formulations deposited into implant sites from coated subcutaneous model implants [13,14].

PLGA is a widely used degradable polymer for fabrication of controlled-release formulations for various pharmaceuticals and biomolecules [43–45]. PLGA microspheres of size range 5–20 μm are used here as the masitinib-releasing matrix. Particles >10 μm in

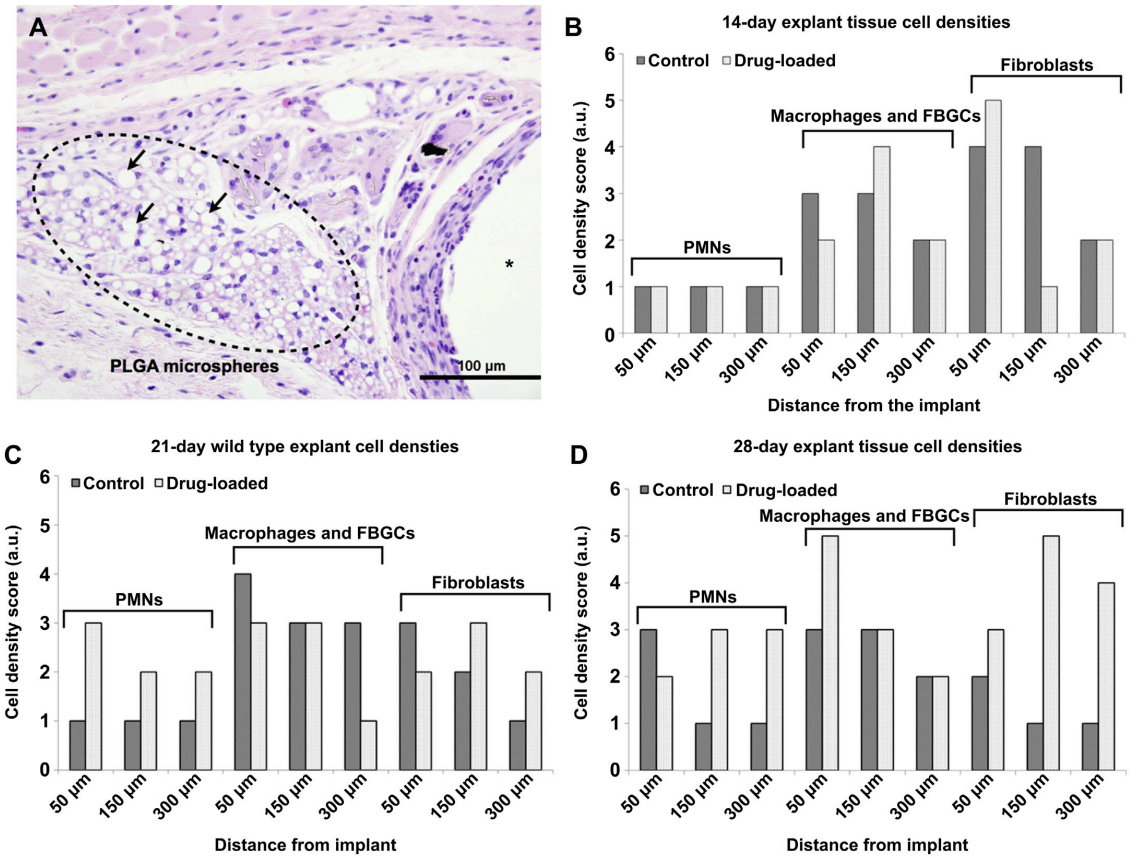

Fig. 5. Inflammatory cell density analysis as a function of distance from the implant interface. A) Histological evidence specific to PLGA microspheres (shown with arrows) around the implant sites; B), C), and D) Inflammatory cell density arbitrary observational scores from multiple histological fields around control and drug-loaded implants for the 14, 21, and 28 day time points, respectively. Location of the implant interface is denoted by the asterisk "*".

diameter are above the threshold of phagocytosis by macrophages [46]. Therefore, cell uptake and possible transport or metabolism of particles in this size range by macrophages should be limited. PLGA microspheres fabricated with different PLGA molecular weights provided a route to control the duration of masitinib release to several different time frames (Fig. 2). Sustained slow-release of the drug is useful for longer-term drug release applications that extend beyond the 4-week study period. A combination of microspheres of different molecular weight PLGAs can be used for a desired release profile with an initial burst release followed by sustained drug release for the desired duration.

These microspheres are deposited near implants via a sacrificial transient soluble polymer matrix on the device that dissolves rapidly upon implantation to avoid hindrance of sensor function while depositing a controlled-release depot of slower-degrading drug-loaded microspheres. A rapidly dissolving, biomedically accepted PEG/PEO carrier allows local tissue site deposition of the controlled-release PLGA microsphere vehicles containing masitinib. Its rapid dissolution (3 minutes) ensures that the carrier matrix does not hinder transport of tissue site glucose and oxygen required by many current clinical CGM sensors. PLGA drug-loaded microspheres are deposited directly in tissue in the implant vicinity (see Fig. 5A, 50–300 μm distant from the implant interface).

As the FBR around both masitinib-releasing and control implants is the collective result of a complex combination of factors including implant-tissue micromotion, both the presence of a monolithic implant (polyester fiber) together with a high surface area, low density implants (PLGA microspheres), and possible surface contamination during implantation (i.e., endotoxin, pathogens), interpreting data for inflammatory responses, especially cell density scores, is challenging and likely not attributed solely to local masitinib pharmacological influences. For example, implant-associated micromotion is known to delay the presence of PMNs at the implant site for days or even weeks after implantation [47]. Histology (Figs. 4–6) shows that implant placement is often directly over the subcutaneous muscle bed due to the thin cutaneous tissue space in this murine model, increasing the possibility for tissue micromotion and muscle irritation.

Inflammatory cell density data suggest that the host inflammatory responses to the implant-tissue interface and that around the microsphere-tissue interface have independent timelines. Cell-associated FBR responses around the fiber implant (distance < 50 μm) seem to follow the normal sequence of events, i.e., acute inflammation (PMNs), transition to macrophage recruitment and formation of FBGCs, recruitment of fibroblasts, on-going chronic inflammation and late tissue remodeling [9], whereas the

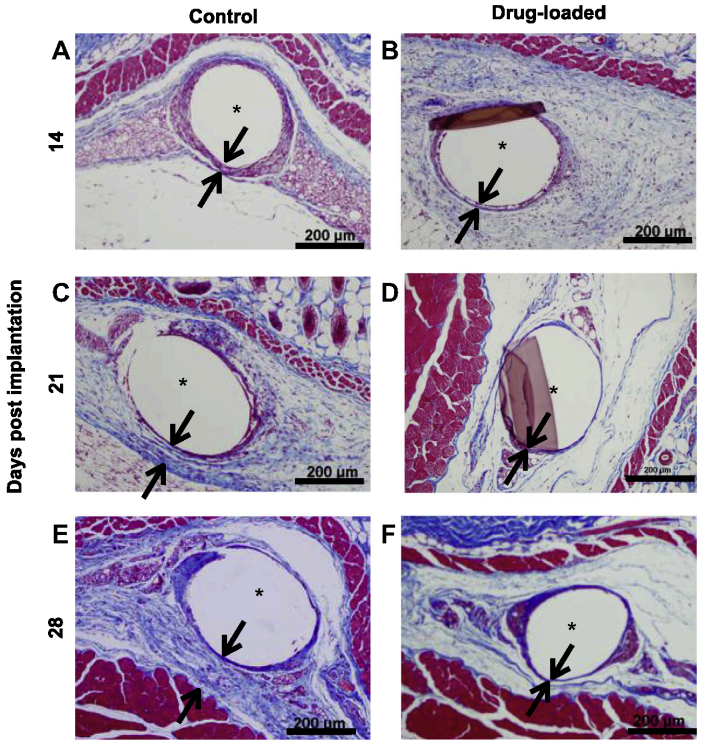

Fig. 6. MTC stained histology slides of A), C), E) control implants and B), D), F) drug-loaded implants for 14, 21 and 28 day time points respectively. Location of the implants is denoted by the asterisk "*". Capsule thicknesses were measured between the arrows shown in the figure. Scale bar: 200 μm.

host response to PLGA microspheres is distinct and more prolonged. The higher density of fibroblasts around masitinib-loaded implants at the 14-day time point (Fig. 5B) suggests granulation tissue formation, tissue remodeling and collagen deposition at the fiber implant surface [46]. Similar high densities of fibroblasts around the masitinib-releasing implants at 150–300 μm where PLGA microspheres are observed at the 28-day time point (Fig. 5D),

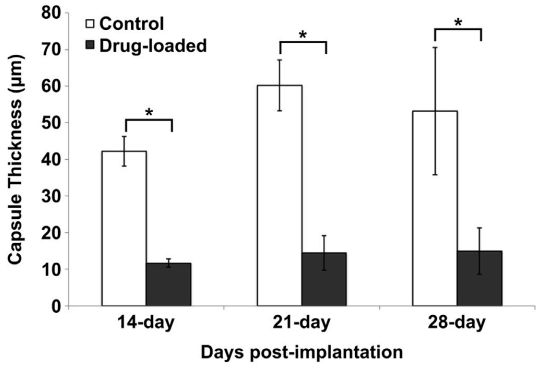

Fig. 7. Plot comparing the capsule thicknesses of control and drug-loaded implants for 14, 21 and 28 day implant studies. $^{*}p < 0.05$ was considered significant.

indicating a distinct tissue response and remodeling timelines for the fiber versus the microspheres. PMN presence around both control and masitinib-releasing implant sites at 21- and 28-day time points (Fig. 5C and D) is longer duration of PMN intensity than usually observed in FBR sites (typically 0–2 days [46]). Previous implant studies in subcutaneous tissue have shown the presence of PMNs around the implant site for up to 90 days after implantation and have attributed their presence to implant micromotion [48]. Hence, extended PMN presence might possibly be attributed to combinations of the effects of implant micromotion against murine dorsal musculature and masitinib-induced delayed FBR. However, capsule thickness data around the implant (see Fig. 7) shows a clear distinction and substantial differences between masitinib-releasing and control implants, with local drug release correlating with statistically significant reductions in fibrous encapsulation thickness. The hypothesis that this effect also produces functional sensor performance differences *in vivo* is the subject of current on-going work. Also, direct detection of implant localized MC activity associated with the FBR (i.e., TKI stabilization of cell degranulation and activation that propagates the FBR) is not possible using histology since degranulated MCs are indistinguishable from tissue-resident macrophages in histology sections.

Apart from confounding effects of other FBR-inducing variables (e.g., implant-associated micromotion, distinct microsphere inflammatory responses), most disruptive trends in cell density data could be attributed to the presence of PLGA microspheres deposited 150–300 μm distant from the implant interface. PLGA microspheres provide a high surface area, low density implant, similar to

foams or highly porous scaffold implants. PLGA microsphere implants in soft tissues have been shown previously to delay foreign body responses by delaying cellular infiltration [46]. High surface area, low density implants have also been known to attenuate typical foreign body responses compared to high density or monolith implants [49]. Separating these two affects is complex and confounds direct interpretation of the host reaction to each implanted foreign body type.

Drug-loaded implants display reduced capsule thicknesses significantly different than control implants at any given time point. Analyte permeabilities through these thinner capsules around masitinib-releasing implants compared to no-drug controls require further investigations using functional CGM sensors. Altered capsule thickness data confirm the working hypothesis that targeting mast cells via c-KIT-associated degranulation pathways with specific pharmacology near implanted biomaterials significantly affects resulting FBR fibrous capsule formation that can adversely affect the longevity and performance of sensor implants.

5. Conclusions

This study demonstrates that local release of the TKI drug, masitinib, from model implant delivery systems can extend beyond 4 weeks, with dosing tailored by PLGA microsphere formulations. Local masitinib release targets tissue site cellular activities to alter capsule deposition in a murine subcutaneous implant model. This is correlated with alterations in the intensity of various inflammatory cell recruitments to implant sites compared to no-drug controls. While observed temporospatial patterns of localized cell recruitment and peri-implant densities are difficult to interpret, local masitinib produces statistically significant, substantially reduced fibrous encapsulation around implants. Formation of a thinner, permeable fibrous capsule can potentially translate to improved sensor (and other implant) performance with longer device lifetimes in clinical use. Functioning CGM combination devices will now be used in this model to evaluate local masitinib delivery on inflammatory and mast cell activation, fibrous deposition and glucose monitoring in real-time *in vivo*.

Acknowledgments

The authors are grateful for support from the University of Utah Research Foundation in the form of both SEED and Technology Commercialization grants. F. Solzbacher has a financial interest in the company, Blackrock Microsystems (USA), that develops and produces implantable neural interfaces and electrophysiological equipment and software.

Appendix A. Supplementary data

Supplementary data related to this article can be found at http://dx.doi.org/10.1016/j.biomaterials.2013.08.090.

References

[1] Epstein AE, Kay GN, Plumb VJ, Dailey SM, Anderson PG. Gross and microscopic pathological changes associated with nonthoracotomy implantable defibrillator leads. Circulation 1998;98:1517–24.
[2] Zhong Y, Bellamkonda RV. Dexamethasone-coated neural probes elicit attenuated inflammatory response and neuronal loss compared to uncoated neural probes. Brain Res 2007;1148:15–27.
[3] Kvist PH, Iburg T, Bielecki M, Gerstenberg M, Buch-Rasmussen T, Hasselager E, et al. Biocompatibility of electrochemical glucose sensors implanted in the subcutis of pigs. Diabetes Technol Ther 2006;8:463–75.
[4] Wisniewski N, Moussy F, Reichert WM. Characterization of implantable biosensor membrane biofouling. Fresenius' J Anal Chem 2000;366:611–21.
[5] Moussy F. Implantable glucose sensor: progress and problems. Proc IEEE Sensors 2002;1:270–3.
[6] Cunningham DD, Stenken JA. In vivo glucose sensing. Wiley; 2009.
[7] Frost MC, Meyerhoff ME. Implantable chemical sensors for real-time clinical monitoring: progress and challenges. Curr Opin Chem Biol 2002;6:633–41.
[8] Wilson GS, Gifford R. Biosensors for real-time in vivo measurements. Biosens Bioelectron 2005;20:2388–403.
[9] Anderson JM, Rodriguez A, Chang DT. Foreign body reaction to biomaterials. Semin Immunol 2008;20:86–100.
[10] Singarayar S, Kistler PM, De Winter C, Mond H. A comparative study of the action of dexamethasone sodium phosphate and dexamethasone acetate in steroid-eluting pacemaker leads. Pacing Clin Electrophysiol 2005;28:311–5.
[11] Gerritsen M, Jansen JA, Lutterman JA. Performance of subcutaneously implanted glucose sensors for continuous monitoring. Neth J Med 1999;54:167–79.
[12] Updike SJ, Shults MC, Rhodes RK, Gilligan BJ, Luebow JO, von Heimburg D. Enzymatic glucose sensors. Improved long-term performance in vitro and in vivo. ASAIO J 1994;40:157–63.
[13] Wu P, Grainger DW. Drug/device combinations for local drug therapies and infection prophylaxis. Biomaterials 2006;27:2450–67.
[14] Avula M, Grainger DW. Addressing medical device challenges with drug/device combination. In: Siegel R, Lyu SP, editors. Drug-device combinations for chronic diseases. New York: Jon Wiley & Sons; 2013.
[15] Klueh U, Dorsky DI, Kreutzer DL. Enhancement of implantable glucose sensor function in vivo using gene transfer-induced neovascularization. Biomaterials 2005;26:1155–63.
[16] Hickey T, Kreutzer D, Burgess D, Moussy F. In vivo evaluation of a dexamethasone/PLGA microsphere system designed to suppress the inflammatory tissue response to implantable medical devices. J Biomed Mater Res 2002;61:180–7.
[17] Norton L, Koschwanez H, Wisniewski N, Klitzman B, Reichert W. Vascular endothelial growth factor and dexamethasone release from nonfouling sensor coatings affect the foreign body response. J Biomed Mater Res A 2007;81:858–69.
[18] Hetrick EM, Prichard HL, Klitzman B, Schoenfisch MH. Reduced foreign body response at nitric oxide-releasing subcutaneous implants. Biomaterials 2007;28:4571–80.
[19] Ward WK, Quinn MJ, Wood MD, Tiekotter KL, Pidikiti S, Gallagher JA. Vascularizing the tissue surrounding a model biosensor: how localized is the effect of a subcutaneous infusion of vascular endothelial growth factor (VEGF)? Biosens Bioelectron 2003;19:155–63.
[20] Takahashi H, Wang Y, Grainger DW. Device-based local delivery of siRNA against mammalian target of rapamycin (mTOR) in a murine subcutaneous implant model to inhibit fibrous encapsulation. J Control Release 2010;147:400–7.
[21] Zdolsek J, Eaton J, Tang L. Histamine release and fibrinogen adsorption mediate acute inflammatory responses to biomaterial implants in humans. J Transl Med 2007;5:31.
[22] Tang L, Jennings TA, Eaton JW. Mast cells mediate acute inflammatory responses to implanted biomaterials. Proc Natl Acad Sci U S A 1998;95:8841–6.
[23] Ward WK, Troupe JE. Assessment of chronically implanted subcutaneous glucose sensors in dogs: the effect of surrounding fluid masses. ASAIO J 1999;45:555–61.
[24] Ward WK, Wood MD, Casey HM, Quinn MJ, Federiuk IF. The effect of local subcutaneous delivery of vascular endothelial growth factor on the function of a chronically implanted amperometric glucose sensor. Diabetes Technol Ther 2004;6:137–45.
[25] Thevenot PT, Baker DW, Weng H, Sun M-W, Tang L. The pivotal role of fibrocytes and mast cells in mediating fibrotic reactions to biomaterials. Biomaterials 2011;32:8394–403.
[26] Klueh U, Kaur M, Qiao Y, Kreutzer DL. Critical role of tissue mast cells in controlling long-term glucose sensor function in vivo. Biomaterials 2010;31:4540–51.
[27] Reber L, Da Silva CA, Frossard N. Stem cell factor and its receptor c-Kit as targets for inflammatory diseases. Eur J Pharmacol 2006;533:327–40.
[28] Dubreuil P, Letard S, Ciufolini M, Gros L, Humbert M, Casteran N, et al. Masitinib (AB1010), a potent and selective tyrosine kinase inhibitor targeting KIT. PLoS ONE 2009;4:e7258.
[29] Paul C, Sans B, Suarez F, Casassus P, Barete S, Lanternier F, et al. Masitinib for the treatment of systemic and cutaneous mastocytosis with handicap: a phase 2a study. Am J Hematol 2010;85:921–5.
[30] Savage DG, Antman KH. Imatinib mesylate — a new oral targeted therapy. N Engl J Med 2002;346:683–93.
[31] Distler JH, Jungel A, Huber LC, Schulze-Horsel U, Zwerina J, Gay RE, et al. Imatinib mesylate reduces production of extracellular matrix and prevents development of experimental dermal fibrosis. Arthritis Rheum 2007;56:311–22.
[32] Gilfillan AM, Tkaczyk C. Integrated signalling pathways for mast-cell activation. Nat Rev Immunol 2006;6:218–30.
[33] Piette F, Belmin J, Vincent H, Schmidt N, Pariel S, Verny M, et al. Masitinib as an adjunct therapy for mild-to-moderate Alzheimer's disease: a randomised, placebo-controlled phase 2 trial. Alzheimers Res Ther 2011;3:16.
[34] Mitry E, Hammel P, Deplanque G, Mornex F, Levy P, Seitz JF, et al. Safety and activity of masitinib in combination with gemcitabine in patients with advanced pancreatic cancer. Cancer Chemother Pharmacol 2010;66:395–403.
[35] Le Cesne A, Blay JY, Bui BN, Bouche O, Adenis A, Domont J, et al. Phase II study of oral masitinib mesilate in imatinib-naive patients with locally advanced or

metastatic gastro-intestinal stromal tumour (GIST). Eur J Cancer 2010;46:1344–51.
[36] Tebib J, Mariette X, Bourgeois P, Flipo RM, Gaudin P, Le Loet X, et al. Masitinib in the treatment of active rheumatoid arthritis: results of a multicentre, open-label, dose-ranging, phase 2a study. Arthritis Res Ther 2009;11:R95.
[37] O'Donnell PB, McGinity JW. Preparation of microspheres by the solvent evaporation technique. Adv Drug Deliv Rev 1997;28:25–42.
[38] Klueh U, Liu Z, Cho B, Ouyang T, Feldman B, Henning TP, et al. Continuous glucose monitoring in normal mice and mice with prediabetes and diabetes. Diabetes Technol Ther 2006;8:402–12.
[39] Luna L. Histopathologic methods and color atlas of special stains and tissue artifacts. 1st ed. Gaithersburg, MD: American Histolabs, Inc; 1992.
[40] Daneshian M, Guenther A, Wendel A, Hartung T, von Aulock S. In vitro pyrogen test for toxic or immunomodulatory drugs. J Immunol Methods 2006;313:169–75.
[41] Coster S, Gulliford MC, Seed PT, Powrie JK, Swaminathan R. Monitoring blood glucose control in diabetes mellitus: a systematic review. Health Technol Assess 2000;4(i–iv):1–93.
[42] Tamborlane WV, Beck RW, Bode BW, Buckingham B, Chase HP, Clemons R, et al. Continuous glucose monitoring and intensive treatment of type 1 diabetes. N Engl J Med 2008;359:1464–76.
[43] Fu K, Pack DW, Klibanov AM, Langer R. Visual evidence of acidic environment within degrading poly(lactic-co-glycolic acid) (PLGA) microspheres. Pharm Res 2000;17:100–6.
[44] Golub JS, Kim Y-t, Duvall CL, Bellamkonda RV, Gupta D, Lin AS, et al. Sustained VEGF delivery via PLGA nanoparticles promotes vascular growth. Am J Physiol Heart Circ Physiol 2010;298:H1959–65.
[45] Hickey T, Kreutzer D, Burgess D, Moussy F. Dexamethasone/PLGA microspheres for continuous delivery of an anti-inflammatory drug for implantable medical devices. Biomaterials 2002;23:1649–56.
[46] Anderson JM, Shive MS. Biodegradation and biocompatibility of PLA and PLGA microspheres. Adv Drug Deliv Rev 1997;28:5–24.
[47] Butler K, Puckett A, Benghuzzi H. Quantitative analysis of the cellular components of the fibrous tissue matrix surrounding ALCAP, HA, and TCP bioceramics using adult male rats as a model. Biomed Sci Instrum 1999;35:267–72.
[48] Butler K, Benghuzzi H, Puckett A. Cytological evaluation of the tissue-implant reaction associated with S/C and I/P implantation of ALCAP and HA bioceramics in vivo. Pathol Res Pract 2001;197:29–39.
[49] Brauker JH, Carr-Brendel VE, Martinson LA, Crudele J, Johnston WD, Johnson RC. Neovascularization of synthetic membranes directed by membrane microarchitecture. J Biomed Mater Res 1995;29:1517–24.

CHAPTER 4

FOREIGN BODY RESPONSE TO IMPLANTED BIOMATERIALS IN A MAST CELL-DEFICIENT *KIT*$^{W\text{-}SH}$ MURINE MODEL

M. Avula[a], A.N. Rao[b], L.D. McGill[c], D.W. Grainger[a,b*], F. Solzbacher[a,d]

[a]Department of Bioengineering, University of Utah, Salt Lake City, UT 84112 USA

[b]Department of Pharmaceutics and Pharmaceutical Chemistry, University of Utah, Salt Lake City, UT 84112 USA

[c]Associated Regional and University Pathologist Laboratories, University of Utah, Salt Lake City, UT 84112 USA

[d]Department of Electrical and Computer Engineering, University of Utah, Salt Lake City, UT 84112 USA

[*]corresponding author – David W. Grainger, david.grainger@utah.edu,
Tel: 801 581 3715; Fax: 801 581 3674

Keywords: host response, medical device, continuous glucose monitoring, sensors, encapsulation, inflammation mast cells, tyrosine kinase inhibitor, local drug delivery, PLGA microspheres, combination device, implants

---

Submitted to Acta Biomaterialia, 2013

4.1 Abstract

Mast cells are recognized for their functional role in wound healing, allergic and inflammatory responses, host responses that are frequently detrimental to implanted biomaterials if extended beyond acute reactivity. These tissue reactions are especially impacting to the performance of sensing implants such as continuous glucose monitoring (CGM) devices. Our hypothesis that effective blockade of mast cell activity around implants could alter the host foreign body response (FBR) and enhance the *in vivo* lifetime of these implantable devices motivated this study. Stem cell factor (SCF) and its ligand c-KIT receptor are critically important for mast cell survival, differentiation, and degranulation. Therefore, a mast cell-deficient sash mouse model was used to assess mast cell relationships to the *in vivo* performance of CGM implants. Additionally, local delivery of a tyrosine kinase inhibitor (TKI) that inhibits c-KIT activity was also used to evaluate the role of mast cells in modulating the FBR. Model sensor implants comprising polyester fibers coated with a rapidly dissolving polymer coating containing drug-releasing degradable microspheres were implanted subcutaneously in sash mice for various time points, and the FBR was evaluated for chronic inflammation and fibrous capsule formation around the implants. No significant differences were observed in the foreign body capsule formation between control and drug-releasing implant groups in mast cell-deficient mice. However, fibrous encapsulation was significantly greater around the drug-releasing implants in sash mice compared to drug-releasing implants in wild-type (e.g., mast cell competent) mice. These results provide insights into the role of mast cells in the FBR, suggesting that mast cell deficiency provides alternative pathways for host inflammatory responses to implanted biomaterials.

4.2 Introduction

Host foreign body response (FBR) to implanted biomaterials plagues the performance of several implanted biomedical devices, particularly soft tissue sensor-actuator type implants such as pacemakers and continuous glucose sensors. The FBR is mediated by a complex series of tissue inflammatory events modulated by several cell types recruited as part of the normal wound healing process. Dissolution, degradation, and/or complete phagocytosis of certain foreign objects (e.g., pathogens, foreign proteins, nano- and microparticles) resolves the FBR and normal wound healing is restored. Implants with prolonged tissue residence, generally lacking the ability to be cleared from a tissue site via natural mechanisms, alter the tissue wound healing response in chronic inflammatory conditions, producing fibrous encapsulation of the foreign body and hallmark foreign body giant cells [1]. Fibrous encapsulation often isolates the implanted foreign body from normal host tissue sites. This capsule is dense and frequently poorly vascularized, altering sensor electrical responses, blocking transport of analytes to sensors, compromising functional performance, and disposing these sites to infection.

The intensity and impact of the FBR depends upon recruitment and reactivity of several key cell mediators, including polymorphonuclear neutrophils (PMNs), monocytes, macrophages, mast cells, and fibroblasts [2]. Each cell type has a specific role in modulating the local tissue response to wounding (i.e., implant placement) and subsequent healing, including chronic inflammation and the FBR [3]. The role of mast cells (MCs) in the FBR is associated with mediating the host response by secreting cytokines and cell mediators through cell activation and degranulation of their prominent intracellular granules [2]. MC precursors derive from hematopoietic stem cells in the bone marrow and are recruited through chemotactic inflammatory signaling to wound sites where they mature and activate. MCs are found ubiquitously in all tissues,

particularly associated with vasculature and nerves, and also in proximity epithelial surfaces such as airways and skin. MC survival and differentiation depends on presentation of the ligand of their membrane-resident c-KIT receptor also known as stem cell factor (SCF) [4-6]. The c-KIT receptor is primarily expressed on hematopoietic stem cells and mast cells [7]. SCF/c-KIT interactions result in mast cell activation and degranulation, prompting secretion of vasodilators (histamine), chemokines, cytokines (e.g., IL-4, IL-13) and prostaglandins [8-11].

MCs act as a primary cell-based host defense mechanism, mediating allergic responses and inflammatory responses. They have also been shown to influence neovascularization and tissue remodeling [12]. MC degranulation in the presence of antigens or allergens produces cell secretion of granules containing IL-4 and IL-13 that provide chemotactic gradients to recruit macrophages, and histamine and serotonin to dilate the vasculature to facilitate greater access to the inflammatory cells arriving at the wound site [2].

The MC role in the implant-associated FBR was recently described using a wild-type C57BL/6 mouse subcutaneous model and a local pharmacological approach. Inhibition of tissue site MC activation and degranulation was attempted using local delivery of a tyrosine kinase inhibitor, masitinib [13]. Reduced thickness of the foreign body capsule formed around implants was demonstrated *in vivo* for up to 28 days post-implantation. A similar study using hernia mesh implants [14] demonstrated that blocking mast cell degranulation with cromolyn treatment reduced inflammation and fibrosis around the subcutaneous implant site. In the context of CGM sensor implants, Klueh et al. [15] recently probed the MC role in the performance of implanted CGM sensors in murine cutaneous implant models. When compared to MC-sufficient wild-type C57BL/6 cohorts, implants in their knockout $Kit^{w\text{-}Sh}$ (sash) (MC-deficient) mutant mice exhibited stable CGM responses for up to 28 days, suggesting a critical MC role in

modulating host tissue response to implanted sensors. Mechanisms for this observation require further study and elucidation.

Previous studies in MC-deficient sash mice also show normal wound healing in cutaneous wounds in the absence of mast cells [16]. Our prior work describes thinner fibrous capsule formation around masitinib-releasing implants than that around control implants in wild-type mice, suggesting that stabilizing MCs alone does not completely avoid FBR fibrosis [13]. These results have produced a further idea that the use of a MC-stabilizing drug in wild-type mice might alter the local tissue response to implants, but may not completely avoid it as fibrous encapsulation of foreign implants has also been observed in the absence of MCs [15, 16]. Klueh et al. [15] report dramatically reduced inflammation and fibrosis around subcutaneous implants in mast cell-deficient mice, while Nauta et al. [16] observed no discernable differences in collagen concentrations in the scar tissue around cutaneous wound sites among MC-deficient and analogous wild-type mice. However, wound healing models in these two studies were significantly different: CGM sensor insertion requires an approximate 600 μm-diameter percutaneous access [15] while cutaneous wounds [16] were 6 mm in diameter. Interestingly, glucose sensor CGM implants functioned normally even with early capsules surrounding them, indicating that the early capsule is permeable to essential analytes (i.e., glucose and oxygen for this CGM) required for glucose sensing. Additionally, these studies have diametrically opposite conclusions regarding the role of MCs in modulating the FBR. Hence, this strategy needs further investigation to understand the complex MC mechanisms involved in FBR and if they can be exploited in the context of implant-associated healing and device integration.

Here, we evaluate the effect of the c-KIT-inhibiting drug, masitinib, in implant-associated MC functions in MC-deficient mutant sash mice. The intent is to assess the role of MCs in host tissue responses to implanted biomaterials. Masitinib is a relatively

new tyrosine kinase inhibitor shown to be an effective inhibitor of MC proliferation *in vitro* and *in vivo* [17] and therefore was chosen to release from the implanted CGM interface to inhibit mast cell degranulation in a device-based local delivery formulation. Apart from being a potent inhibitor of c-KIT, masitinib has also been shown to inhibit platelet-derived growth factor receptor (PDGFR), intracellular kinase Lyn, and fibroblast growth factor receptor 3 (FGFR3) that play a role in tissue remodeling, inflammatory, and allergic responses [17].

Mast cell-deficient sash mice (B6.Cg-*KitW-sh*/HNihrJaeBsmGlliJ) have been used as the strain of choice for studying MC deficiency-related conditions [18]. In this context, polyester fiber model implants as sensor surrogates were coated with rapidly dissolving polymer film loaded with degradable polymer microsphere controlled release formulations of masitinib to alter the healing dynamics in subcutaneous tissues of mast cell-deficient sash mice implanted for 14, 21, and 28 days.

4.3 Materials and Methods

4.3.1 Materials

Poly(lactic-co-glycolic acid) (PLGA) was purchased from Lakeshore Biomaterials (now Evonik Biomaterials, USA). Polyethylene glycol (PEG) (MW 20,000), polyethylene oxide (PEO) (MW 100,000), poly(vinyl alcohol) (PVA, average MW 30-70 kDa), and solvents dichloromethane (DCM), chloroform, ethanol, methanol, and acetonitrile were purchased from Sigma Aldrich, USA. Trifluoroacetic acid (TFA) was purchased from Fisher Scientific, USA. Masitinib drug was purchased from Selleck Chemicals, USA. Commercial polyester fiber (Trilene, 300 μm diameter, Berkley Fishing, USA) was cleaned using 70% ethanol before use. Ultrapure water (Millipore-filtered ASTM Grade II) was used for all experiments.

4.3.2 Implant fabrication

Implant fabrication was accomplished as described in a recent publication [13]. Briefly, PLGA polymer microspheres were fabricated using established solvent-evaporation techniques either with masitinib at a concentration of 1 mg/ml or without masitinib (blank controls), and mixed with aqueous PEG/PEO solution at a concentration of 350 mg/ml. Polyester fiber sensor model implants were coated with the PEG-PLGA microsphere solution using a 2-part aluminum mold and flash-freezing, and the resulting coating was lyophilized for 12 hours to obtain the implants coated with a rapidly soluble polymer film containing drug-loaded microspheres. Both drug-releasing and control implants (i.e., PLGA microspheres, no drug) were fabricated using this procedure.

Intended masitinib load within each implant was calculated based on drug dosing values from Dubreuil et al. [17], with subcutaneous tissue density values obtained from Kyrzywicki et al. [19], and assumptions about the intended tissue delivery volume surrounding the implant (see Figure 4.1A). A dose of 60 mg/kg/day was considered potent by assuming complete drug clearance each day from the tissue bed surrounding the implant. Subcutaneous tissue density of 1 g/cc and a targeted tissue drug exposure depth of 200 μm around each implant (illustrated in Figure 4.1A) were considered, and the resulting dosing values were extrapolated for 30-day release for targeting final drug load on the implant. A margin of safety of 1.5x was used in calculating the drug loading/implant to accommodate this required drug load and assumptions. Post-fabrication, coated implants were tested for viable bacterial contamination using blood agar cultures for a 24-hour incubation period. USP chromogenic LAL assay (Lonza, USA) was used to test for endotoxin content on the final implants.

Drug loading and release for each implant was characterized using high performance liquid chromatography (HPLC) and a UV detector at 283nm for masitinb. A Zorbax Eclipse C18 column (4.6 mm × 250 mm, 5μm, Agilent Technologies, USA) was

used for drug quantification using a method with 2 mobile phases (A and B) developed with a 30-minute cycle time. TFA in water (1%) was used as mobile phase A and TFA in acetonitrile (1%) was used as mobile phase B. The HPLC assay involved gradient flow of mobile phase B at 100% initially and ending the cycle at 0% (100% mobile phase A) at a flow rate of 1 ml/min.

4.3.3 In vivo implant studies

Male sash (B6.Cg-*KitW-sh*/HNihrJaeBsmGlliJ) mice (12-14 weeks) were purchased from Jackson Laboratories (USA). Animals were divided into 3 cohorts for 14, 21, and 28-day study time points with n=7 for each time point. Each animal was implanted subcutaneously with one blank control and one masitinib-releasing sensor model implant parallel to the spine in the dorsal regions, as illustrated in Figure 4.1B. All procedures involving the use of animals for this study were approved by the institutional animal care and use committee (IACUC) at the University of Utah.

Surgical implant procedures were adapted with slight modifications from that recently published in a similar context [13, 20]. Each animal was anesthetized using 1-2.5% isofluorane (in 1 L/min of oxygen) administered through a nose cap throughout the procedure. Animals were placed on a warming water pad to maintain body temperature for the duration of surgery and recovery. An area of 6×4 cm^2 on the back of the animal was shaved and the exposed skin treated with povidone-iodine solution to create an aseptic environment at the surgical site. A sterile 18G needle was used to gently puncture the skin and to inject the wound site with 100 µl of pyrogen-free 0.9% NaCl solution to create a subcutaneous “pocket” for the implantation procedure. The implant was gently inserted through the puncture into the subcutaneous pocket created with the NaCl solution such that the entire implant is placed subcutaneously under the animal’s skin without any protrusions, and the perforated skin was then sealed with skin glue

(Nexcare Skin Care, USA). The animal was then removed from anesthesia and allowed to recover on the warming pad before being moved to its cage. Animals were housed in individual cages in 12-hour dark/light cycles for the duration of the study; food and water were provided ad libitum. Implanted mice were divided into 3 cohorts with different study end points of 14, 21, and 28 days.

4.3.4 Explant histological analysis

At each time point, animals were euthanized using 100% CO_2 in a bell jar and the entire tissue bed surrounding each implant including the implant was harvested intact for histology. Harvested tissue was fixed in 10% neutral buffered formalin (Fisher Scientific) for 48 hours with the formalin being replaced after 24 hours. The fixed tissue was then sent to Associated Regional and University Pathologists (ARUP, USA) Laboratories for further processing and histological analytical guidance. Tissue samples were sectioned and stained with hematoxylin and eosin (H&E) stain to identify cell nuclei and to quantify inflammatory cell densities, and with Masson's trichrome stain to identify fibrosis and to quantify capsule thicknesses around implants.

4.3.5 Inflammatory cell densities measurement

Cell densities on H&E-stained sections of implant tissue were determined microscopically by scoring the number of cells surrounding each implant in five representative 40x fields per sample. Cell density was expressed as a representative score of the number of cells present per field. Neutrophils and plasma cells, macrophages and foreign body giant cells, and fibroblasts were identified visually by morphology and scored at radial distances of 50 μm, 150 μm, and 300 μm from the implant/tissue interface for both control and masitinib-releasing implants. These cells were chosen to represent those typical of the foreign body response, with neutrophils

representing the acute wound stage infiltrates, while macrophages and fibroblasts represent more chronic FBR and tissue resolution stages, respectively [2].

4.3.6 Capsule thickness measurement

Tissue sections stained with both H&E and Masson's trichrome were observed under bright field microscopy using 10x and 20x objectives, and images were captured and analyzed. Capsule thickness from fibrosis around each implant was measured at the interface of the implant and adipose tissue on the apical side, and also the interface of the implant and muscle tissue on the basal side. Multiple random locations (n=5 per implant site, N=7 implants) at these interfaces were chosen for the capsule thickness measurements using ImageJ software. Capsule thicknesses are also compared with values obtained around identical implant sites in MC-competent mice [13] to analyze the effect of locally released masitinib on subcutaneous murine fibrosis in the presence and absence of MCs.

4.3.7 Statistical significance

All data are expressed as the mean ± 1 standard deviation and compared with an ANOVA test. Capsule thickness data for control implants were compared with masitinib-releasing implants for identical time points using Student's T-test assuming equal variance. Data were considered statistically significant for $p < 0.05$.

4.4 Results

4.4.1 Implant fabrication and characterization

PLGA microspheres (5-20 μm diameter) were obtained from the fabrication method [13]. This size range is generally accepted to be beyond the phagocytosable range of tissue site phagocytes [21, 22] eliminating confounding effects of undesired cell particle uptake and processing.

An aqueous mixture of PEG/PEO solution and PLGA microsphere suspension was used to coat polyester fiber model implants using 2-part aluminum molds and cryogenic processing to produce the resulting implant matrices [13]. The resulting PEG-PLGA composite coatings were previously shown to dissolve *in vitro* in less than 3 minutes [13]. The PEG-PLGA microsphere-coated implants were characterized for drug loading and release using HPLC analysis. Masitinib loading in the PLGA component of the composite implant coating was determined to be 11.2±1.2 μg/implant (mean ± standard deviation, n=3) by HPLC analysis (LOD = 73 ng/ml). This dosing is ~1.5X the theoretically calculated dose required to target mast cells in a 200 μm-thick tissue volume surrounding the implant site at a desired loading of 7.5 μg/implant, assuming complete tissue site clearance each day over the dosing interval. Blood agar cultures with the implants showed no bacterial colony formation after 24 hours of culture. LAL assay results show endotoxin content less than 0.1 ng/implant – a negligible amount compared to the reported endotoxin clearance rate of 5 ng/kg/hr [23].

4.4.2 Inflammatory cell densities around implants in vivo

H&E-stained tissue preparations exhibit variable distributions of different inflammatory and wound-recruited cell densities for both control and masitinib-releasing implant sites at each time point, as shown in Figure 4.2. Inflammatory cell densities around the implant site were scored for 3 cell types: neutrophils (PMNs), macrophages and foreign body giant cells (FBGCs), and fibroblasts, all representative of the acute inflammation, chronic inflammation, and tissue remodeling phases of the FBR, respectively.

Observed tissue site cell densities for control (PLGA blank, no drug) vs. drug loaded composite implant coatings for these different cell types were evaluated for different time points: 14 days, 21 days, and 28 days, at distances of 50 μm, 150 μm, and

300 μm from implant-tissue interface. Cell densities were scored in arbitrary units (a.u.) as 1-normal, 2-moderate, 3-medium, 4-high, and 5-severe by direct observation of multiple randomly selected histological sections from sash mast cell-deficient mice.

Cell density assessment for the 14-day time point in sash mast cell-deficient mice is shown in Figure 4.3A. Around control implants, PMNs exhibit high densities at the implant surface and decrease in numbers with increasing distance from the implant surface. This trend is seen in all cell types analyzed in this study around the control implants. For drug-releasing implants, PMNs and fibroblasts are found in high numbers in zones at greater distances from the implant site (i.e, from 50 μm to 150 μm) – not directly at the implant interface - and decrease in density further away from the implant surface (to 300 μm). Macrophages around drug-releasing implants steadily decrease in density with increasing distance away from the implant while their numbers peak around the PLGA microspheres at 150 μm and decrease at 300 μm distances from control implant surfaces.

The 21-day time-point cell density profile is shown in Figure 4.3B but in contrast to earlier time points exhibit no clear trends among the different cell types surrounding both the control and drug-loaded implants in sash subcutaneous tissue. In the control implant group, PMN cell density increases consistently with increasing distance from the implant, whereas macrophage density initially increases and then decreases over the same measured distance. Fibroblast numbers remain steady until 150 μm distance from the implant and then decrease to 300 μm. In the drug-loaded group, PMN density is roughly constant to a distance of 150 μm and then increases slightly, similar to their corresponding density in the control implant group. Macrophages are roughly constant at 50 μm and 150 μm and then decrease at 300 μm distance from the implant. Fibroblasts initially increase near the implant and then decrease from 50 μm to 300 μm.

For the 28-day time point (Figure 4.3C), PMN cell density increases slightly from the control implant surface and then remains constant from 150 μm to 300 μm. In contrast, PMN density is constant around the drug-loaded implants at any distance. Macrophage density is comparable among the drug-loaded and control implants from 50 μm to 300 μm. Fibroblast density decreases between 150 μm and 300 μm for the control implants and increases between the same distance points around drug-loaded implants.

Overall, the qualitative analysis shows a comparable cell density profile between control and drug-loaded implant sites, with most tissue locations exhibiting similar or ±1 a.u. difference in cell density scores.

4.4.3 Implant capsule thickness

Masson's trichrome-stained (MTC) histology preparations were used to measure fibrous capsule thickness formed around implants at the different explant time points. Capsule thicknesses were measured at multiple locations between the arrows, as shown in Figure 4.4A-4.4F. Figure 4.4G shows capsule thickness plots for both implant types at respective time points. Capsule thickness values are averaged for measurements taken from 5 random locations on each implant site in 7 individual implant sites (i.e., n=5 for N=7). Capsule thickness values for control implant sites were found to be 42.5±5.6 μm, 34.6±6.3 μm, and 41.6±5.2 μm for 14-, 21-, and 28-day time points, respectively. Thicknesses were 38.9±11.5 μm, 34.4±6.2 μm, and 42.4±6.2 μm for capsules around the masitinib-releasing implant sites for these same respective time points. These measurements do not show statistically significant differences between control and masitinib-releasing implant groups (p>0.05) for all time points, as shown in Figure 4.4G.

4.4.4 Comparisons of implant fibrosis between mast cell-competent wild-type and sash mast cell-deficient implant sites

Capsule thickness values for 14-, 21- and 28-day time points for both the control and masitinib-releasing implants compared for MC-competent and sash MC-deficient mice are compared in Figure 4.5 [13]. For identically prepared implants in the wild-type mice, capsule thickness values for control implant sites were found to be 42.2±4 μm, 60.2±6.9 μm, and 53.2±17.4 μm for 14-, 21-, and 28-day time points, respectively.[12] In contrast, capsule thicknesses were substantially reduced to 11.7±1.1 μm, 14.4±4.7 μm, and 14.4±6.3 μm for tissue around masitinib-releasing implant sites in wild-type MC-competent mice. In sash MC-deficient mice, fibrous capsule thickness values around control implants were comparable to that in wild-type mice except for the 21-day time point. Interestingly, values for capsule thicknesses around masitinib-releasing implants in sash mice were significantly higher than in the same drug-releasing implants in wild-type mice at the same time points.

4.5 Discussion

We report *in vivo* influences of local release of the tyrosine kinase inhibitor, masitinib, at subcutaneous implant sites in MC-deficient sash mice to evaluate the possibility to eliminate MC effects on the FBR. This has been motivated by the need to improve performance from implanted feedback and reporting devices such as CGM sensors that are adversely affected by tissue site FBR. The rate of CGM adoption by patients to monitor glycemic indices and mitigate long-term effects of diabetes is increasing. The effects of host response on these implanted devices has limited their FDA-approved lifetimes to less than a week in tissues. Evidence from several studies shows that MCs play an important role in mediating the wound healing response to

implanted biomaterials [24]. Pharmacological influences on MC function at implant sites could provide new insights into FBR and implant response.

In this regard, recent studies by Klueh et al. [15] have shown reduced FBR to implanted CGM sensors in sash mouse models deficient in MCs. Specifically, they have shown uninterrupted CGM response over a 28-day period in sash mice that was only lost when bone marrow-derived MCs were injected at the implant site, suggesting the importance of MCs in modulating the FBR. We tested their theory by seeking to replicate their results using local drug release to inhibit mast cell degranulation at the implant site. Our previous study [13] showed that local delivery of MC-targeting masitinib from surfaces of implanted model sensors reduced capsule formation around subcutaneous implant sites in wild-type mouse models. This study now extends that approach in MC-deficient sash mice mutants to understand FBR pharmacological modulation in the absence of MCs.

4.5.1 Inflammatory cell densities at the implant-tissue site

The model implant used in this study is a cleaned, endotoxin-free cylindrical monolithic polyester fiber with low surface area that is coated with a rapidly soluble PEG layer containing porous PLGA microspheres as drug carriers. This coating is not crosslinked and highly soluble, allowing immediate dissolution and disintegration upon implantation to disperse the PLGA contents into the local tissue bed surrounding the implant. This results in no interference with CGM function if used in the context of a sensor. It also results in tissue site deposition of two very different types of foreign bodies, i.e,, a low surface area monolithic polymer fiber, and a low-density, high surface area degradable polymer microsphere. Previous literature has shown that FBR to high surface area implants proceeds at a slower rate, as infiltrating inflammatory cells require more time to traverse through the porous structure of such implants [3, 25]. The

presence of significant PMNs around the 28-day tissue explant sites (Figure 3C), a cell type typically not found after this time duration around implants, can be attributed to this phenomenon. Cell density analysis for the 14-day study (Figure 3B) shows increasing PMN density moving away from the implant-tissue interface, suggesting the dispersed presence of PLGA microspheres around the implant site. This observation helps explain the variations in cell densities around implant sites as the local densities around PLGA foreign bodies are different from the average densities in adjacent tissues.

Since the host inflammatory responders encounter two distinct implant types (i.e,, polymer monolithic fiber and porous PLGA microspheres), FBR modulation is distinct for each of them. The local variations in implantations and tissue bed distributions of implant coating contents from the implant, and cell densities for various cell types are comparable between control and drug-loaded implant sites for a given time point. Observed PLGA microspheres located at distances of 150 μm from the implant surface indicate that their drug load is released to tissue some 200 μm from the implant interface. This can be correlated to the increase in inflammatory cell densities observed at 150 μm from the implant surface, as seen in Figure 4.3.

4.5.2 Capsule thickness

Capsule thicknesses compared in this study for sash MC-deficient mice show no significant differences between control and drug-loaded implant groups. Interestingly, no appreciable changes in capsule thicknesses are seen at the 14-, 21- and 28-day time points. This result is distinct from that show previously for identical implants in wild-type MC-competent mice [13], indicating distinct differences in subcutaneous tissue pharmacology to masitinib in MC-deficient mice. MC absence in the sash models could facilitate different inflammatory reactions and tissue remodeling kinetics, possibly due to absence of MC-derived vasoactive agents normally that permit greater influx of

inflammatory cells to the injury/implantation site. Interestingly, capsules around drug-loaded implants in wild-type mice are thinner than their analogous capsules in the sash MC-deficient mice [13]. Capsule thickness data from Figure 4.4G can be correlated to the fibroblast cell densities around implant sites in Figure 4.3. Fibroblast density at 50 μm from the implant surface increases from 14 to 21 days and then attenuates at 28 days to the 14-day levels, suggesting that fibroblast density undergoes little to no net change for the various time points.

Several studies have shown comparable cutaneous wound healing in wild-type and MC-deficient mice [16, 26, 27]. The effects of MC-absence on wound healing have been debated to have either positive or negative impacts on tissue remodeling processes [16, 24]. MC injections at the implant site have shown to precipitously drop CGM sensor response in both wild-type and sash mice, suggesting that their presence intensifies collagen formation or results in increased vasoconstriction, limiting blood flow to the implant site [15].

Results from this study showing that collagen formation around implants is not being affected by masitinib release supports either that the drug is mainly targeting MCs and hence ineffective in their absence in the sash model, or that the FBR in sash mice is independent of the various targets of masitinib (i.e., FGFR3, PDGFR, Lyn kinase) - all of which have been shown to be interdependent on MC activity [17, 28, 29]. As an indicator of common TKI bioactivity pathways, masitinib mesylate has been shown to reduce production of extracellular matrix and prevent the development of experimental non-implant fibrosis [30]. Nonetheless, masitinib is selective in inhibiting recombinant human c-KIT receptor (IC_{50} 200 ± 40nM), and platelet-derived growth factor receptor (PDGFR) while weakly inhibiting other type III tyrosine kinase receptors, including fibroblast growth factor receptor 3 (FGFR3) and FCεRI receptor. Imatinib inhibits a broader range of receptors [17]. These receptors when bound to ligands like IgE, SCF, C3a, PAMPs, etc.,

result in mast cell activity and degranulation [31], leading to increased inflammatory cell activity. In the absence of mast cells in sash mice however, masitinib appears to be ineffective in regulating collagen production by fibroblasts. This could mean that sash mice have developed an alternative wound site inflammatory response system acting mostly independently of MC activity.

4.6 Conclusions

The absence of MCs in the sash mouse implant response does not significantly alter the fibrous encapsulation of implanted biomaterials. The use of local masitinib as a TKI capable of inhibiting c-KIT receptors on MCs and other cells does not alter FBR perceptibly in the absence of MCs as evidenced by the similarity in inflammatory cell densities around drug-releasing and control implant sites. Similarly, fibrous capsule formation around implanted biomaterials shows similar thicknesses around control and drug-releasing implants in the MC-deficient sash model. Correspondingly, capsule thickness is almost constant over time, correlated with the constant fibroblast cell density observed around the implants as implant time increases. Capsule thickness around drug-releasing implants in sash mice is higher when compared to thickness values around analogous drug-releasing implants in wild-type mice, suggesting an alternative pathway for inflammatory responses in mast cell-deficient mice that proceeds to rapid, reliable fibrosis as an expected FBR endpoint in the absence of MC mediators. This indicates that the pathways that recruit and stimulate fibroblast deposition of matrix, especially collagens, in the sash model must be highly operative.

4.7 Acknowledgements

The authors acknowledge support from the University of Utah Research Foundation in the form of both SEED and Technology Commercialization grants. P. Hogrebe (Utah) is thanked for his support and help in technical discussions.

4.8 Disclosure

Author F. Solzbacher has a financial interest in the company Blackrock Microsystems (USA) that develops and produces implantable neural interfaces and electrophysiological equipment and software, none of which is used in this study.

4.9 References

[1] Jay SM, Skokos EA, Zeng J, Knox K, Kyriakides TR. Macrophage fusion leading to foreign body giant cell formation persists under phagocytic stimulation by microspheres in vitro and in vivo in mouse models. J Biomed Mater Res A 2010;93:189-99.

[2] Anderson JM, Rodriguez A, Chang DT. Foreign body reaction to biomaterials. Semin Immunol 2008;20:86-100.

[3] Anderson JM, Shive MS. Biodegradation and biocompatibility of PLA and PLGA microspheres. Adv Drug Delivery Rev 1997;28:5-24.

[4] Huang E, Nocka K, Beier DR, Chu TY, Buck J, Lahm HW, et al. The hematopoietic growth factor KL is encoded by the Sl locus and is the ligand of the c-kit receptor, the gene product of the W locus. Cell 1990;63:225-33.

[5] Williams DE, Eisenman J, Baird A, Rauch C, Van Ness K, March CJ, et al. Identification of a ligand for the c-kit proto-oncogene. Cell 1990;63:167-74.

[6] Zsebo KM, Wypych J, McNiece IK, Lu HS, Smith KA, Karkare SB, et al. Identification, purification, and biological characterization of hematopoietic stem cell factor from buffalo rat liver--conditioned medium. Cell 1990;63:195-201.

[7] Okayama Y, Hunt TC, Kassel O, Ashman LK, Church MK. Assessment of the anti-c-kit monoclonal antibody YB5.B8 in affinity magnetic enrichment of human lung mast cells. J Immunol Methods 1994;169:153-61.

[8] Columbo M, Horowitz EM, Botana LM, MacGlashan DW, Jr., Bochner BS, Gillis S, et al. The human recombinant c-kit receptor ligand, rhSCF, induces mediator release from human cutaneous mast cells and enhances IgE-dependent mediator release from both skin mast cells and peripheral blood basophils. J Immunol 1992;149:599-608.

[9] Takaishi T, Morita Y, Hirai K, Yamaguchi M, Ohta K, Noda E, et al. Effect of cytokines on mediator release from human dispersed lung mast cells. Allergy 1994;49:837-42.

[10] Taylor AM, Galli SJ, Coleman JW. Dexamethasone or cyclosporin A inhibits stem cell factor-dependent secretory responses of rat peritoneal mast cells in vitro. Immunopharmacology 1996;34:63-70.

[11] Taylor WE, Najmabadi H, Strathearn M, Jou NT, Liebling M, Rajavashisth T, et al. Human stem cell factor promoter deoxyribonucleic acid sequence and regulation by cyclic 3',5'-adenosine monophosphate in a Sertoli cell line. Endocrinology 1996;137:5407-14.

[12] Dvorak AM. Basophil and mast cell degranulation and recovery. New York: Plenum Press; 1991.

[13] Avula MN, Rao AN, McGill LD, Grainger DW, Solzbacher F. Modulation of the foreign body response to implanted sensor models through device-based delivery of the tyrosine kinase inhibitor, masitinib. Biomaterials 2013;34:9737-46.

[14] Orenstein SB, Saberski ER, Klueh U, Kreutzer DL, Novitsky YW. Effects of mast cell modulation on early host response to implanted synthetic meshes. Hernia 2010;14:511-6.

[15] Klueh U, Kaur M, Qiao Y, Kreutzer DL. Critical role of tissue mast cells in controlling long-term glucose sensor function in vivo. Biomaterials 2010;31:4540-51.

[16] Nauta AC, Grova M, Montoro DT, Zimmermann A, Tsai M, Gurtner GC, et al. Evidence that mast cells are not required for healing of splinted cutaneous excisional wounds in mice. PLoS ONE 2013;8:e59167.

[17] Dubreuil P, Letard S, Ciufolini M, Gros L, Humbert M, Casteran N, et al. Masitinib (AB1010), a potent and selective tyrosine kinase inhibitor targeting KIT. PLoS ONE 2009;4:e7258.

[18] Grimbaldeston MA, Chen CC, Piliponsky AM, Tsai M, Tam SY, Galli SJ. Mast cell-deficient W-sash c-kit mutant Kit W-sh/W-sh mice as a model for investigating mast cell biology in vivo. Am J Pathol 2005;167:835-48.

[19] Krzywicki HJ, Chinn KS. Human body density and fat of an adult male population as measured by water displacement. Am J Clin Nutr 1967;20:305-10.

[20] Klueh U, Liu Z, Cho B, Ouyang T, Feldman B, Henning TP, et al. Continuous glucose monitoring in normal mice and mice with prediabetes and diabetes. Diabetes Technol Ther 2006;8:402-12.

[21] Hirota K, Hasegawa T, Hinata H, Ito F, Inagawa H, Kochi C, et al. Optimum conditions for efficient phagocytosis of rifampicin-loaded PLGA microspheres by alveolar macrophages. J Control Release 2007;119:69-76.

[22] Wang Y, Tran KK, Shen H, Grainger DW. Selective local delivery of RANK siRNA to bone phagocytes using bone augmentation biomaterials. Biomaterials 2012;33:8540-7.

[23] Daneshian M, Guenther A, Wendel A, Hartung T, von Aulock S. In vitro pyrogen test for toxic or immunomodulatory drugs. J Immunol Methods 2006;313:169-75.

[24] Weller K, Foitzik K, Paus R, Syska W, Maurer M. Mast cells are required for normal healing of skin wounds in mice. FASEB J 2006;20:2366-8.

[25] Brauker JH, Carr-Brendel VE, Martinson LA, Crudele J, Johnston WD, Johnson RC. Neovascularization of synthetic membranes directed by membrane microarchitecture. J Biomed Mater Res 1995;29:1517-24.

[26] Egozi EI, Ferreira AM, Burns AL, Gamelli RL, Dipietro LA. Mast cells modulate the inflammatory but not the proliferative response in healing wounds. Wound Repair Regen 2003;11:46-54.

[27] Iba Y, Shibata A, Kato M, Masukawa T. Possible involvement of mast cells in collagen remodeling in the late phase of cutaneous wound healing in mice. Int Immunopharmacol 2004;4:1873-80.

[28] Urtz N, Olivera A, Bofill-Cardona E, Csonga R, Billich A, Mechtcheriakova D, et al. Early activation of sphingosine kinase in mast cells and recruitment to FcepsilonRI are mediated by its interaction with Lyn kinase. Mol Cell Biol 2004;24:8765-77.

[29] Crivellato E, Beltrami CA, Mallardi F, Ribatti D. The mast cell: an active participant or an innocent bystander? Histol Histopathol 2004;19:259-70.

[30] Distler JH, Jungel A, Huber LC, Schulze-Horsel U, Zwerina J, Gay RE, et al. Imatinib mesylate reduces production of extracellular matrix and prevents development of experimental dermal fibrosis. Arthritis Rheum 2007;56:311-22.

[31] Gilfillan AM, Tkaczyk C. Integrated signalling pathways for mast-cell activation. Nat Rev Immunol 2006;6:218-30.

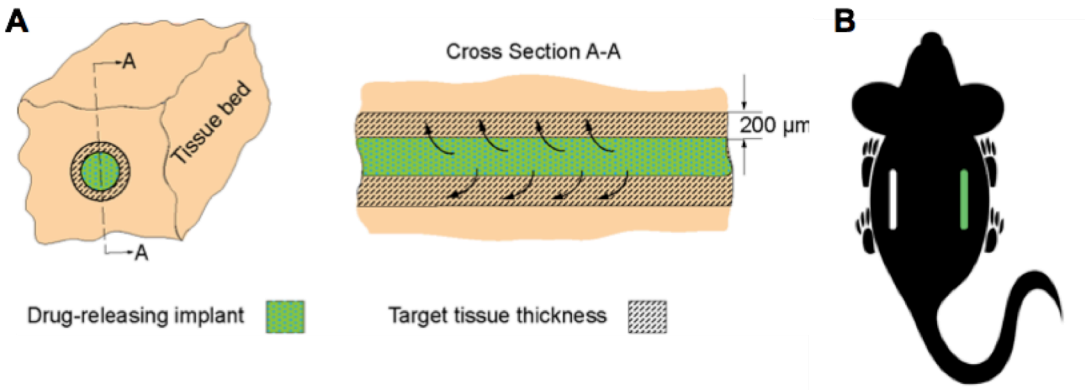

Figure 4.1: Illustration of implant and locations of implantation. **(A)** Implant drug-loading calculation geometric volume model used for drug dosing to local tissue sites into 200-micron thick cylindrical tissue volume adjacent to the implant, and (**B)** bilateral dorsal implant locations in a sash knock-out mouse.

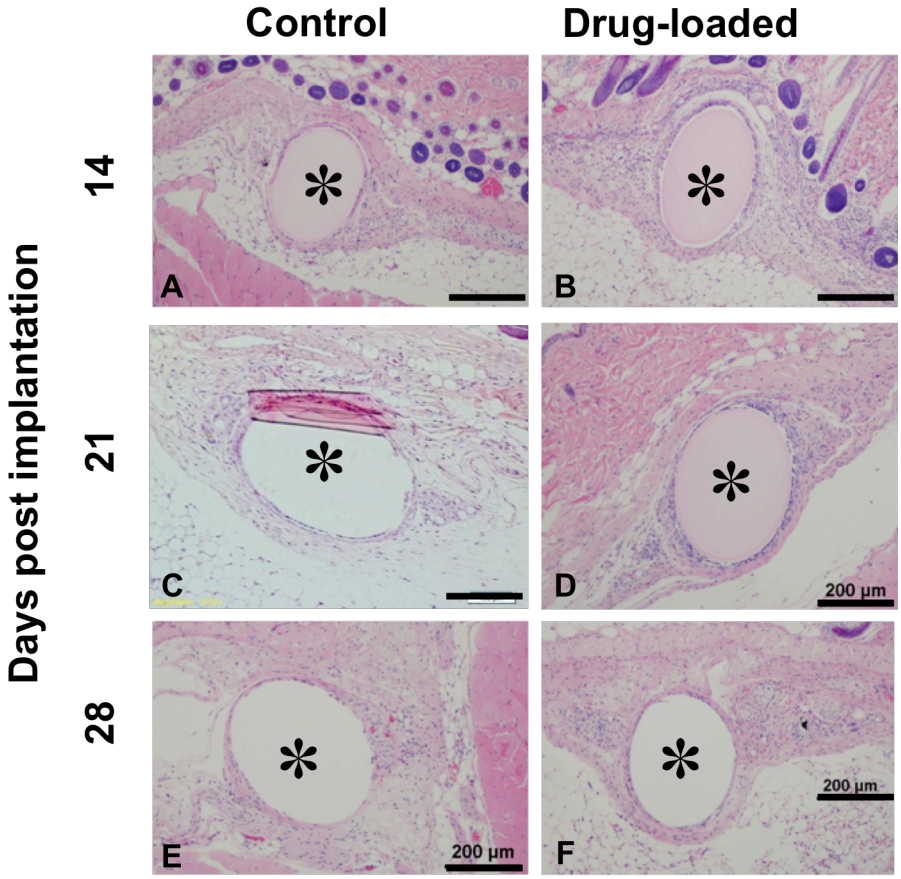

Figure 4.2: H&E stained histology slides showing subcutaneous tissue sites around A), C) and E) control (PLGA microparticle blank) PEG polymer-coated implants and B), D) and F) PLGA microparticle drug-loaded, PEG-polymer-coated implants for 14, 21, and 28-day implants in sash mast cell-deficient mice, respectively. The '*' symbol represents the fiber implant site. Magnification is 20x and scale bar is 200 µm.

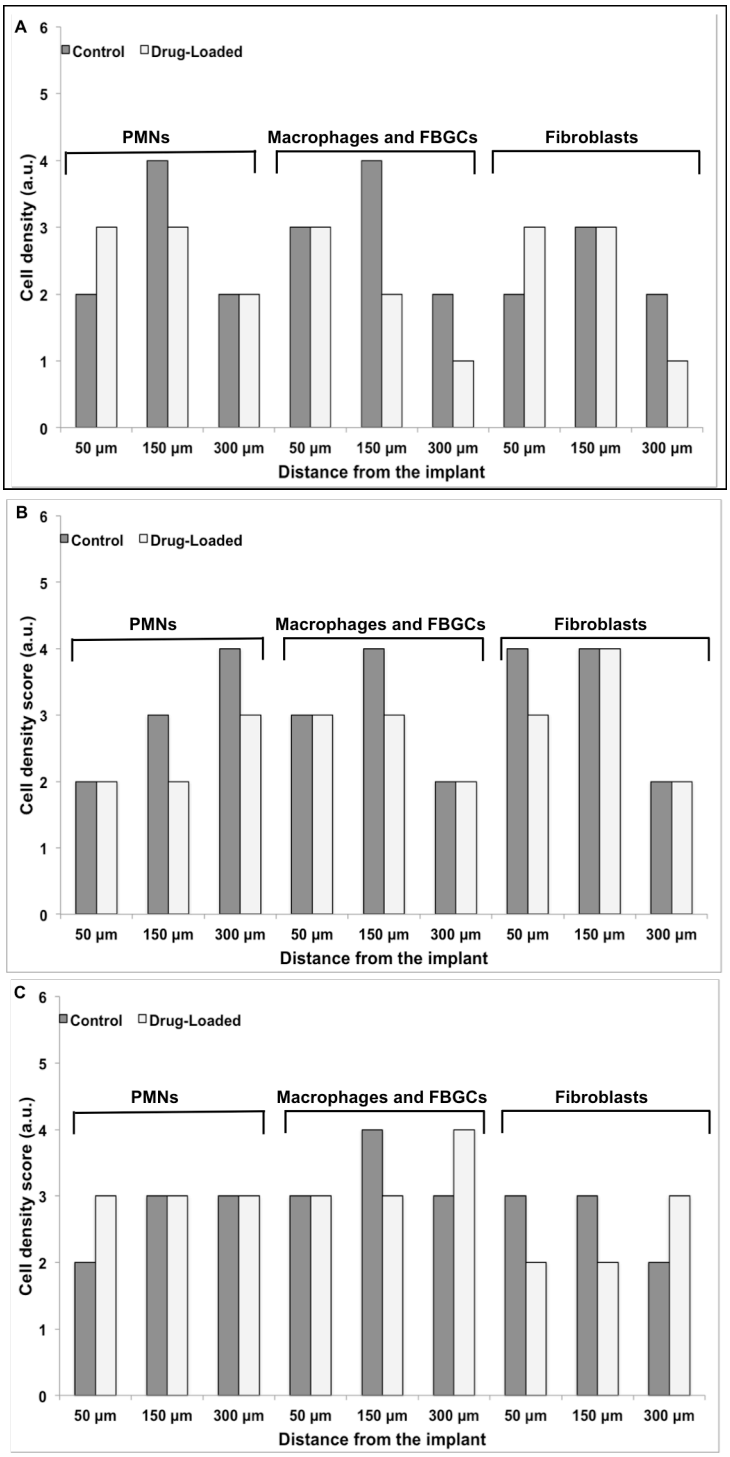

Figure 4.3: Inflammatory cell densities of representative cells contributing to the foreign body response as a function of distance from the implant-tissue interface for A) 14-day, B) 21-day, and C) 28-day implant sites in sash mast cell-deficient mice.

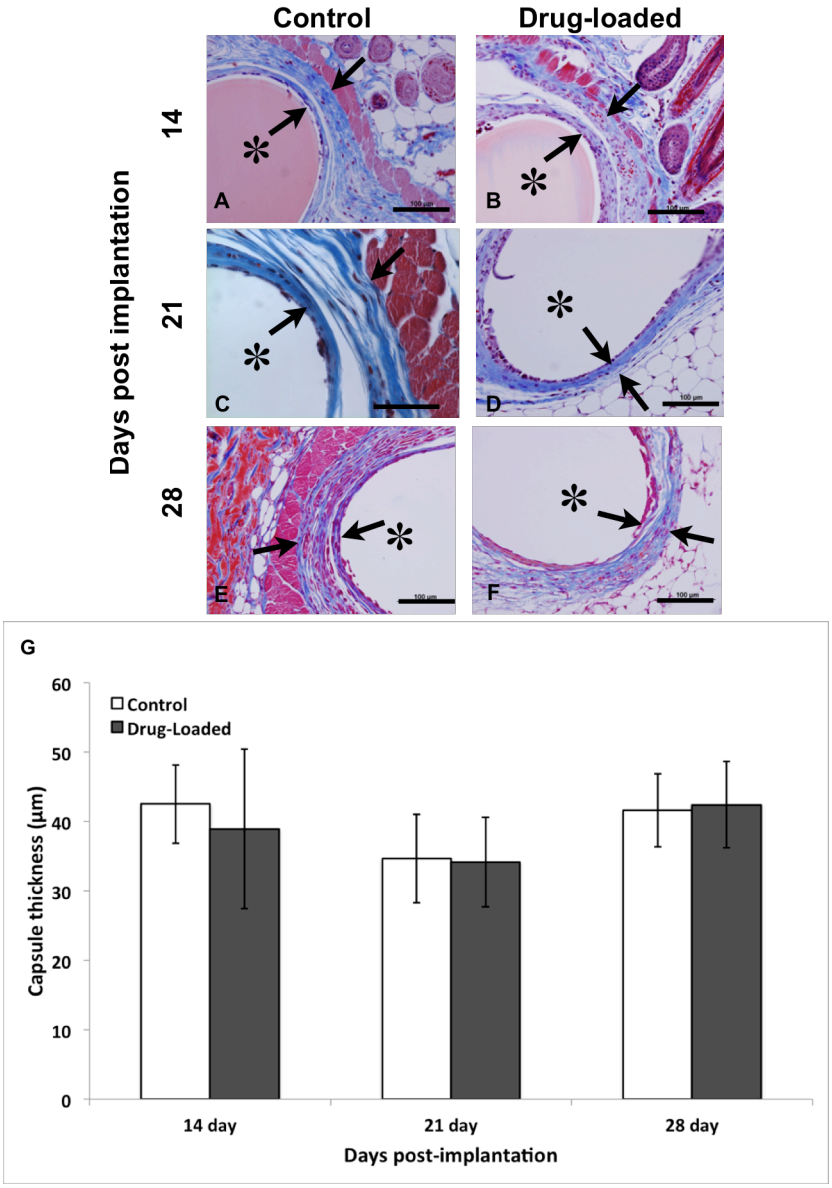

Figure 4.4: Masson's trichrome stained histology slides showing subcutaneous tissue sites around A), C), and E) control (PLGA microparticle blank) PEG polymer-coated implants and B), D), and F) PLGA microparticle drug-loaded, PEG-polymer-coated implants for 14, 21, and 28-day implants, respectively. The '*' symbol represents the implant site. Magnification is 20x and scale bar is 200 µm. G) Comparison of foreign body capsule thickness between control and drug-loaded implant sites in sash mast cell-deficient mice.

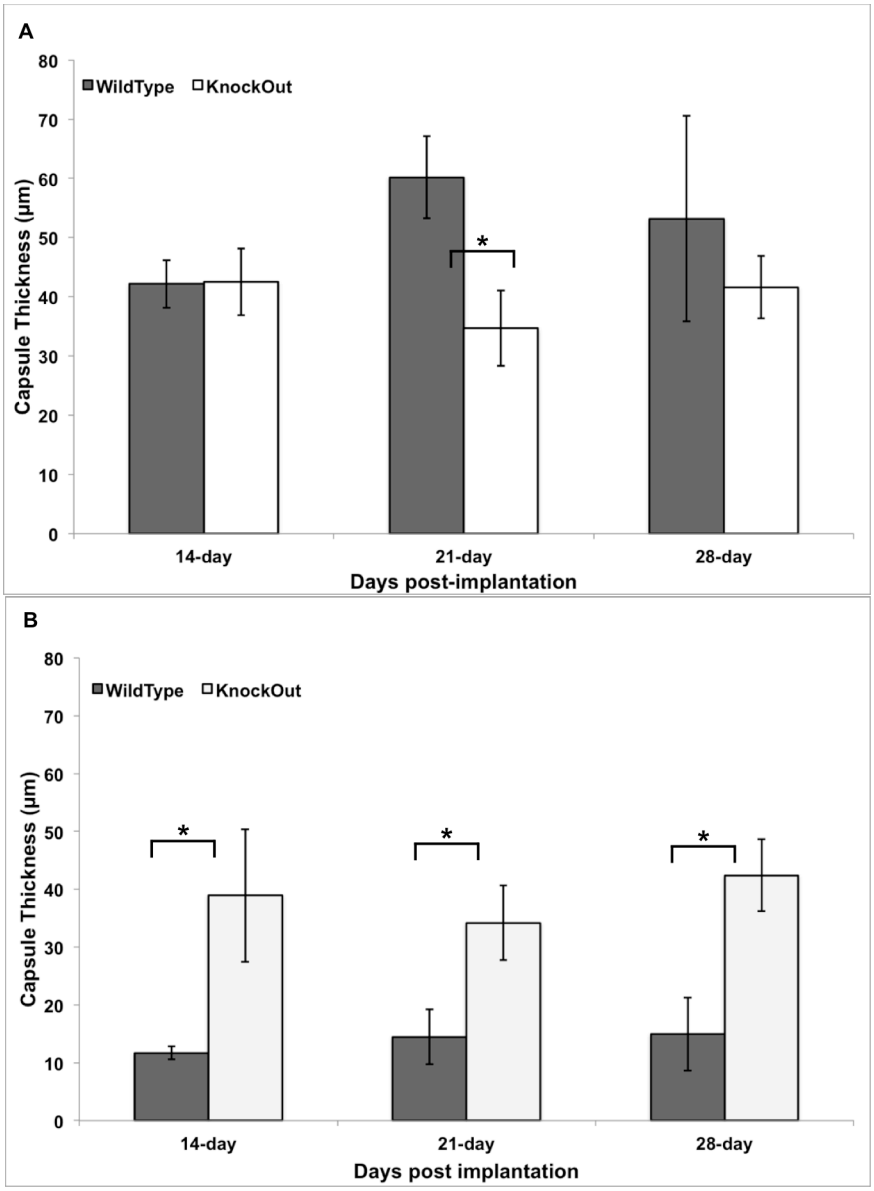

Figure 4.5: Comparison of foreign body capsule thickness between wild-type (taken from data reported in Ref. 12 and plotted here) and sash mast cell-deficient mice for: A) control, and B) drug-loaded implant sites. *$p < 0.05$.

CHAPTER 5

LOCAL RELEASE OF MASITINIB AFFECTS IMPLANTABLE CONTINUOUS GLUCOSE SENSOR PERFORMANCE

M. Avula[1], D. Jones[2], A.N. Rao[3], B. Feldman[4], L.D. McGill[5], D.W. Grainger[1,3*], F. Solzbacher[1,6]

[1]Department of Bioengineering, University of Utah, Salt Lake City, UT 84112 USA

[2]Department of Endocrinology, University of Utah, Salt Lake City, UT 84112 USA

[3]Department of Pharmaceutics and Pharmaceutical Chemistry, University of Utah, Salt Lake City, UT 84112 USA

[4]Abbott Diabetes Care, Alameda, CA USA

[5]Associated Regional and University Pathologist Laboratories, University of Utah, Salt Lake City, UT 84112 USA

[6]Department of Electrical and Computer Engineering, University of Utah, Salt Lake City, UT 84112 USA

[*]corresponding author – David W. Grainger, david.grainger@utah.edu

Keywords: host response, medical device, continuous glucose sensors, encapsulation, mast cells, tyrosine kinase inhibitor, local drug delivery, PLGA microspheres, combination device

---

Article in preparation

5.1 Abstract

Continuous glucose monitoring (CGM) sensors have long been recognized as beneficial for improving long-term glycemic control in the context of diabetes. Subcutaneous sensor fouling and fibrous encapsulation resulting from the host foreign body response (FBR) reduces sensor sensitivity to glucose and eventual produces sensor failure. Several combination device strategies have been evaluated using CGM sensors that release drug payloads locally to tissue sites to mitigate FBR-mediated sensor failure. Here, the mast cell-targeting tyrosine kinase inhibitor, masitinib, was released from polymer microspheres delivered from the surfaces of commercial CGM needle-type implanted sensors. Targeting the mast cell c-Kit receptor and inihibting mast cell activation and degranulation, the local masitinib delivery around the CGM sought to reduce fibrosis around the sensor and extend its functional lifetime in subcutaneous sites. Drug-releasing and control CGM implants were tested in murine percutaneous implant studies for 21 days continuously. Drug-releasing implants showed reduced fibrosis around implant sites and relatively stable sensor responses over the period of the study compared to blank microsphere controls.

5.2 Introduction

Nearly 350 million people (5% of world population) suffer from diabetes worldwide [1], including the 25.8 million Americans (8.3% of the population) who require regular glucose monitoring. Tight regulation of blood glucose has been convincingly shown to reduce diabetes morbidity and mortality [2], leading to a standard of care that demands intensive glucose monitoring. While most glucose monitoring involves painful, inconvenient finger sticks to extract blood, subcutaneous continuous glucose monitoring (CGM) sensors have been clinically available since 1999 as an alternative [3-6].

Currently, four subcutaneous CGM systems are approved for patient self-implantation and marketed, with “real-time” glucose reporting every 1–5 minutes, and with alarm functions for hypo- and hyperglycemia [7, 8]. Three CGMs are needle-type subcutaneous designs: the Freestyle Navigator (Abbott Diabetes Care, Alameda, CA), the Guardian Real-Time (Medtronic MiniMed, Northridge, CA) [9-11], Dexcom G4 Platinum (Dexcom, San Diego, CA). The fourth (GlucoDay, Menarini Diagnostics) is a microdialysis-type sensor. All commonly measure glucose *in situ* amperometrically via the classic Clark glucose oxidase reaction [4-6]. However, as this analyte reaction requires co-transport of tissue glucose and oxygen to the electrode buried within the needle sensor membrane in order to produce the redox chemistry required for sensing, interference with either transport or with the redox chemistry proves problematic to reliable glycemic reporting.

Among several clinical CGM interferents, the host foreign body response (FBR) remains most problematic, limiting human performance to several days once implanted. The FBR involves a complex set of cascades of cell reactions and cytokines in the implant site. Initially, the acute host response is essentially a normal wound healing response to address the wound created by the implant placement. This immediate inflammatory response around the CGM produces confounding influences on glucose response until the acute local tissue reaction subsides to steady state – a phenomenon called “burn in” [7, 12, 13]. However, without implant removal or complete degradation, this acute response to the implant transitions to a chronic inflammatory response that no longer resembles wound healing but has distinct features, including release of inflammatory cytokines IL-4 and IL-13 that accelerate recruitment of inflammatory and immune cells to the implant site [14], formation of unique foreign body giant cells, and finally, fibroblasts that deposit excess collagen and matrix proteins [14-18]. The endpoint of this chronic host response is a fibrous sheath that surrounds the implant, many tens of

microns thick and avascular [17, 19, 20]. This physical collagenous barrier formation (shown in Figure 5.1) frequently hinders analyte transport between host tissue and the CGM, limiting the functional lifetime of this device in subcutaneous sites [14].

As a result of the host-implant response, regulatory approvals for most of these devices in humans are several days instead of the weeks-to-months shown to characterize reliable CGM operation reliably *in vitro*. Significantly, all four FDA-approved sensors exhibit instability over the approved implantation and sensing period (3-7 days), and their pre-implant single-point calibration is thought to be good for only 12 hours [7]. Despite intensive research over two decades, CGM glucose sensing performance under sustained chronic implantation (>14 days) remains a major challenge primarily due to the host's acute and chronic foreign body response (FBR) to the implanted sensor. Given the current performance issues dogging CGMs, barriers to expanding their clinical utility and patient benefits are notable. Longer-term implantable CGM sensors would facilitate the development of a closed-loop glucose sensor–insulin pump system that could improve the quality of life of millions of diabetes patients as an artificial pancreas with dynamic, feedback-driven response [21].

Strategies to improve CGM sensor lifetimes in tissue have focused on refined signal processing [22], improved surface fouling resistance by applying specific coatings to sensor surfaces to inhibit protein and cell adhesion [17, 23], CGM device design refinements, and modifying the CGM as a combination device that releases a drug payload locally from the implant modify local cell and tissue reactions [24-27]. To date, none of these approaches has demonstrated profound changes in the host implant site response to improve CGM functional duration.

CGM surface coatings containing bioactive nitric oxide [28-30], dexamethasone [31-33], and vascular endothelial growth factor (VEGF) [34, 35] both attempt to limit sensor fouling while exploiting a local pharmacological strategy to attenuate the intensity

of the acute phase host inflammatory reaction. Each locally released drug and associated coating matrix approach has formulation, loading, and stability issues, different dosing requirements for given potencies, and different tissue targets. Dexamethasone seeks to inhibit fibroblast production of collagen around the sensor, while VEGF prompts local angiogenesis to endow the FBR fibrotic capsule around the sensor with effective permeability, sufficiently perfused for effective trans-capsular glucose and oxygen transport to the sensor. Significantly, these drug-release approaches have addressed cell targets and behaviors well downstream, as well as temporally and spatially distinct from the early acute-phase FBR mast cell and leukocyte initiating reactivities around the implant.

Mast cells (MC) play a critical role in mediating acute tissue inflammatory responses. Located perivascularly throughout all tissues MCs are mobilized during any inflammatory response [36]. MC degranulation of histamine and other pro-inflammatory mediators including heparin, cytokines (e.g., TNF-alpha), chemokines, and many proteases together with fibrinogen adsorption are recognized as powerful inducers of acute inflammatory responses to implanted biomaterials [37, 38]. MC-released cytokines and chemotaxis along with histamine and serotonin release result in vasodilation and increased recruitment of phagocytes to the implant site. Their connection with the foreign body reaction is well recognized [26, 27, 39]. Specific to CGMs, Klueh et al. [40] have recently compared MC behavior *in vivo* on CGM sensor implant performance in both wild-type and MC-deficient mice. Significantly, they confirmed using CGM signal-to-noise ratio (S/N) and analyte response time as a function of implant time that MCs play a major role in the host FBR around CGMs. Importantly, this effect was linked to subsequent fibrous capsule formation around the CGM that impedes sensor function [40].

Elucidating how MCs orchestrate the host FBR has been elusive. One new clue is that stem cell factor (SCF), the ligand of the MC-specific c-KIT tyrosine kinase receptor, is an important growth factor for MC survival, proliferation, differentiation, and degranulation processes [41]. The link between the MC-specific SCF/MC c-KIT pathway and the intensity of acute phase of the inflammatory response appears critical in MC function and degranulation reactions [42].

Here, we describe use of the newly screened tyrosine kinase inhibitor (TKI), masitinib, shown effective in inhibiting the SCF receptor, c-KIT, on MCs. Masinitib offers potent control of MC reactivity [43, 44] by binding competitively to the ATP-binding c-KIT receptor, blocking its critical tyrosine kinase signaling activity. ***Importantly, this pharmacological action stabilizes mast cells from degranulating or activating***. Use of masitinib to control MC activation in the context of the FBR is unknown. We proposed that its pharmacology could be exploited to benefit CGM function by formulation into a local release coating applied to CGM sensors and implanted subcutaneously in wild type C57BL/6 mice and monitored for CGM function *in situ* for 21 days.

5.3 Materials and Methods

5.3.1 Materials

Poly(lactic-co-glycolic acid) (PLGA) was purchased from Surmodics Biomaterials (now Evonik Biomaterials, USA), and masitinib was purchased from Selleck Chemicals (Houston, USA). Wild-type C57BL/6 mice (12-week old males) were purchased from Jackson Laboratories (Bar Harbor, USA) for the *in vivo* studies. A multichannel potentiostat (CH Instruments model CHI1000C, Austin, USA) was used to interface with CGM sensors to record their *in vitro* and *in vivo* responses. All chemicals were purchased from Sigma Aldrich (USA).

5.3.2 Glucose sensor surface modification, drug loading, and in vitro testing

Modified Freestyle Navigator™ sensors (Abbott Diabetes Care, Alameda, CA) were used for this study. Sensors were coated with a PEG matrix-PLGA microsphere composite formulation as described previously [45, 46]. Briefly, PLGA microspheres containing masitinib were prepared using solvent-evaporation method and then mixed in aqueous PEG solution and the resulting formulation is coated around the commercial CGM sensors cryogenically using a 2-part aluminum mold. Control implant coatings were prepared with a similar process with identical ingredients except masitinib.

A sample of 3 sensors were tested before and after coating in 1x phosphate buffered saline solution (PBS) at 37°C with both 0 and 90 mg/dL glucose concentration to evaluate coating perturbations on the CGM sensor performance in terms of glucose sensitivity and response time.

5.3.3 Sensor implantation procedure

Sensors were implanted with slight modifications from the procedures described by Klueh et al. [40, 47, 48]. Each sensor is tested in 1x PBS at 90 mg/dl glucose to provide *in vitro* calibration values before murine implantation. Mice were anesthetized with 2% isofluorane administered through a nose cap. Fur on back of each animal was clipped in an area of 6×4 cm^2 and cleaned with povidone-iodine solution to create an aseptic location for sensor implantation. A sterile 18G needle was then used to create a point-of-insertion for the CGM sensor. Corneal scissors were used to blunt-dissect the pocket to create space for the sensor. A CGM sensor is inserted into the pocket through the point-of-insertion. The sensor is then glued to the skin using Newskin™ Skin Glue and secured with surgical staples. A thin strip of Velcro™ is then strapped around the animal's abdomen to secure the CGM sensor and avoid relative motion against the skin

at its percutaneous entry. The animals were allowed to recover and housed individually in modified cages to enable securing the sensor wiring and were provided with food and water ad libitum. Sensors were then connected to individual recording channels on the multipotentiostat to continuously monitor glucose levels for a period of 21 days.

5.3.4 Data monitoring and processing

Glucose response current was collected every 60 seconds from the sensors. Moving average glucose values were processed with 120-minute frequency to smoothen the response and to observe the trends over a 21-day period. Raw data are plotted and the 120-minute moving average data are overlapped onto the plot.

Daily maximum and minimum values for each glucose sensor were recorded and plotted with respect to time to observe and better understand the trends of the glucose sensor data.

5.3.5 Histological evaluation

Animals were euthanized and tissue beds surrounding the sensor implant site were harvested at the end of the time period and processed for histological analysis. Tissue slides were fixed in 10% neutral buffered formalin and sent to Associated Research and University Pathologists (ARUP, USA) labs for staining with Hematoxylin and Eosin (H&E), and Masson's Trichrome (MTC) stains. Tissue sites were evaluated for fibrous encapsulation around implant sites from multiple sites on multiple slides for each implant.

5.4 Results

5.4.1 CGM sensor modification

Clinically approved CGM sensors were coated with the PEG-PLGA microsphere composite formulation shown to dissolve completely within a few minutes when exposed

to PBS [45]. This leaves the PLGA microspheres deposited in the tissue bed around the sensor without any sensor interference from a coating [45]. Figure 5.2A shows both the PEG/PLGA composite coated and uncoated sensors. Modified animal housing cages allow wire tethers to extend from the implanted sensors in the animals to the multichannel potentiostat, as shown in Figures 5.2B and 5.2C. Sensor testing before and after polymer coating exhibited less than 10% (i.e., +4.9 to -9.1%) change in response at 90 mg/dl glucose challenge in PBS at 37°C (shown in Figures 5.3A and 5.3B). This minor change is attributed to slight variations resulting from different *in vitro* temperature or experimental variables.

5.4.2 CGM response

Figure 5.4 shows implant CGM *in vivo* response from masitinib-releasing and control implants. Raw sensor output in nA is plotted together with a calibration axis (double right y-axis) since each sensor exhibited different calibrations. Measured glucose values ranged from 100–200 mg/dl over the first few days. All sensors exhibit an initial drop in glucose values for the first few days after implantation (i.e., sensor burn in). Sensor response fluctuates as a result of variations in normal animal activity (i.e., glycogen release) and in blood glucose due to food intake. Figure 5.4A shows the response from a drug-releasing implant that is relatively consistent and stable compared to control implant output. CGM response from drug-releasing implants seen from the 120-minute moving average data is consistent over the implantation period whereas a marked loss of glucose sensitivity is observed in control sensors, as seen in Figures 5.4B-5.4D.

5.4.3 Histology analysis

Analysis of Masson's trichrome-stained histology tissue sites from 21-day implant harvests shows very little inflammation around drug-releasing implant sites and

comparatively higher amounts of fibrosis around control implants as characterized by the blue collagen staining seen in Figure 5.5A and 5.5B. A thin layer of collagen 1-2 cell layers thick could be observed around drug-releasing implants whereas a uniform region of collagen deposition was observed in control implants.

5.5 Discussion

Strategies to enable continuous and reliable CGM sensor response in tissue sites for longer durations than existing implantation times (e.g., currently ~1 week) is currently a major challenge plaguing long-term CGM performance. Several combination device strategies have sought to use on-board drug delivery from the sensor to "condition" the implant site pharmacologically and enhance the local sensor-tissue interface [24-30]. Tissue mast cells have been shown to be important to eliciting the FBR around CGM sensors during the acute inflammatory response stage, affecting their tissue site performance [40]. Targeting the SCF/c-KIT pathway to inhibit degranulation and activation pathways in tissue mast cells around implantable CGM sensors exploits the pharmacology of the TKI, masitinib. Previous work has shown reductions in the fibrous capsule thickness formed around masitinib-releasing nonfunctional sensor model implants [45]. That this observed reduced fibrosis around masitinib-releasing implants translates to improved CGM response *in vivo* was pursued in this study.

PEG-PLGA microsphere composite coatings were designed to dissolve within minutes of implantation to allow unhindered glucose access to the sensor surface [45, 46]. This coating shows no significant effect on the sensors' glucose sensitivity: less than 10% change is observed in sensor signal outputs tested *in vitro* before and after coating in a glucose standard. The coating also does not appear to affect sensor performance in the *in vivo* studies as well. A normal "break-in" period is observed in sensor response from control implants, during which sensitivity drops immediately after implantation (see

Figure 5.4) as has been previously observed in several studies [7, 12, 13]. Drug-releasing implants show relatively reduced sensor break-in responses during this early implantation period (data not shown), suggesting lower intensities of tissue inflammatory responses around these implants during acute stages.

Sensor response over the entire duration of the 21-day study, characterized by the moving average data (Figure 5.4), shows a clear distinction in responses between drug-releasing and control implants. Drug-releasing implants exhibit stable glucose values with consistent, periodic fluctuations attributed to animal physical activity and food consumption, whereas in the control implants loss of sensor function is observed in various forms. For example, data from sensor 413C shown in Figure 5.4B exhibit a clear change in glucose fluctuations, specifically after day 14, which can be attributed to limited glucose availability to the sensor.

Maximum and minimum glucose value trend plots shown in Figure 5.5 provide a better understanding to CGM response for a given sensor. Data shown in Figure 5.5A and 5.5C from the control implants show a consistent degradation of sensor signal as evidenced by the decreasing difference between the maximum and minimum values for a given time point. The moving sensor data and the daily maximum and minimum trend data suggest that the CGM sensors get decreasing access to environmental glucose over the duration of the study. Control CGM implants exhibit a greater loss in glucose sensitivity compared to the durg-treated CGM sensors. This loss in sensitivity can be attributed to the steric hindrance of the fibrous capsule surrounding the implants and can also be attributed to the consumption of glucose by the various cell types involved in mediating the foreign body response to the implants.

Histology evaluation shows reduced inflammation and collagen deposition around masitinib-releasing implants compared to control implants at 21 days (Figure 5.6). The effect of masitinib in targeting fibroblasts via mast cell-stabilization and through

the inhibition of fibroblast growth factor receptor 3 (FGFR3) might contribute to this collagen difference [43, 46]. Klueh et al. [40] recently reported similar reduced fibrosis around subcutaneous implants in mast cell-deficient sash mouse models.

Use of the mouse subcutaneous implant model to evaluate the effects of the host FBR on CGM performance is more appropriate for short-term investigative studies than longer-term implants due to notable dissimilarities in their dermal physiology compared to humans. Intrinsically thin dermis combined with the presence of a muscle layer adjacent to the dermis without significant cutaneous adipose in these animals contributes to increased mechanical micromotion from subcutaneous muscle twitches upon implantation that is minimal or absent in human tissues. This murine muscle micromotion can be further exacerbated by tethering the external portion of the CGM implant to the recording device and allowing the animals free movement while tethered for 21 days [49]. The relative size of the actual CGM implant approved for human use compared to the animal's body can even further result in micromotion-associated tissue responses that are independent of the implantation and tethering process. Lastly, human CGMs are recommended clinically to be best placed in subdermal adipose tissue in humans [50], a situation very unlikely in the murine model given their lack of such adipose in skin. All of these differences are likely contributing factors to fluctuations observed in the implanted CGM sensor outputs. Evaluating the CGM sensors and effects of local drug release targeting mast cell-implant activation responses relevant to the FBR might be more accurately performed in porcine models with their dermal tissue physiology similar to humans.

5.6 Conclusions

CGMs modified to release the TKI inhibitor, masitinib, exhibit stable glucose readings *in vivo*. Sensor performance is improved providing improved glucose sensing

in the presence of masitinib. Reduced glucose sensor sensitivity can be attributed to the consumption of glucose by cells surrounding the implant site. Masitinib-releasing PEG-PLGA microsphere coating on CGM sensors show reduced collagen formation around the implant site, suggesting that local tissue mast cell and fibroblast functions are affected by the drug. Implant-associated micromotion can be causing the fluctuations in the sensor response.

5.7 Acknowledgements

The authors acknowledge support from the University of Utah Research Foundation in the form of both SEED and Technology Commercialization grants. D. Sze, B. Cho, R. Caldwell, and P. Hogrebe are thanked for their support and help in technical discussions. Author F. Solzbacher has a financial interest in the company Blackrock Microsystems (USA) that develops and produces implantable neural interfaces and electrophysiological equipment and software, none of which is used in this study.

5.8 References

[1] Danaei G, Finucane MM, Lu Y, Singh GM, Cowan MJ, Paciorek CJ, et al. National, regional, and global trends in fasting plasma glucose and diabetes prevalence since 1980: systematic analysis of health examination surveys and epidemiological studies with 370 country-years and 2.7 million participants. The Lancet. 2011;378:31-40.

[2] Coster S, Gulliford MC, Seed PT, Powrie JK, Swaminathan R. Monitoring blood glucose control in diabetes mellitus: a systematic review. Health Technol Assess. 2000;4:i-iv, 1-93.

[3] Bode BW, Gross TM, Thornton KR, Mastrototaro JJ. Continuous glucose monitoring used to adjust diabetes therapy improves glycosylated hemoglobin: a pilot study. Diabetes Res Clin Pract. 1999;46:183-90.

[4] Chase HP, Kim LM, Owen SL, MacKenzie TA, Klingensmith GJ, Murtfeldt R, et al. Continuous subcutaneous glucose monitoring in children with type 1 diabetes. Pediatrics. 2001;107:222-6.

[5] Ludvigsson J, Hanas R. Continuous subcutaneous glucose monitoring improved metabolic control in pediatric patients with type 1 diabetes: a controlled crossover study. Pediatrics. 2003;111:933-8.

[6] Tanenberg R, Bode B, Lane W, Levetan C, Mestman J, Harmel AP, et al. Use of the Continuous Glucose Monitoring System to guide therapy in patients with insulin-treated diabetes: a randomized controlled trial. Mayo Clinic proceedings Mayo Clinic. 2004;79:1521-6.

[7] Wilson GSZ, Y. Introduction to the Glucose Sensing Problem. In Vivo Glucose Sensing. Hoboken, NJ: John Wiley; 2010.

[8] Liao KC, Hogen-Esch T, Richmond FJ, Marcu L, Clifton W, Loeb GE. Percutaneous fiber-optic sensor for chronic glucose monitoring in vivo. Biosens Bioelectron. 2008;23:1458-65.

[9] Jungheim K, Wientjes K, Heinemann L, Lodwig V, Koschinsky T, Schoonen A. Subcutaneous continuous glucose monitoring. Diabetes Care. 2001;24:1696.

[10] Koschwanez H, Reichert W. In vitro, in vivo and post explantation testing of glucose-detecting biosensors: Current methods and recommendations. Biomaterials. 2007;28:3687-703.

[11] Wilson G, Hu Y. Enzyme-based biosensors for in vivo measurements. Chem Rev. 2000;100:2693-704.

[12] Gifford R, Kehoe J, Barnes S, Kornilayev B, Alterman M, Wilson G. Protein interactions with subcutaneously implanted biosensors. Biomaterials. 2006;27:2587-98.

[13] Wisniewski N, Moussy F, Reichert W. Characterization of implantable biosensor membrane biofouling. Fresenius' J Anal Chem. 2000;366:611-21.

[14] Anderson JM, Rodriguez A, Chang DT. Foreign body reaction to biomaterials. Semin Immunol. 2008;20:86-100.

[15] Murch AR, Grounds MD, Marshall CA, Papadimitriou JM. Direct evidence that inflammatory multinucleate giant cells form by fusion. J Pathol. 1982;137:177-80.

[16] Frost MC, Meyerhoff ME. Implantable chemical sensors for real-time clinical monitoring: progress and challenges. Curr Opin Chem Biol. 2002;6:633-41.

[17] Wilson GS, Gifford R. Biosensors for real-time in vivo measurements. Biosens Bioelectron. 2005;20:2388-403.

[18] Miller KM, Rose-Caprara V, Anderson JM. Generation of IL-1-like activity in response to biomedical polymer implants: a comparison of in vitro and in vivo models. J Biomed Mater Res. 1989;23:1007-26.

[19] Gerritsen M, Jansen JA, Lutterman JA. Performance of subcutaneously implanted glucose sensors for continuous monitoring. Neth J Med. 1999;54:167-79.

[20] Wisniewski N, Moussy F, Reichert WM. Characterization of implantable biosensor membrane biofouling. Fresenius' J Anal Chem. 2000;366:611-21.

[21] Cobelli C, Renard E, Kovatchev B. Artificial pancreas: past, present, future. Diabetes. 2011;60:2672-82.

[22] Facchinetti A, Sparacino G, Cobelli C. Modeling the error of continuous glucose monitoring sensor data: critical aspects discussed through simulation studies. J Diabetes Sci Technol. 2010;4:4-14.

[23] Wisniewski N, Reichert M. Methods for reducing biosensor membrane biofouling. Colloids Surf B Biointerfaces. 2000;18:197-219.

[24] Hickey T, Kreutzer D, Burgess D, Moussy F. Dexamethasone/PLGA microspheres for continuous delivery of an anti-inflammatory drug for implantable medical devices. Biomaterials. 2002;23:1649-56.

[25] Hickey T, Kreutzer D, Burgess D, Moussy F. In vivo evaluation of a dexamethasone/PLGA microsphere system designed to suppress the inflammatory tissue response to implantable medical devices. J Biomed Mater Res. 2002;61:180-7.

[26] Ward WK, Wood MD, Casey HM, Quinn MJ, Federiuk IF. The effect of local subcutaneous delivery of vascular endothelial growth factor on the function of a chronically implanted amperometric glucose sensor. Diabetes Technol Ther. 2004;6:137-45.

[27] Ward WK, Troupe JE. Assessment of chronically implanted subcutaneous glucose sensors in dogs: The effect of surrounding fluid masses. ASAIO J. 1999;45:555-61.

[28] Nichols SP, Le NN, Klitzman B, Schoenfisch MH. Increased In Vivo Glucose Recovery via Nitric Oxide Release. Anal Chem. 2011;83:1180-4.

[29] Nablo BJ, Prichard HL, Butler RD, Klitzman B, Schoenfisch MH. Inhibition of implant-associated infections via nitric oxide release. Biomaterials. 2005;26:6984-90.

[30] Hetrick EM, Prichard HL, Klitzman B, Schoenfisch MH. Reduced foreign body response at nitric oxide-releasing subcutaneous implants. Biomaterials. 2007;28:4571-80.

[31] Bhardwaj U, Sura R, Papadimitrakopoulos F, Burgess DJ. Controlling acute inflammation with fast releasing dexamethasone-PLGA microsphere/pva hydrogel composites for implantable devices. J Diabetes Sci Technol. 2007;1:8-17.

[32] Hickey T, Kreutzer D, Burgess DJ, Moussy F. Dexamethasone/PLGA microspheres for continuous delivery of an anti-inflammatory drug for implantable medical devices. Biomaterials. 2002;23:1649-56.

[33] Ju YM, Yu B, West L, Moussy Y, Moussy F. A dexamethasone-loaded PLGA microspheres/collagen scaffold composite for implantable glucose sensors. J Biomed Mater Res A. 2010;93:200-10.

[34] Golub JS, Kim Y-t, Duvall CL, Bellamkonda RV, Gupta D, Lin AS, et al. Sustained VEGF delivery via PLGA nanoparticles promotes vascular growth. Am J Physiol Heart Circ Physiol. 2010;298:H1959-H65.

[35] Sung J, Barone PW, Kong H, Strano MS. Sequential delivery of dexamethasone and VEGF to control local tissue response for carbon nanotube fluorescence based micro-capillary implantable sensors. Biomaterials. 2009;30:622-31.

[36] Krishnaswamy G, Ajitawi O, Chi DS. The human mast cell: an overview. Methods in molecular biology (Clifton, NJ). 2006;315:13-34.

[37] Zdolsek J, Eaton J, Tang L. Histamine release and fibrinogen adsorption mediate acute inflammatory responses to biomaterial implants in humans. J Transl Med. 2007;5:31.

[38] Tang L, Jennings TA, Eaton JW. Mast cells mediate acute inflammatory responses to implanted biomaterials. Proc Natl Acad Sci U S A. 1998;95:8841-6.

[39] Thevenot PT, Baker DW, Weng H, Sun M-W, Tang L. The pivotal role of fibrocytes and mast cells in mediating fibrotic reactions to biomaterials. Biomaterials. 2011;32:8394-403.

[40] Klueh U, Kaur M, Qiao Y, Kreutzer DL. Critical role of tissue mast cells in controlling long-term glucose sensor function in vivo. Biomaterials. 2010;31:4540-51.

[41] Reber L, Da Silva CA, Frossard N. Stem cell factor and its receptor c-Kit as targets for inflammatory diseases. Eur J Pharmacol. 2006;533:327-40.

[42] Reber L, Da Silva CA, Frossard N. Stem cell factor and its receptor c-Kit as targets for inflammatory diseases. Eur J Pharmacol. 2006;533:327-40.

[43] Dubreuil P, Letard S, Ciufolini M, Gros L, Humbert M, Casteran N, et al. Masitinib (AB1010), a potent and selective tyrosine kinase inhibitor targeting KIT. PLoS ONE. 2009;4:e7258.

[44] Paul C, Sans B, Suarez F, Casassus P, Barete S, Lanternier F, et al. Masitinib for the treatment of systemic and cutaneous mastocytosis with handicap: a phase 2a study. Am J Hematol. 2010;85:921-5.

[45] Avula MN, Rao AN, McGill LD, Grainger DW, Solzbacher F. Modulation of the foreign body response to implanted sensor models through device-based delivery of the tyrosine kinase inhibitor, masitinib. Biomaterials. 2013;34:9737-46.

[46] Avula MN, Rao AN, McGill LD, Grainger DW, Solzbacher F. Foreign Body Response To Implanted Biomaterials in a Mast Cell-deficient Kitw-Sh Murine Model. Acta Biomater. 2013;Submitted.

[47] Klueh U, Dorsky DI, Kreutzer DL. Enhancement of implantable glucose sensor function in vivo using gene transfer-induced neovascularization. Biomaterials. 2005;26:1155-63.

[48] Klueh U, Liu Z, Cho B, Ouyang T, Feldman B, Henning TP, et al. Continuous glucose monitoring in normal mice and mice with prediabetes and diabetes. Diabetes Technol Ther. 2006;8:402-12.

[49] Helton KL, Ratner BD, Wisniewski NA. Biomechanics of the sensor-tissue interface-effects of motion, pressure, and design on sensor performance and the foreign body response-part I: theoretical framework. J Diabetes Sci Technol. 2011;5:632-46.

[50] Nielsen JK, Djurhuus CB, Gravholt CH, Carus AC, Granild-Jensen J, Orskov H, et al. Continuous glucose monitoring in interstitial subcutaneous adipose tissue and skeletal muscle reflects excursions in cerebral cortex. Diabetes. 2005;54:1635-9.

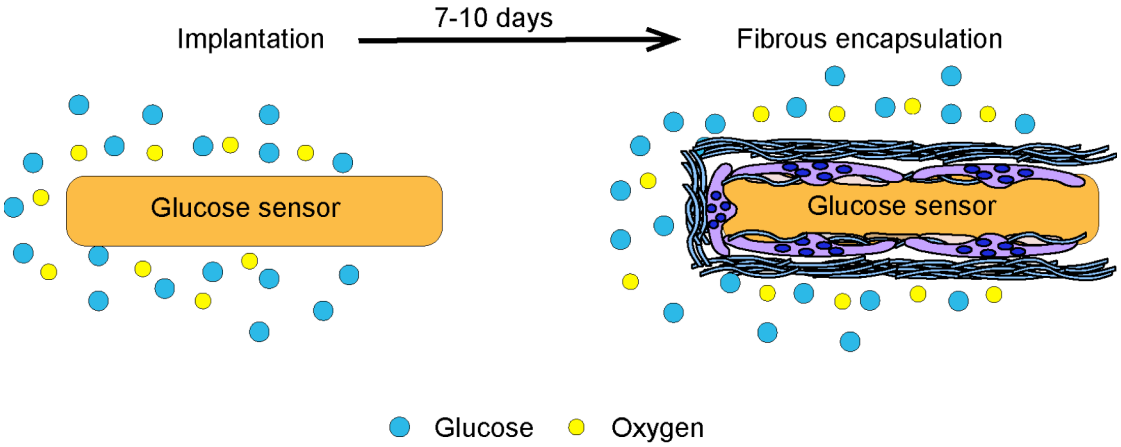

Figure 5.1: Conceptual depiction of the collagenous encapsulation of implanted CGM sensors *in vivo* after 7-10 days of implantation.

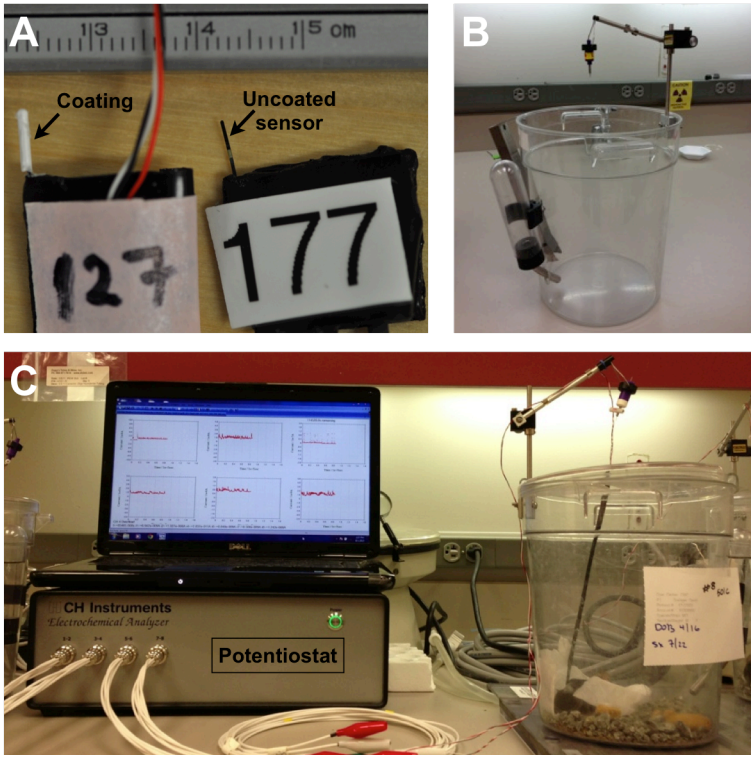

Figure 5.2: Sensor and experimental setup. A) CGM sensors before and after coating, B) modified cage for housing mice with CGM implants during the long-term 21-day implant study, and C) test station used to interface with implant CGM and the multichannel recording device.

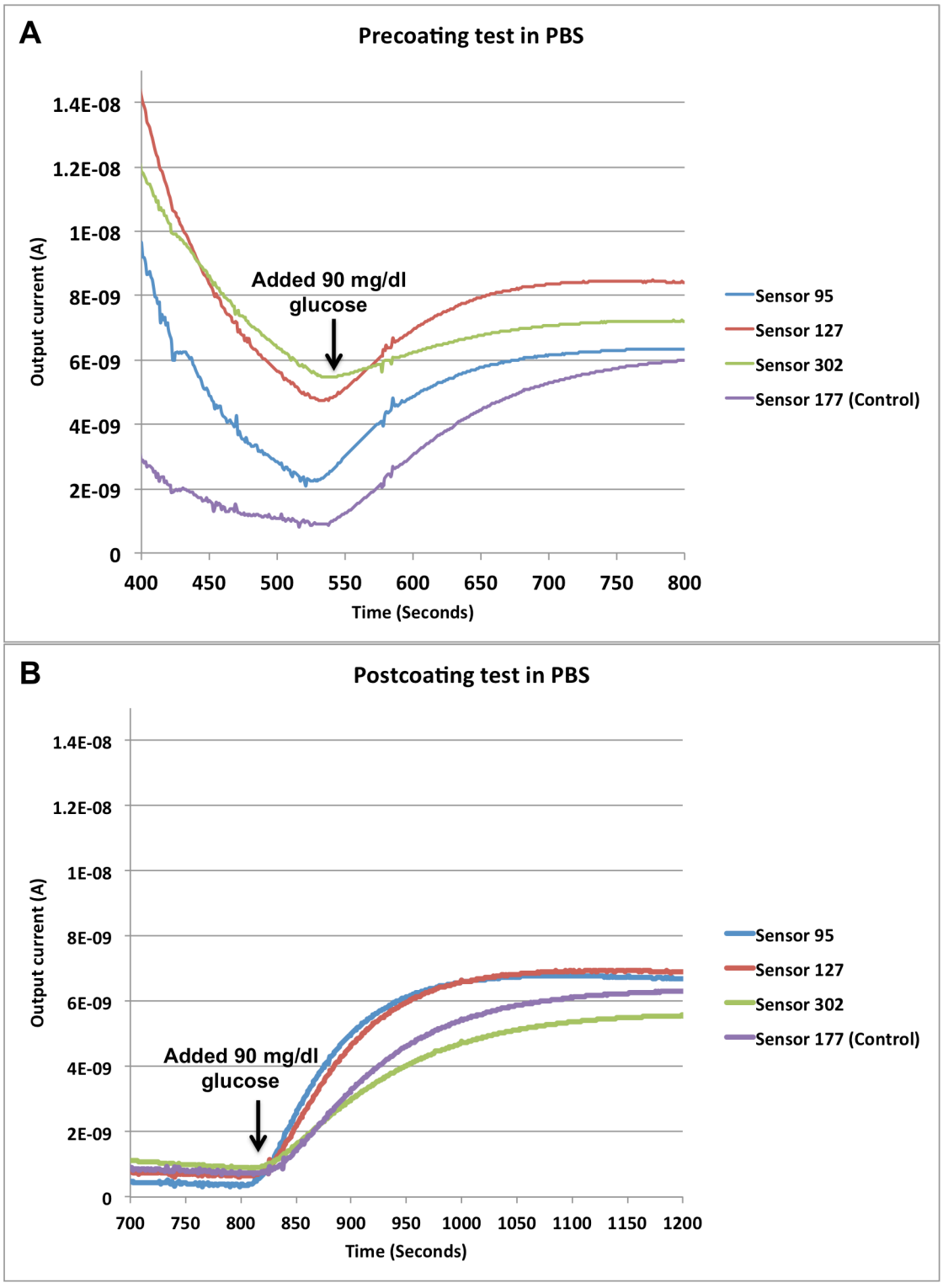

Figure 5.3: Sensor response to *in vitro* dynamic glucose change from 0 to 90 mg/dl: A) before modifying coating, and B) after PEG/PLGA composite coating.

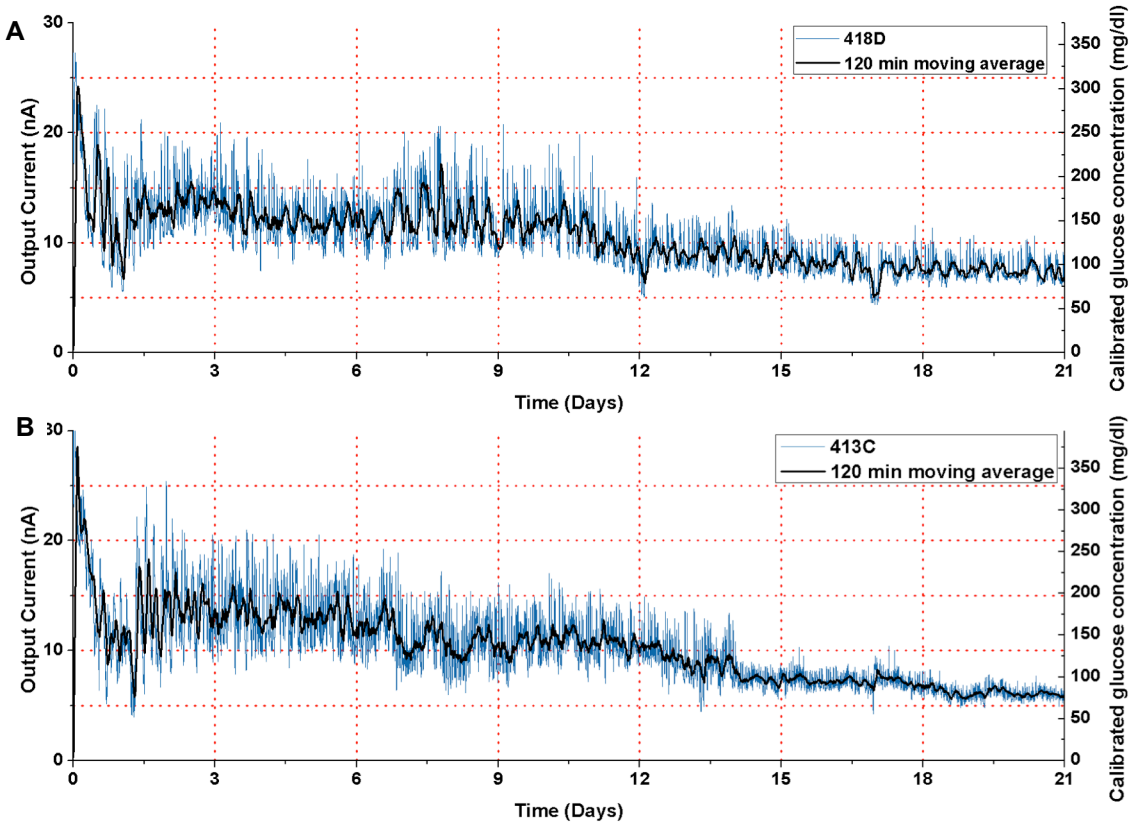

Figure 5.4: Implanted CGM sensor response monitored in real-time for 21 days by direct wired CGM implants in murine subcutaneous sites: A) Drug-releasing CGM, and B) control CGM sensors. Y-axis, left is raw amperometic output; y-axis right is calibrated glucose measurements.

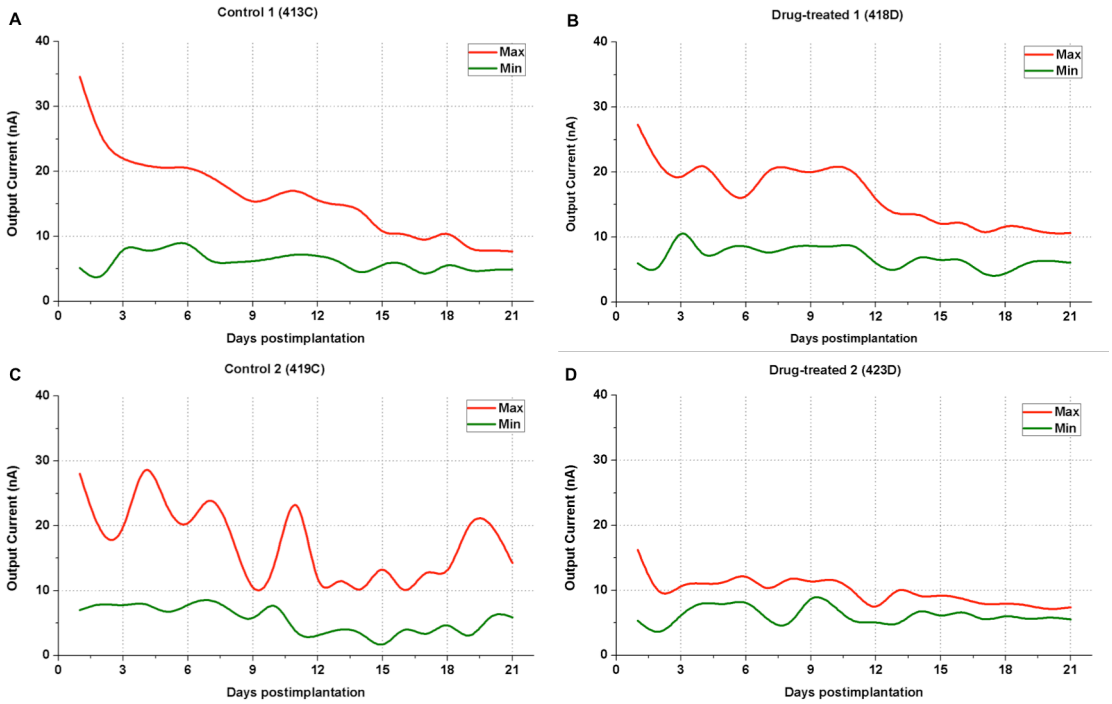

Figure 5.5: Plot showing daily maximum and minimum values of CGM sensor response. A) and C) Control implants, and B) and D) Drug-treated implants.

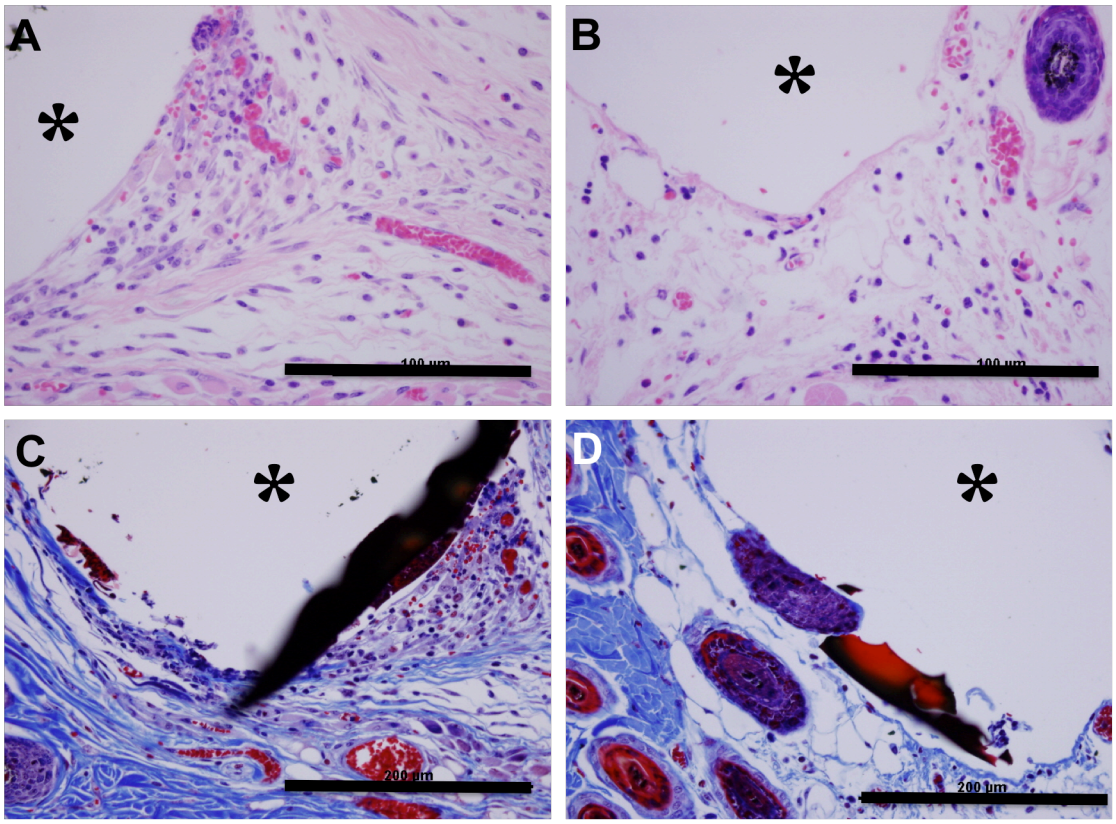

Figure 5.6: H&E stained tissue sites for A) control (blank), and B) drug-releasing coated implants; Masson's trichrome stained tissue sites for: C) control (blank), and D) drug-releasing coated implants explanted after 21 days in murine subcutaneous sites. '*' shows the location of the implant site. Scale 200 µm.

CHAPTER 6

SUMMARY OF RESEARCH AND SUGGESTED FUTURE WORK

This closing chapter presents a summary of the major results in addressing the motivation for the research, and selected technical recommendations for future studies. Diabetes mellitus is an epidemic characterized by chronic hyperglycemia resulting from insufficient production or tolerance to insulin. Nearly 350 million people (5% of world population) suffer from diabetes worldwide [1], including the 25.8 million Americans (8.3% of the population) who require regular glucose monitoring. Treatment has direct and indirect costs of about $218 billion annually (2007) [2]. Tight regulation of blood glucose has been convincingly shown to reduce diabetes morbidity and mortality [3], leading to a standard of care that demands intensive glucose monitoring.

Alternatives to the current CGM sensor implants lasting less than a week need to be developed for long-term reliable glucose monitoring that would enable the development of closed-loop insulin delivery systems that are extremely beneficial to younger patients. Long-term fully implantable sensors will improve the device performance while reducing the costs and discomfort associated with needle type percutaneous implants. Fully implantable sensors eliminate the problems associated with percutaneous implants such as infection of the wound site, fibrosis associated with tethering of the implants, adhesion problems of the transmitter base to the epidermis, etc. Problems with wireless charging and telemetry exist with the conception of such systems and can be adopted from other existing devices such as pacemakers and improvements in low power wireless data communication technology. The successful

culmination of this project would be the combination of a fully implantable sensor device and an efficient targeting of early phase tissue response to delay and/or modify FBR and the associated fibrous encapsulation.

6.1 Chapter 3: Modulation of the Foreign Body Response to Implanted Sensor Models Through Device-based Delivery of the Tyrosine Kinase Inhibitor, Masitinib

6.1.1 Motivation for this work

Continuous glucose monitoring (CGM) sensors are adversely affected by the host foreign body response. Fibrous encapsulation resulting from the FBR degrades the sensing ability of CGM sensors by "walling-off" the sensor from the essential analytes such as glucose and oxygen. Mast cells among several other cell types and cell-signaling molecules are known to play a key role in mediating the formation of this fibrous capsule [4]. Mast cells play a critical role in the acute inflammatory response by degranulating and secreting key cell-signaling molecules, including vasodilators like histamine and serotonin, and inflammatory cell recruiting cytokines like IL-4 and IL-13 [4-8]. We hypothesized that targeting mast cell degranulation would result in a less intense FBR and hence could be used to improve the longevity and performance of CGM sensors. To test our hypothesis, we chose masitinib – a newly developed tyrosine kinase inhibitor to target mast cell degranulation via the targeting of c-KIT receptor known to be essential for mast cell survival, proliferation, and degranulation [9, 10].

6.1.2 Summary of research work

Polyester fibers were chosen as the sensor model implants that would mimic the dimensions and material properties of a CGM sensor. Masitinib release in the local tissue surrounding the implant could be efficiently managed by the formulation of a local delivery mechanism. Poly (D,L-lactic-co-glycolic acid) (PLGA) is a well-studied

biodegradable polymer commonly commercially used as a drug delivery vehicle for various agents (e.g., peptides, hormones, siRNA, DNA, VEGF, protein therapeutics, and small molecules) [11-16]. PLGA of three different intrinsic viscosities was selected as the drug carrier and was formulated into 5-20 μm diameter microspheres to avoid phagocytosis. *In vitro* release kinetics were determined for 30 days to characterize the release profiles of the drug. The microspheres were then combined with an aqueous solution of PEG-PEO mixture that was chosen as the matrix material to transiently hold microspheres around the implants until implantation. The PEG-PLGA microsphere coating was fabricated around the implants using mold coating techniques. The coated sensor models were then implanted in murine subcutaneous tissue for 14, 21, and 28 days and the tissue surrounding the implant sites was analyzed using histology to evaluate the effect of mast cells on FBR.

6.1.3 Critical assessments

A coating formulation that could transiently contain drug-releasing microspheres around the implant could be developed. The coating design allowed it to completely disintegrate in bodily fluids upon implantation, thereby releasing the microspheres in the vicinity of the implant and enabling unhindered implant-tissue interactions. Histology analysis showed complex inflammatory cell densities around the implantation site. The complexity can be attributed to the presence of two distinct implant types, i.e., a monolith, low surface area polyester fiber sensor model, and a low density, high surface area, and foam-like disintegrated PEG-PLGA microsphere coating. The presence of these distinct implant types would cause the FBR to the implants to proceed independently with two separate timelines for the various cell arrivals causing a complicated inflammatory cell density. However, the capsule thickness assessments around the sensor model implants show a clear and significant reduction in the thickness

values around drug-releasing implants compared to the control implant sites. These results would suggest that mast cells play an important role in mediating capsule formation around implants. Although the results show a clear decrease in capsule thickness around the drug-releasing implant sites, it is unclear if these capsules are permeable to glucose and oxygen – the two most important molecules for the detection of glucose, to the sensor surface.

6.2 Chapter 4: Foreign Body Response to Implanted Biomaterials in a Mast Cell-deficient Kit$^{w\text{-}Sh}$ Murine Model

6.2.1 Motivation for this work

In Chapter 2, we had tested the effect of masitinib-releasing implants on the tissue response and the subsequent fibrous capsule resulting from it. Masitinib is a potent inhibitor of c-KIT receptor that is critical for mast cell survival. Therefore, masitinib-releasing implants are expected to downregulate mast cell degranulation and result in lower fibrosis of implants. We have seen evidence for this downregulation of mast cell activity in the form of reduced capsule thickness around masitinib-releasing implants in wild-type mice. To ensure that masitinib is only affecting mast cell activity, we needed to test the drug in mast cell-deficient sash mouse model. By testing both control and drug-releasing implants in the sash mouse model, the effect of masitinib could be understood on the modulation of FBR. Additionally, FBR can be studied in the absence of mast cells.

6.2.2 Summary of research work

In this study, polyester fiber sensor models were coated with the PEG-PLGA microsphere coating and implanted in mast cell-deficient sash mouse model for 14-, 21-, and 28-day time points. At the end of each time point, the animals were euthanized and

the tissue bed surrounding the implant sites was harvested and histological analysis was performed.

6.2.3 Critical assessments

Masitinib release in sash mice did not seem to effect the capsule formation around the implant site. Capsule thickness values around control and drug-releasing implants seemed to be similar and the inflammatory cell densities were found to be comparable. Capsule thickness assessment has also shown that there is no comparable increase in the fibrosis among the 14-, 21-, and 28-day implant sites. However, the capsule thickness values around drug-releasing implants around sash mice were found to be significantly higher when compared to those in wild-type mice. These results indicate that the modulation of FBR in the absence of mast cells has an alternative pathway and that the fibrosis manifests earlier than in mast cell sufficient mice and remains largely unchanged for long-term implants.

6.3 Chapter 5: Local Release of Masitinib Affects Implantable Continuous Glucose Sensor Performance

6.3.1 Motivation for this work

In Chapters 2 and 3, the effect of masitinib and the role of mast cells in modulating FBR and the resulting fibrosis were evaluated using sensor models. In this chapter, we designed a study to test commercial CGM sensors that are coated with masitinib-releasing formulation in wild-type mouse for 21 days. The goal of this study was to examine any performance improvements in the masitinib-coated CGM response over a control. Commercial CGM sensors are have FDA-approved implantation times limited to less than a week. The purpose of this study was to examine the possibility of improvements in reliability of glucose sensing values over the FDA-approved periods. This would culminate the work proposed in this dissertation by confirming that targeting

tissue mast cells around the implantation site of a CGM sensor would affect its long-term performance.

6.3.2 Summary of research

In this study, modified Abbott Freestyle Navigator sensors were used as the implants. The PEG-PLGA microsphere coating process was modified for the CGM sensors. PEG-PLGA microsphere-coated sensors were tested before and after the coating process to evaluate the effects of the coating process on the sensor response in terms of sensitivity and response times to glucose changes *in vitro*. The coated sensors were then implanted in wild-type C57BL/6 mice for 21 days. These time points are ~5-7x the FDA-approved implantation time for the sensor. At the end of the time points, the tissue surrounding the sensor implant site was harvested and analyzed using histology for capsule thickness. A sample of implanted sensors were tested postmortem for the respective time points to evaluate their performance

6.3.3 Critical assessments

CGMs modified to release the TKI inhibitor, masitinib, exihibit stable glucose readings *in vivo*. Sensor performance is improved providing consistent glucose sensing in the presence of masitinib. Masitinib-releasing PEG-PLGA microsphere coating on CGM sensors show reduced collagen formation around the implant site, suggesting that local tissue mast cell and fibroblast functions are affected by the drug. Implant-associated micromotion can be causing the fluctuations in the sensor response.

6.4 Suggested Future Work

6.4.1 Hollow fiber implants

From our studies, we have shown that fibrosis and fibrous capsule formed around implants is being affected by the use of masitinib to target mast cells. However,

evaluating the nature of the capsule that is formed around drug-releasing implants is essential to understanding the ability of sensor implants to perform for longer durations under mast cell inactivity. A study designed specifically to understand the nature and permeability of the capsule could involve the use of a microdialysis hollowfiber probe (Cuprophan, outer diameter, 0.25 mm, inner diameter, 0.20 mm; length, 15 mm) can be coated with masitinib-releasing formulation and implanted subcutaneously in a murine model. Microdialysis can be performed in these implants for extended periods to ensure glucose transport through the capsule formed in the presence of masitinib to evaluate the permeability of the capsule. Each animal can be implanted with two microdialysis catheters – one control and one drug-releasing implant. This experiment would A) help in understanding the nature of the capsule formed and B) examine the period of time that the drug can be effectively used to reduce the FBR. At the end of the study, fluorescently-labeled glucose 2-NBDG (2-(N-(7-nitrobenz-2-oxa-1,3-diazol-4-yl)amino)-2-deoxyglucose) can be injected into the hollow fiber to visually examine the permeability of the capsule during histology analysis [17]. The extent of dye-penetration into the surrounding capsule can be characterized to further understand the nature of the capsule.

6.4.2 Bone marrow-derived mast cell injections

To test our hypothesis that inhibiting mast cell degranulation results in a reduced FBR, we have conducted studies with local delivery formulations of masitinib in both mast cell sufficient (Chapter 3) and deficient (Chapter 4) mouse models. To further prove the role of mast cells, we could inject *in vitro*-cultured bone-marrow derived tissue mast cells at the CGM sensor implant sites. A similar experiment in mast cell-deficient sash mice implanted with CGM sensors has shown a precipitous drop in glucose measurements within a few days of mast cell injections [18]. Bone marrow derived mast

cells can be culture as described in [18, 19]. Injections of 10^4 to 10^5 cells in pyrogen free saline at the implant site of the sensor could be performed. CGM response can be monitored for one week after the injection of the mast cells to observe any recovery from mast cell injection effects.

6.4.3 Dose escalation studies and the effect of combination of masitinib and anti-inflammatory drugs

The results from this work show significant reduction of fibrous capsule thicknesses around masitinib-releasing implants. The dosage used in these studies was empirical targeting 200 μm thick tissue surrounding the implant site. A randomized dose-escalation study to investigate the dose-response relationship of masitinib could be investigated. Different dosages of 23 μg/implant and 35 μg/implant (i.e., 2x and 3x the current dosage) could be used to evaluate the result of increased drug dosing on the fibrous encapsulation. These studies will give the appropriate dose to mitigate FBR for a given time point.

Mouse models are difficult to handle with a tethered wired sensor setup due to their relatively small body size with respect to the sensor size. Current CGM sensors detect glucose levels in the interstitial fluid in subcutaneous adipose tissue and the mouse model does not possess sufficient adipose tissue for accurate CGM sensor functioning [20, 21]. Zucker diabetic fatty (ZDF) rats are a commonly used animal model in diabetes studies [22]. ZDF rats provide sufficient adipose tissue for CGM sensing and are easier to handle compared to C57Bl/6 mice for long-term CGM testing.

In this dissertation work, we have focused on targeting mast cell degranulation that is widely recognized as a key initiator and orchestrator of host-mediated FBR to implants. However, the release of masitinib does not directly target inflammation and inflammatory cells. Keeping this in view, a future experiment can be designed that uses

a drug formulation containing a combination of masitinib and an anti-inflammatory drug. Aspirin is an anti-inflammatory drug that has shown to reduce fibrosis and inflammation around the implant sites [23]. PLGA microsphere formulations of both dexamethasone and aspirin have been previously developed [24]. Quantified amounts of aspirin PLGA microspheres along with masitinib PLGA microspheres can be coated onto CGM implants and their combined effect on the FBR and resulting fibrosis can be studied. It also needs to be verified if the combination of these drugs counteracts each other's effect [25].

Estimating an appropriate number of test subjects to observe statistically significant differences in responses from control and drug-treated groups is very important to obtain relevant results. Sample size for CGM sensor studies in mice can be calculated based on the capsule thickness data obtained from model implants in wild type mice studies. Assuming a 20% difference in the means of capsule thickness values among the control and treated groups, and a 90% power with a *p*-value of 0.05 (from the table below), the needed sample size can be calculated using Lamorte's sample size calculator to be 15 animals per group, i.e., 30 animals for control and drug-treated groups for a single time point of 21-days. The detailed calculation is shown in Table 6.1.

6.4.4 Sterilization methods

The work done in this dissertation used aseptic processes to reduce the possibility of bacterial contamination of the implants that has been confirmed with LPS experiments. However, there is a need to develop a reliable sterilization method to reduce the bio burden of these implants. Thermal methods of sterilization are unusable for these implants given their polymeric constituents, a majority of which are irreversibly damaged at high temperatures needed for such sterilization methods. Ethylene oxide and sterrad methods tried during our studies have shown to collapse the porous

structure of the coating that would result in slower dissolution of the coating components. Radiation sterilization is known to result in reducing the molecular weights and accelerating the degradation rates of PLGA [26]. A low temperature, radio-frequency glow discharge (RFGD) plasma treatment sterilization method was developed for treating polyester devices [27]. While the RFGD plasma was shown to induce surface cross-linking or branching of the polymer, it did not affect polymer crystallinity, mechanical properties, or overall melting temperature [28]. The sterilization efficiency of plasma gas was demonstrated by a 10^5 reduction of bacteria, bacterial endospores, yeast and bacterial viruses within 90 s of exposure to an atmospheric uniform glow discharge plasma [29], indicative of a similar sterilization efficiency to that of ETO and gamma. RFGD plasma sterilization at 100 W for 4 minutes has shown no volume change and a slight increase in the molecular weight of PLGA scaffolds [30] and can be adopted for the sterilization of the coatings developed in this dissertation.

6.5 References

[1] Danaei G, Finucane MM, Lu Y, Singh GM, Cowan MJ, Paciorek CJ, et al. National, regional, and global trends in fasting plasma glucose and diabetes prevalence since 1980: systematic analysis of health examination surveys and epidemiological studies with 370 country-years and 2.7 million participants. The Lancet. 2011;378:31-40.

[2] Centers for Disease Control and Prevention. National diabetes fact sheet: national estimates and general information on diabetes and prediabetes in the United States. In: Services DoHaH, editor. Atlanta, GA: U.S.: Centers for Disease Control and Prevention; 2011.

[3] Coster S, Gulliford MC, Seed PT, Powrie JK, Swaminathan R. Monitoring blood glucose control in diabetes mellitus: a systematic review. Health Technol Assess. 2000;4:i-iv, 1-93.

[4] Anderson JM, Rodriguez A, Chang DT. Foreign body reaction to biomaterials. Semin Immunol. 2008;20:86-100.

[5] Krishnaswamy G, Ajitawi O, Chi DS. The human mast cell: an overview. Methods in molecular biology (Clifton, NJ). 2006;315:13-34.

[6] Ward WK, Troupe JE. Assessment of chronically implanted subcutaneous glucose sensors in dogs: The effect of surrounding fluid masses. ASAIO J. 1999;45:555-61.

[7] Ward WK, Wood MD, Casey HM, Quinn MJ, Federiuk IF. The effect of local subcutaneous delivery of vascular endothelial growth factor on the function of a chronically implanted amperometric glucose sensor. Diabetes Technol Ther. 2004;6:137-45.

[8] Thevenot PT, Baker DW, Weng H, Sun M-W, Tang L. The pivotal role of fibrocytes and mast cells in mediating fibrotic reactions to biomaterials. Biomaterials. 2011;32:8394-403.

[9] Dubreuil P, Letard S, Ciufolini M, Gros L, Humbert M, Casteran N, et al. Masitinib (AB1010), a potent and selective tyrosine kinase inhibitor targeting KIT. PLoS ONE. 2009;4:e7258.

[10] Reber L, Da Silva CA, Frossard N. Stem cell factor and its receptor c-Kit as targets for inflammatory diseases. Eur J Pharmacol. 2006;533:327-40.

[11] Capan Y, Woo BH, Gebrekidan S, Ahmed S, DeLuca PP. Preparation and characterization of poly (D, L-lactide-co-glycolide) microspheres for controlled release of poly (L-lysine) complexed plasmid DNA. Pharm Res. 1999;16:509-13.

[12] Wang D, Robinson DR, Kwon GS, Samuel J. Encapsulation of plasmid DNA in biodegradable poly (,-lactic-co-glycolic acid) microspheres as a novel approach for immunogene delivery. J Control Release. 1999;57:9-18.

[13] Woodrow KA, Cu Y, Booth CJ, Saucier-Sawyer JK, Wood MJ, Saltzman WM. Intravaginal gene silencing using biodegradable polymer nanoparticles densely loaded with small-interfering RNA. Nat Mater. 2009;8:526.

[14] Sinha V, Trehan A. Biodegradable microspheres for protein delivery. J Control Release. 2003;90:261-80.

[15] Okada H, Toguchi H. Biodegradable microspheres in drug delivery. Crit Rev Ther Drug Carrier Syst. 1995;12:1.

[16] Soppimath KS, Aminabhavi TM, Kulkarni AR, Rudzinski WE. Biodegradable polymeric nanoparticles as drug delivery devices. J Control Release. 2001;70:1-20.

[17] Yoshioka K, Takahashi H, Homma T, Saito M, Oh KB, Nemoto Y, et al. A novel fluorescent derivative of glucose applicable to the assessment of glucose uptake activity of Escherichia coli. Biochim Biophys Acta. 1996;1289:5-9.

[18] Klueh U, Kaur M, Qiao Y, Kreutzer DL. Critical role of tissue mast cells in controlling long-term glucose sensor function in vivo. Biomaterials. 2010;31:4540-51.

[19] Razin E, Ihle JN, Seldin D, Mencia-Huerta JM, Katz HR, LeBlanc PA, et al. Interleukin 3: A differentiation and growth factor for the mouse mast cell that contains chondroitin sulfate E proteoglycan. J Immunol. 1984;132:1479-86.

[20] Cengiz E, Tamborlane WV. A tale of two compartments: interstitial versus blood glucose monitoring. Diabetes Technol Ther. 2009;11 Suppl 1:S11-6.

[21] Nielsen JK, Djurhuus CB, Gravholt CH, Carus AC, Granild-Jensen J, Orskov H, et al. Continuous glucose monitoring in interstitial subcutaneous adipose tissue and skeletal muscle reflects excursions in cerebral cortex. Diabetes. 2005;54:1635-9.

[22] Srinivasan K, Ramarao P. Animal models in type 2 diabetes research: an overview. Indian J Med Res. 2007;125:451-72.

[23] Malik AF, Hoque R, Ouyang X, Ghani A, Hong E, Khan K, et al. Inflammasome components Asc and caspase-1 mediate biomaterial-induced inflammation and foreign body response. Proc Natl Acad Sci U S A. 2011;108:20095-100.

[24] Xiao CD, Shen XC, Tao L. Modified emulsion solvent evaporation method for fabricating core-shell microspheres. Int J Pharm. 2013;452:227-32.

[25] Norton L, Koschwanez H, Wisniewski N, Klitzman B, Reichert W. Vascular endothelial growth factor and dexamethasone release from nonfouling sensor coatings affect the foreign body response. J Biomed Mater Res A. 2007;81:858-69.

[26] Deshpande P, Ramachandran C, Sefat F, Mariappan I, Johnson C, McKean R, et al. Simplifying corneal surface regeneration using a biodegradable synthetic membrane and limbal tissue explants. Biomaterials. 2013;34:5088-106.

[27] Gogolewski S, Mainil-Varlet P, Dillon JG. Sterility, mechanical properties, and molecular stability of polylactide internal-fixation devices treated with low-temperature plasmas. J Biomed Mater Res. 1996;32:227-35.

[28] Ayhan F, Ayhan H, Piskin E. Sterilization of Sutures by Low Temperature Argon Plasma. J Bioact Compat Polym. 1998;13:65-72.

[29] Kelly-Wintenberg K, Hodge A, Montie TC, Deleanu L, Sherman D, Roth JR, et al. Use of a one atmosphere uniform glow discharge plasma to kill a broad spectrum of microorganisms. AVS; 1999. p. 1539-44.

[30] Holy CE, Cheng C, Davies JE, Shoichet MS. Optimizing the sterilization of PLGA scaffolds for use in tissue engineering. Biomaterials. 2001;22:25-31.

Table 6.1: Sample size estimation for future *in vivo* studies using Lamorte's sample size calculator

	Anticipated Values						
	Mean	**Stan. Dev**					
Control	31	5		Difference in means=		19.35	%
Drug-treated	25	5					
The cells in the table below show the estimated number of subjects needed in each							
group in order to demonstrate a statistically significant difference at "p" values							
ranging from 0.10 - 0.01and at varying levels of "power".							
	Power is the probability of finding a statistically significant difference at						
a given "P" value with the specified number of subjects in each group.							
	Sample Size Needed in Each Group						
alpha level		**Power**					
("p" value)		**95%**	**90%**	**80%**	**50%**		
0.10		15	12	9	4		
0.05		18	15	11	5		
0.02		22	18	14	8		
0.01		25	21	16	9		